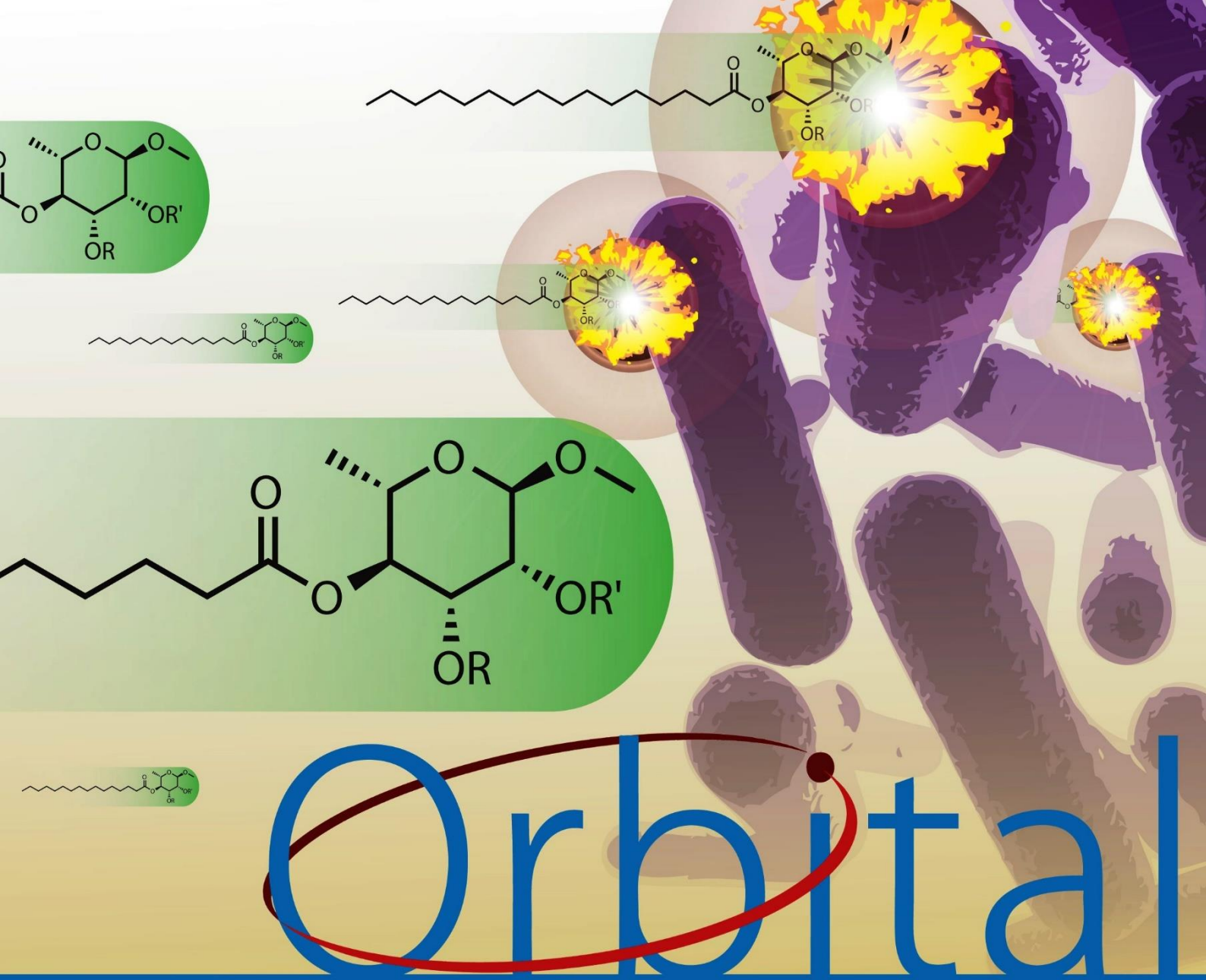

Orbital

The Electronic Journal of Chemistry

JANUARY-MARCH, 2014
VOLUME 6, NUMBER 1
ISSN 1984-6428

Synthesis and antimicrobial study of some methyl 4-O-palmitoyl α-L-rhamnopyranoside derivatives

Published by the
Institute of Chemistry of the Federal University of Mato Grosso do Sul
Campo Grande, Brazil

www.orbital.ufms.br

Orbital - Vol. 6 No. 1 - January-March 2014

Table of Contents

FULL PAPERS

SHORT COMMUNICATIONS

Orbital: The Electronic Journal of Chemistry
journal homepage: www.orbital.ufms.br
ISSN 1984-6428

| Vol 6 | | No. 1 | | January-March 2014 |

Full Paper

Physico-Chemical and In-vitro Microbial Studies of Newly Synthesis Organometallic Complexes

Isam Hussain T. Al-Karkhi

College of Dentistry, University of Baghdad, Bab Al Mozam, Baghdad, Iraq

Article history: Received: 05 October 2013; revised: 09 March 2014; accepted: 28 March 2014. Available online: 02 April 2014.

Abstract: Drugs normally synthesized to use as medication to treat diseases like cancer and microbial infections, these synthesized drugs were interested more than naturally-derived drugs which have been shows low activity or not as efficient against diseases. A new ligand 3-methylbenzyl (2Z)-2-[1-(pyridin-4-yl)ethylidene]hydrazine carbodithioate (PE3MBC) and its Cd(II), Cu(II), Co(II) and Zn(II) metal complexes. The new ligand and metal complexes were characterized via various physico-chemical and spectroscopic techniques. Cd(II) complex show more activity against microbes and against cancer cell line MCF-7, while other complexes does not shows activity like cadmium complex, all the complexes does not shows any activity against MDAMB-231 cell line. The fatal of the cancer and the microbes cell was due to inhibition of DNA synthesis which was probably due to chelating with metals complexes, or could be referred to lipophilicity, presence of hydrophobic moiety in the complex molecule, also could be due to steric effects and electronic effects.

Keywords: organometallic; cytotoxicity; microbes

1. INTRODUCTION

Schiff bases have often been used as chelating ligands in coordination chemistry. Schiff base with donors (N, O, S, etc) have structure similarities with neutral biological systems and due to presence of imine group are utilized in elucidating the mechanism of transformation of rasemination reac-tion in biological system [1].

Thiosemicarbazide and its derivatives as ligands with potential sulphur and nitrogen bands are interesting and have gained special attention due to their importance in medicinal and pharmaceutical field. They show biological activities including antibacterial antifungal, antidiabetic, antitumor, antiproliferative, anticancer, herbicidal, anticorrosion and anti-inflammatory activities [2].

It is well known that the shape of a certain molecule is the most important factor that affects drug activity [3]. The four major factors that affect the properties of a drug are: its ability to chelate to metal ions, its lipophilicity, steric effects and electronic effects. It is clear that the lipophilicity (Fat-loving) is one of the compound character itself which increases the cell permeability and may cause an intracellular reduction of the active M(II) species which leads to the activation of oxygen that cause lethal for microbes [4, 5].

Heterocycles such as, pyrimidine, pyridine and quinolone have been under investigation as they play important roles in biological systems [5]. The criteria should include the presence of hydrophobic moieties in the synthetic drug molecule.

A new ligand 3-methylbenzyl (2*Z*)-2-[1-(pyridin-4-yl)ethylidene]hydrazine carbodithioate (PE3MBC) and its Cd(II), Cu(II), Co(II) and Zn(II) metal complexes has been synthesized and characterized successfully. The biochemistry, cytotoxicity and bioactivity of the newly synthesized organic compounds were under focus in this study to discover the factors that affected the antimicrobial and cytotoxic activity.

2. MATERIAL AND METHODS

Experimental

Carbon, hydrogen, nitrogen and sulfur analyses were carried out using a Leco CHNS-932 analyzer.

*Corresponding author. E-mail: isamhtk@hotmail.com

The molar conductivity measurements were carried out using Wissenschaftlich-TechnischWerk- -statten 8120. Melting points of the synthesized compounds were determined by open capillary and are uncorrected. Melting point apparatus of Gallenkamp M.F.B 600.01 was used. ^{1}H NMR spectra and ^{13}C spectra were recorded on Jeol (JNM-ECA400) 400 MHz NMR spectrometer. Compounds were visualized under UV using UV-Vis 160A in the range of wave number (200-1100 nm). IR spectra were recorded using KBr on Shimadzu FTIR 8300 in the wavelength range of (4000-400) cm^{-1}. The magnetic susceptibility values using (Magnetic Susceptibility Balance), of Johnson mattey catalytic system division using an atomic absorption technique by Perkin-Elmer-5000 to (Cu^{+2}, Ni^{+2}, Cd^{+2} and Zn^{+2}) metal ions.

Preparation of 3-methylphenylhydrazinecarbodithioate (3MBC)

Potassium hydroxide (0.2 mol) was dissolved in absolute ethanol (70 mL). To this solution, hydrazine hydrate (0.2 mol) was added and the mixture was cooled in an ice-salt bath to 0 °C. Carbon disulphide (0.2 mol) was added dropwise with constant stirring over a period of one hour. The two layers that subsequently formed were separated using a separating funnel. The light-brown lower layer was dissolved in 40% ethanol (60 mL) below 5 °C. The mixture was kept in an ice-bath and to it, 3-methylbenzyl chloride (0.2 mol) was added dropwise with vigorous stirring of the mixture. The sticky white product, (3MBC), which formed was filtered and left to dry overnight in a desiccator over anhydrous silica gel. (Yield: 75%, m.p. 130 °C). IR (KBr cm^{-1}): ν(C=N) 1612, ν(N=N) 1046, ν(C=SS) 975 ν (NH)/NH_2) 3398.

Preparation of 3-methylbenzyl (2Z)-2-[1-(pyridin-4-yl)ethylidene]hydrazinecarbodithioate (PE3M-BC)

3-methylbenzyl hydrazinecarbodithioate (0.01 mol) was dissolved in hot acetonitrile (100 mL). This was added to an equimolar solution of 1-(pyridin-4-yl)ethanone in ethanol (10 mL). The mixture was heated and stirred for 30 minutes and then allowed to stand for a few hours, after which yellow crystals formed, which were filtered off and recrystallised from acetonitrile. Yields were fairly high, ca. 85%, C: 59.23(60.29), H: 5.54(5.43), N: 12.65(13.32) and S: 22.03(20.33).

IR (KBr cm^{-1}): ν(C=N) 1592, ν(N=N) 1060, ν(C=SS) 824 ν (NH)/NH_2) 3081.

^{1}H-NMR (DMSO δ ppm): 13.52 (singlet 1H, NH), 7.06-8.55 (multiple 13H, Ar-H), 4.42 (singlet 2H, S-CH_2). 2.29 (singlet 3H, –CH_3). ^{13}C-NMR (DMSO δ ppm): 197.57 (C=S), 149.80 (C=N), 120.18-146.67 (Ar-H), 39.29 (-S-CH_2), 20.95 (CH_3).

The general mechanism for the formation of the Schiff base shown in Scheme 2:

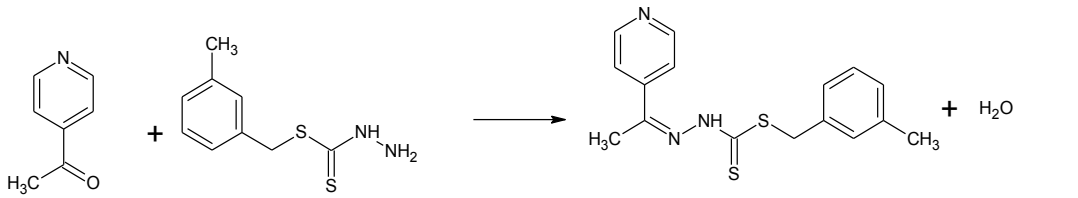

Scheme 1. Condensation reaction of PE3MBC.

Preparation of metal complexes

A hot ethanolic solution of M[acetate/nitrate] .nH_2O[M = Cu(II), Ni(II), Cd(II) and Zn(II)] (0.001 mol in 25 ml) were mixed with a solution of PE3MBC in 1:1 acetonitrile: ethanol (0.002mol in 50 mL) and the resulting mixture were heated for ~30 minutes. The solids precipitated were filtered, washed with cold ethanol and dried in a desiccator over silica gel. Yields: 62-74%.

IR (KBr cm^{-1}) for Cd(II) metal complex: ν(C=N) 1601, ν(N=N) 1083, ν(C=SS) 827.

IR (KBr cm^{-1}) for Cu(II) metal complex: ν(C=N) 1591, ν(N=N) 1089, ν(C=SS) 821.

IR (KBr cm^{-1}) for Ni(II) metal complex: ν(C=N) 1573, ν(N=N) 1081, ν(C=SS) 832.

IR (KBr cm^{-1}) for Zn(II) metal complex: ν(C=N) 1585, ν(N=N) 1090, ν(C=SS) 880.

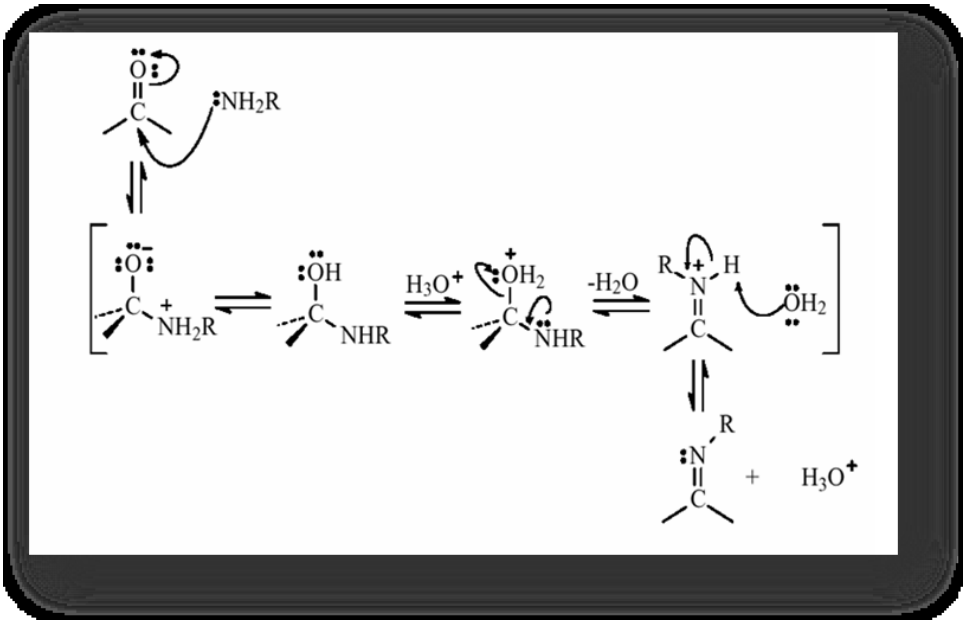

Scheme 2. Formation of the Schiff Base

3. RESULTS AND DISCUSSION

All the synthesized compounds were purified by recrystallization in ethanol. The sharp melting point and the of matching the experimental CHNS data with the theoretical. The characterization of the synthesized compounds and their structures was confirmed using, UV-visible, magnetic susceptibility and molar conductivity. Table 1 shows the physical constant data of synthesized compounds, while Table 2 shows the characterization data as depicted below.

Table 1. Physical properties of the synthesized compounds.

Compound	Color	Melting Point	Molecular Formula	Yield%
3MBC	White	131	$C_9H_{12}N_2S_2$	75%
PE3MBC	Yellow	208	$C_{16}H_{17}N_3S_2$	85%
$Cu(PE3MBC)_2$	Dark Brown	184	$C_{32}H_{32}CuN_6S_4$	67%
$Ni(PE3MBC)_2$	Golden brown	215	$C_{32}H_{32}NiN_6S_4$	68%
$Zn(PE3MBC)_2$	Golden Yellow	190	$C_{32}H_{32}ZnN_6S_4$	71%
$Cd(PE3MBC)_2$	Yellow	205	$C_{32}H_{32}CdN_6S_4$	74%

Table 2. Molar conductivity, Magnetic Susceptibility and UV- Vis Spectroscopy of metal complexes.

Complex	Λ (S cm^2 mol^{-1})	μ_{eff} (BM) at 298K	λ_{max} (Log ε) nm)
PE3MBC	-	-	326 (2.91)
$Cu(PE3MBC)_2$	5.03	1.79	285 (3.45), 427 (3.63), 641 (0.31)
$Ni(PE3MBC)_2$	8.45	Diamagnetic	329 (3.19), 445 (2.65), 885 (0.31)
$Zn(PE3MBC)_2$	1.27	Diamagnetic	252 (3.45), 291 (3.12)
$Cd(PE3MBC)_2$	3.98	Diamagnetic	305 (3.02)

Antimicrobial activity

The antimicrobial activities of the compounds were qualitatively determined by a modified disc diffusion method. A lawn of microorganisms was prepared by pipetting and evenly spreading inoculum (10-4 mL, adjusted turbidometrically to 105–106 cfu/mL (cfu: colony forming units) on to agar set in Petri dishes, using nutrient agar (NA) for the bacteria

and potato dextrose agar (PDA) for fungi. Whatman No. 1 filter paper discs of 6 mm diameter were impregnated with dimethyl sulphoxide (DMSO) stock solution of the compound (100 mg/mL) and dried under sterile conditions. The dried discs were then placed on the previously inoculated agar surface. The plates were inverted and incubated for 24 h at 37 °C for bacteria and 30 °C for fungi. Antimicrobial activity was indicated by the presence of clear inhibition zones around the discs.

Seven pathogenic microbes were used to test the biological potential of the compounds: (i) Methicillin resistant *Staphylococcus* (MRSA), (ii) *Bacillus subtilis*-wild type (B29) (*B. Sabtilis*), (iii) *Pseudomonas aeruginosa* (60690) (*P. aeruginosa*), (iv) *Candida albicans* (CA), (v) *Aspergillus ochraceous* (398) (*A. ochraceous*), (vi) *Saccharomyces cereviceae* (20341) (*S. cereviceae*) and *Salmonella choleraesuis*. The sources of microbes and culture maintenance were as previously described. The antimicrobial activity of the extracts was qualitatively determined by a modified disc diffusion method [6, 7]. Streptomycin was used for antibacterial control while Nystatin was used as antifungal control. Measurement of inhibitory activity as described by Hufford and Clark, the lowest concentration that completely inhibited microbial growth recorded as the minimum inhibitory concentration (MIC, $\mu g.cm^{-3}$) [8]**.** Table 3 shows the antimicrobial activity of the compounds.

It has been observed that the Schiff base was not active against the tested bacteria and fungi the inhibition diameters (18 mm) which is less than that of the commercially available standard, Nystatin (22 to 27 mm), indicating that it was less effective. However, Metal complexes were found to be more active against the selected bacteria and fungi compare to the ligand. Streptomycin (22–24 mm), especially that of the Cd(II) complex, which had inhibition diameters as high as 26 mm. The Cadmium is well known with its toxicity, in addition to that, the methyl group in PE3MBC also reduces the water solubility of the complex and its ability to hydrogen bond.

Table 3. Qualitative antimicrobial analysis of the ligand and its metal complexes.

Complex	Inhibition diameters (mm)						
	Bacterial Strains				**Fungal Strains**		
	MRSA	**P. Aer**	**S. Cho**	**B. Sub**	**C. Alb**	**A. Och**	**S. Cer**
3MBC	17	17	16	18	18	18	18
PE3MBC				12			
$Cd(PE3MBC)_2$	21	16	17	26			
$Cu(PE3MBC)_2$							
$Ni(PE3MBC)_2$	14			14			
$Zn(PE3MBC)_2$	10	14	10	10			
Streptomycin	**24**	**22**	**23**	**22**			
Nystatin					22	23	27

This higher antibacterial activity of the metal complexes compared to ligand is may be due to the change in structure due to coordination and chelating tends to make metal complexes act as more powerful and potent bacteriostatic agents, thus inhibiting the growth of the bacteria. Furthermore, chelation reduces the polarity of the metal ion mainly due to the partial sharing of its positive charge with the donor groups within the chelate ring system. Such chelation increases the lipophilic nature of the central metal atom, which favors its permeation more efficiently through the lipid layer of the microorganism, thus destroying them more forcefully. Thus, all complexes showed more increased activity than the corresponding ligand and the two antibacterial drugs [9-11].

Cytotoxic activity

The MCF-7 (Human Breast cancer cells with positive estrogen receptor) and the MDA-MB-231 (Human Breast cancer cells with negative estrogen receptor) cell lines were obtained from the National Cancer Institute, U.S.A. The cells were cultured in RPMI-1640/DMEM (Sigma) medium supplemented with 10% fetal bovine serum. Cytotoxicity was

determined using the microtitration of 3-(4,5-dimethylthiazol-2-yl)-2,5-diphenyl tetrazolium bromide (MTT) assay (Sigma, USA) as reported by Mosmann [6]. Controls that contained only cells were included for each sample. Cytotoxicity was expressed as IC_{50}, i.e. the concentration that reduced the absorbance of treated cells by 50% with reference to the control (untreated cells). Tamoxifen was used as a standard cytotoxin. Table 4 shows the activity of the compounds against 2 cancer cell lines.

Table 4. Cytotoxic data of the ligand and its transition metal complexes.

Complex	IC50(µg/ml)	
	MCF-7	MDA-MB-231
3MBC	8.7	Inactive
P33MBC	Inactive	Inactive
$Cd(PE3MBC)_2$	4.7	4.5
$Cu(PE3MBC)_2$	7.3	15.2
$Ni(PE3MBC)_2$	17.8	Inactive
$Zn(PE3MBC)_2$	5.9	17
Tamoxifen	**5.1**	**5.4**

IC_{50} < 5.0 µg cm^{-3}- strongly active, IC_{50} 5.0 < 10.0 µg cm^{-3}- moderately active, IC_{50} 10.0 < 25.0 µg cm^{-3}- weakly active, IC_{50} > 25.0 µg cm^{-3}- not active. IC_{50} (µg cm^{-3}) = Cytotoxic dose at 50% i.e. the concentration to reduce growth of cancer cells by 50%. MCF-7= Human Breast Carcinoma Cells with Positive Estrogen Receptor, MDA-MB-231 = Human Breast Carcinoma Cells with Negative Estrogen Receptor

The complexes were more cytotoxic towards the MCF-7 cells than the MDA-MB-231 cells (Table 4) meaning that the structure or part of the structure of the complexes is complementary to the stereo electronic structure of the positive estrogen receptor responsible for the desired biological action. Receptors are specific areas of proteins and glycoproteins embedded in cellular membranes or in the nuclei of living cells [10], which may open ion channels or release secondary messengers when bonded to a favourably shaped molecule. If a tumor is estrogen-receptor positive (ER-positive), it has receptors that react with estrogen and it is more likely to grow in a high-estrogen environment. ER-negative tumors do not have any receptors that react with estrogen and are usually not affected by the levels of estrogen and are not inhibited by well-known anti-cancer drug, Tamoxifen [6, 12, 13]. Tamoxifen has been used to treat breast cancer by blocking the binding of estrogens to the estrogen receptor [13].

The increased activity of the metal chelates can be explained on the basis of chelation potent bactericidal agents and to antifungal agent, thus killing more of the bacteria than the ligand. It is observed that, in a complex, the positive charge of the metal is partially shared with the donor atoms present in the ligand, and there may be π-electron delocalization over the whole chelating. This increases the lipophilic character of the metal chelate and favors its permeation through the lipoid layer of the bacterial membranes. Also, there are other factors which also increase the activity, such as solubility, conductivity and bond length between the metal and the ligand. The mode of action may involve the formation of a hydrogen bond through the azomethine nitrogen and oxygen atom with the active centers of the cell constituents, resulting in interference with the normal cell process. The variation in the effectiveness of different compounds against different organisms depend either on the impermeability of the cells of the microbes or the difference in ribosomes of microbial cells [14].

A complex that is used as a therapeutic chelating agent should have the following characteristics. Chelates occur naturally in biological systems as enzymes and involve mainly transition metal ions. A pathogenic organism can be killed or inhibited by introducing a ligand having a greater affinity for an essential metal ion than the natural ligand, forming a stable, inert chelate [15]. Chelation reduces the polarity of the molecule making it more lipophilic and hence allowing for more binding sites and interactions in the cell membranes, as cell membranes consists of lipids, polysaccharides and proteins amongst others. This would allow the molecule to penetrate the cell membrane easily to reach the cell's DNA, to bind to the nucleoside bases in the DNA and inhibiting its biosynthesis [16, 17]. Hence, it is probably the complex is unable to hydrogen bond due to the presence of different substituents; it is unable to interact with the DNA and proteins in the cell and cause cell apoptosis and is less

effective as an antimicrobial or anti-cancer agent [11]. The increase in the size of the complex allows for a better interaction with the hydrophobic pocket in the target site of the bacteria/fungi which might strengthen the binding of the complex to the microbe, destroying the cell wall and ultimately killing the microbe [10]. Cadmium has the largest size comparing with other metals used in this study.

There are many factors that affect potential drug behavior in the biological system. Some of these include the rigidity of the molecule, the number of rings in the system, nature of bonding, the conformation and stereochemistry, presence of a pharmacophore, number of methyl groups and the degree of unsaturation. All of these affect the lipophilicity and hydrophobicity of the complexes. This in turn plays a huge role in determining whether the complexes would be able to interact with the receptors on the cell membrane, and with the DNA in the nuclei of the cell, ultimately leading to cell death. It is of interest to note that the complexes exhibit approximately equal inhibition to the standard antibiotic which reveals the biological efficiency of these complexes and showed the possibility to be useful as new drug [18].

4. CONCLUSION

The chelating of DNA with metal complexes will lead to the inhibition of DNA synthesis in cancer cells and microbes which result to apoptosis of the cell, this could be probably due to electronic effect, lipophilicitym steric effect or could be to the hydrophobic behaviors to the molecule of the complex.

5. REFERENCE AND NOTES

[1] Kumar, G.; Kumar, D.; Devi, S.; Johari, R.; Singh, C. P. *Eur. J. Med. Chem.* **2010**, *45*, 3056. [CrossRef]

[2] Basu, A. and Das, G. *Inorg. Chim. Acta* **2011**, *372*, 394. [CrossRef]

[3] Gringauz, A. Introduction to medicinal chemistry: how drugs act and why. New York: Wiley-VCH, 1997.

[4] Singh, K.; Barwa, M. S; Tyagi, P. *Eur. J. Med. Chem.* **2006**, *41*, 147. [CrossRef]

[5] Singh, P.; Kaur, P.; Luxami, V.; Kaur, S.; Kumar, S. *Bioorg. Med. Chem*. **2007**, *15*, 2386. [CrossRef]

[6] Mosmann, T. *J. Immunol. Methods* **1983**, *65*, 55. [CrossRef]

[7] Bauer, W. A. *Am. J Clin. Patholog.* **1966**, *45*, 493.

[8] Hufford, D. C.; Clark, M. A.; Studies in Natural Product Chemistry, 2, Amsterdam: Elsevier, 1988.

[9] Geetaa, B.; Shravankumara, K.; Reddy, P. M.; Ravikrishna, E.; Sarangapani, M.; Reddy, K. K.; Ravinder, V. *Spectrochim. Acta Part A* **2010**, *77*, 911. [CrossRef]

[10] Thomas, G.; Medicinal Chemistry: An Introduction. In Anticancer Agents, 3rd ed. New York: John Wiley & Sons, Ltd, 2000.

[11] Hamid, G.; Sara, K.; Maedeh, R.; Davood, F. *Polyhedron* **2013**, *51*, 1. [CrrossRef]

[12] Nguyen, A.; Top, S.; Vessières, A.; Pigeon, P.; Huché, M.; Hillard, E. A.; Jaouen, G. *J. Organomet. Chem.* **2007**, *692*, 1219. [CrossRef]

[13] Sheikh, M. S.; Garcia, M.; Pujol, P.; Fontana, J. A.; Rochefort, H. *Inv Metastasis* **1995**, *14*, 329.

[14] Abdelrazak, M. T.; Mosad, A.; Samy, M.; Naglaa, M. *Spectrochim. Acta Part A* **2012**, *97*, 1172. [CrossRef]

[15] Santosh, K.; Niranjan, M. S.; Chaluvaraju, K. C.; Jamakhandi, C. M.; Kadadevar, D. *J. Curr. Pharm. Res.* **2010**, *1*, 39.

[16] Mehmet, C.; Levent, O.; Mehmet, K.; Ibrahim, E. *Spectrochim. Acta Part A* **2013**, 111, 97. [CrossRef]

[17] Huang, R.; Wallqvist, A.; Covell, D. G. *Biochem. Pharmacol.* **2005**, *69*, 1009. [CrossRef]

[18] Azza, A. A.; Wolfgang, L. *Spectrochim. Acta Part A* **2012**, *95*, 596. [CrossRef]

Orbital: The Electronic Journal of Chemistry
journal homepage: www.orbital.ufms.br
ISSN 1984-6428

| Vol 6 | | No. 1 | | January-March 2014 |

Full Paper

Estudo da Influência do Tempo de Síntese na Obtenção de Hidroxiapatita por Hidrotermal/micro-ondas

Luciana Natália Cividatti[a,b], Valdemir dos Santos[c], Alexandre Urbano[d], Adriana Fernandes da Silva[e], Luiz Henrique Dall'Antonia[a]*.

[a]*Departamento de Química, Universidade Estadual de Londrina (UEL). Londrina-PR, Brazil*
[b]*Universidade Tecnológica Federal do Paraná (UTFPR) Campus Londrina. Londrina-PR, Brazil.*
[c]*LIEC, Universidade Federal de São Carlos (UFSCar). São Carlos-SP, Brazil.*
[d]*Departamento de Física, Universidade Estadual de Londrina (UEL). Londrina-PR, Brazil.*
[e]*Departamento de Odontologia Restauradora da Universidade Federal de Pelotas (UFPel). Pelotas - RS, Brazil.*

Article history: Received: 25 November 2014; revised: 10 January 2014; accepted: 11 February 2014. Available online: 02 April 2014.

Abstract: The hydrothermal system has been widely used in recent years for the synthesis of materials, especially in the synthesis of nanostructured materials. The present work aimed to synthesize hydroxyapatite, since it is characterized by being a biomaterial widely used in bone replacement procedures. The synthesis of this material was conducted via the hydrothermal system combined with the influence of the microwave. The materials obtained in this synthetic route were compared with the material obtained by synthesis in hot plate. Also explored was the influence of synthesis time (10, 20 and 30 min). The synthesized materials were analyzed by X-ray diffraction, Fourier transform infrared spectroscopy and scanning electron microscopy. The results showed that the synthesis heating plate is capable of generating particles of smaller crystallite size and crystallinity equivalent to those of the materials synthesized in hydrothermal system assisted by microwaves. Moreover, the hydrothermal system was only effective in the synthesis of hydroxyapatite for 30 min. Times smaller synthesis in hydrothermal system generated with a mixture of hydroxyapatite with brushite and monetite.

Keywords: hydroxyapatite; hydrothermal; microwave-hydrothermal; hot plate.

1. INTRODUÇÃO

A hidroxiapatita (HAp) é um biomaterial que exibe uma excelente biocompatibilidade com tecidos moles como a pele, músculos, gengiva, e por isso é considerada como a melhor opção para implantes ortopédicos e dentários [1]. A HAp sintética [$(Ca_{10}(PO_4)_6(OH)_2$] vem sendo amplamente utilizada também no reparo de tecidos duros, aumento ósseo, assim como no recobrimento de implantes ou como material de enxerto para ossos e dentes [1,2].

Entretanto, apatitas biológicas (esmalte dentário, dentina e ossos) diferem da HAp sinteticamente produzida em estequiometria, composição, cristalinidade e também em outras propriedades físicas e mecânicas [3]. Além dos fosfatos de cálcio serem considerados como materiais úteis em calcificações biológicas, eles também apresentam grande importância na química, agricultura, bioquímica e bioengenharia [4]. A literatura descreve várias metodologias utilizadas no preparo de cristais de HAp incluindo reações no estado sólido, técnicas de plasma, crescimento de cristais em condições hidrotermais, hidrólise de outros sais de fosfato de cálcio e método sol-gel [2,5-10].

Em condições ideais, os materiais cerâmicos sintetizados, quando utilizados como biomateriais, devem apresentar características físico-químicas, pureza e estrutura cristalina o mais semelhante possível com HAp naturais. As características da HAp dependem de uma série de fatores relativas ao processo de síntese, tais como impurezas, reagentes precursores, morfologia e tamanho de cristal, concentração, pH e temperatura. Além disso, a bioatividade desses materiais também depende do perfil de tratamento térmico para a secagem e sinterização do material [11,12].

O presente trabalho teve por objetivo estudar a influência do tempo de síntese de hidroxiapatita. O

*Corresponding author. E-mail: luizh@uel.br

processo de síntese foi realizado em sistema hidrotermal assistido por micro-ondas (HM), método hidrotermal (H) e em chapa aquecedora (Ch) conduzidos à 120ºC por 10, 20 e 30 min. Os materiais obtidos foram caracterizados por microscopia eletrônica de varredura (MEV), infravermelho por transformada de Fourier (IV) e difração de raio-X (DRX).

2. MATERIAIS E METODOS

Síntese dos materiais

Todos os reagentes utilizados são de grau analítico e foram utilizados sem purificação prévia e todas as soluções foram preparadas utilizando água ultrapura (Millipore Plus), com resistividade de aproximadamente 18 MΩ.cm a 25 °C.

A síntese por precipitação foi realizada a partir da adição controlada e simultânea das soluções de acetato de cálcio ($Ca(CH_3COO)_2$) e hidrogenofosfato de amônia ($(NH_4)_2HPO_4$), em uma solução de acetato de amônia (NH_4CH_3COO), mantendo-se o pH controlado em 8,5 pela adição de amônia (NH_4OH), obtendo-se a razão molar Ca/P em 1,67. Tal procedimento de síntese foi realizado sob agitação constante, em chapa de aquecimento (Ch). O mesmo procedimento foi repetido em sistema hidrotermal (H), onde as soluções precursoras foram misturadas e seladas em um frasco de vidro de reação (100 mL) e mantido em estufa (EL-1.6, Odontobrás), sendo necessários, em média, 30 min para que se atingisse a temperatura desejada. Por fim, o procedimento de síntese também foi realizado em sistema hidrotermal assistido por micro-ondas (HM), utilizando-se um recipiente de Teflon, selado em um reator de inox (HMO-100, LIEC), com rampa de aquecimento de 5ºC/min. Todas as rotas sintéticas foram realizadas à 120ºC por 10, 20 e 30 min.

Caracterização dos materiais

Os grupamentos típicos dos materiais foram analisados por espectroscopia no infravermelho com transformada de Fourier (IR Prestige-21 Shimadzu) na região de número de onda entre 400 e 4000 cm^{-1}, sendo o material imobilizado em pastilhas de KBr. A análise por difração de raios X dos materiais sintetizados, na forma de pó, foram realizadas com um difratômetro X´Pert PRO MPD (Panalytical) utilizando-se radiação CuKα de λ=1,54060 Å. A morfologia das partículas foi observada em microscópio eletrônico de varredura (Quanta 200 FEI, Philips), operado a 30 KeV.

3. RESULTADOS E DISCUSSÕES

A Figura 1 apresenta os difratogramas obtidos para as amostras sintetizadas em chapa aquecedora (Ch), sistema hidrotermal (H) e em sistema hidrotermal assistido por micro-ondas (HM) nos tempos de 10, 20 e 30 min.

A análise por difração de raios X dos materiais sintetizados em sistema hidrotermal mostrou que todas as rotas de síntese, independente do tempo de síntese levaram à formação da HAp, no entanto, quando da síntese em sistema hidrotermal por 10 min e 20 min verificou-se, também, a presença de brushita ($CaHPO_4.2H_2O$) e monetita ($CaHPO_4$). Destaca-se também que quando da síntese em sistema hidrotermal assistido por micro-ondas por 10 e 30 min e em chapa aquecedora por 20 minutos, os picos característicos para HAp apresentam maior intensidade e melhor resolução. Tal fato pode significar uma maior cristalinidade do material obtido. O perfil de difração das amostras de HAp foram indexadas (*Inorganic Crystal Structure Database* - ICSD) como sendo pertencente ao grupo hexagonal (grupo espacial $P6_3/m$, ICSD: 016742).

O fato de a maioria das rotas sintéticas terem levado à formação de HAp, pode ser um indicativo de que, assim como sugerem alguns pesquisadores [13,14], as micro-ondas não possuem a habilidade de aumentar a velocidade de reação ou criar partículas mais bem definidas. Dessa forma, tais efeitos poderiam ser atribuídos como consequência das condições de temperatura e altas pressões que desencadeiam algumas diferenças nos materiais formados.

A média dos tamanhos dos cristalitos, calculada a partir da Equação de Scherrer [15], considerando o plano de difração 002 (Tabela 1) apresentou uma diferença muito pequena entre os materiais sintetizados. Destaca-se, no entanto que, quando da síntese em sistema hidrotermal assistido por micro-ondas o aumento no tempo de síntese leva ao aumento do tamanho de cristalito (aumento de 13%), como era de se esperar, pois em sínteses mais demoradas, o cristal tem um período maior de tempo para nucleação e crescimento. Por outro lado, quando da síntese em chapa aquecedora, aquelas realizadas por 10 e 30 min geraram materiais com tamanho

médio de cristalito muito semelhante entre si e apresentam valores menores (29%), quando comparados com os materiais sintetizados em sistema hidrotermal assistido por micro-ondas.

A síntese em chapa aquecedora por 20 min gerou cristais um pouco maiores (27%) em relação aos obtidos em síntese por 10 e 30 min em chapa aquecedora.

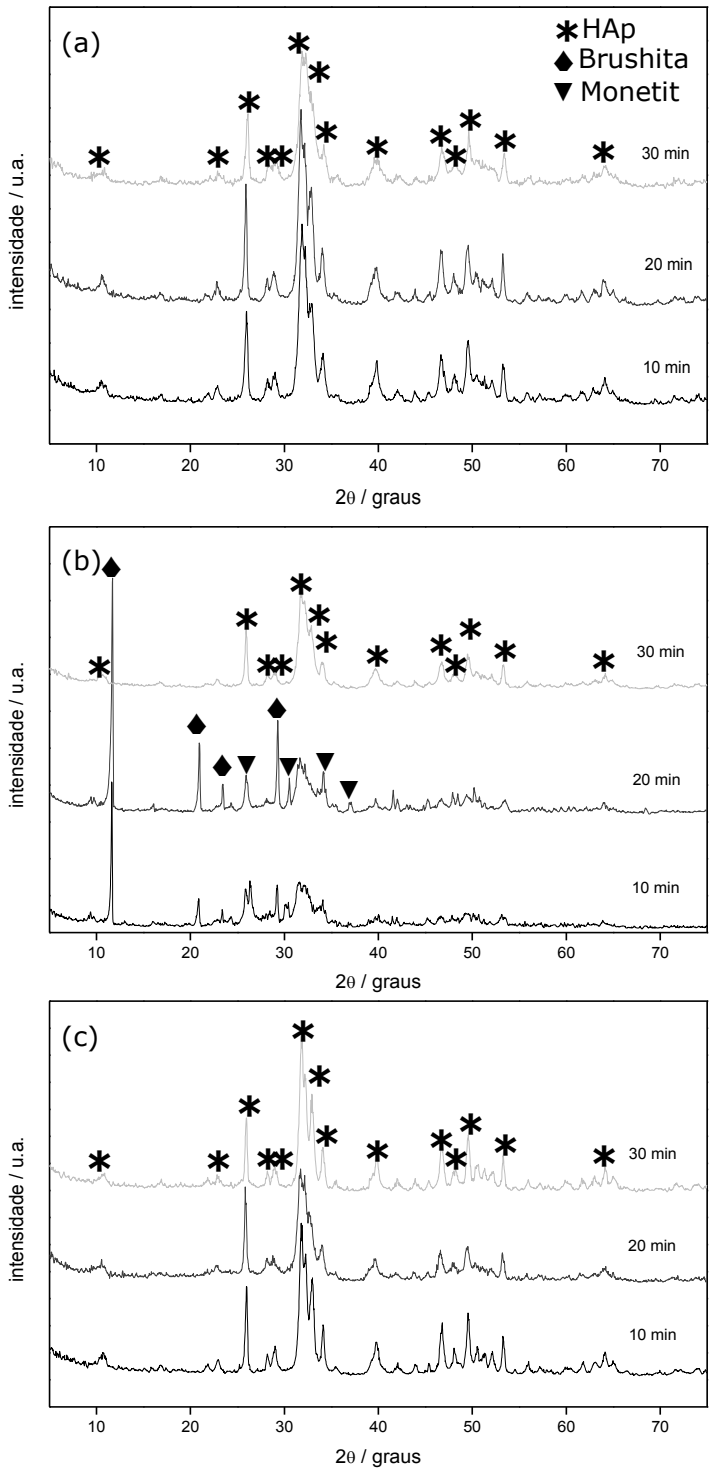

Figura 1. Difratogramas de raios X das amostras obtidas pela síntese da hidroxiapatita conduzida por 10, 20 e 30 min em (a) chapa aquecedora, (b) sistema hidrotermal e (c) sistema hidrotermal assistido por micro-ondas.

Tabela 1. Tamanho de cristalito, calculado a partir da equação de Scherrer, para os materiais sintetizados nas diferentes condições propostas.

	τ (nm)		
	10 min	**20 min**	**30 min**
Chapa Aquecedora	27	35	28
Hidrotermal	*	*	35
Hidrotermal Micro-ondas	39	42	44

*Amostras caracterizadas como sendo misturas.

Considerando-se apenas a síntese em Ch por 30 min que esperava-se a formação de HAp com maior tamanho de cristalito, sugere-se que esta amostra pode ter sofrido uma ruptura espontânea da estrutura, parcial ou integral, devido à expansão volumétrica dos grãos. Destaca-se o fato do difratograma desse material apresentar picos menos intensos, o que caracteriza a amostra como sendo menos cristalina, gerando um alargamento dos picos e consequentemente o valor calculado de tamanho médio de cristalito será menor. Dessa forma, a síntese em Ch por 30 min, gerou partículas menos cristalinas e cristais menores.

O material sintetizado em sistema hidrotermal por 30 min gerou cristais com tamanho intermediário em relação aos outros dois tipos de síntese.

A partir da análise dos tamanhos médios dos cristalitos percebe-se que o aumento da pressão gera cristalitos maiores, visto que os picos de difração tendem a ser mais intensos e apresentar maior largura a meia altura para amostras sintetizadas em pressões mais elevadas. Tal característica pode ser atribuída ao fato de que o aumento da pressão, à temperatura constante, geralmente reduz a mobilidade dos átomos, ocasionando um aumento de elasticidade na superfície dos grãos que induz ao crescimento do grão. Ainda a pressão pode induzir a ordenação da fase amorfa, ou parcialmente desordenada, levando a maiores tamanhos de cristalito [16]. Tais considerações justificam o fato de que o sistema hidrotermal assistido por micro-ondas gere cristalitos maiores.

Os espectros de infravermelho obtidos para as amostras sintetizadas em chapa aquecedora (Ch), sistema hidrotermal (H) e em sistema hidrotermal assistido por micro-ondas (HM) nos tempos de 10, 20 e 30 min são apresentados na Figura 2.

Nota-se que para os materiais sintetizados em chapa aquecedora as bandas características de fosfato são proporcionalmente mais intensas, quando comparadas aos espectros dos materiais obtidos pelas outras rotas sintéticas (H e HM). A presença de duas bandas em 563 e 605 cm^{-1} correspondem ao estiramento característico do grupo O-P-O de fosfato (ν_4 OPO), e a banda presente em 961 cm^{-1} caracteriza o estiramento simétrico P-O de fosfato (ν_1 PO). Essas bandas foram identificadas em todos os espectros, mas são muito mais intensas para os materiais sintetizados em chapa aquecedora por 10 e 20 min. O dubleto localizado na faixa de infravermelho entre 1100 e 1000 cm^{-1} corresponde ao estiramento assimétrico P-O de fosfato (ν_3 PO) [17-20]. Vale ressaltar, porém, que a banda correspondente ao OH^- estrutural (ν OH) típico de HAp [18] (634 e 3571 cm^{-1}), mais uma vez, foram mais características nos espectros obtidos para os materiais sintetizados em chapa aquecedora por 10 e 20 min.

Os resultados de infravermelho apresentados evidenciam que não é necessário um tempo de síntese muito elevado para que se obtenha a HAp e ainda que métodos de sínteses simples, como em chapa aquecedora, são capazes de gerar HAp da mesma forma que métodos mais rebuscados, como o sistema hidrotermal assistido por micro-ondas, gerando, inclusive, materiais com tamanho médio de cristalito menor.

As analises por MEV indicaram que, quando se realiza a síntese em Ch (Fig. 3a, 3b e 3c), independente do tempo de síntese, há predominância de aglomerados de partículas com tendências esféricas. Por outro lado, a síntese em sistema H por 10 e 20 min (Fig. 3d e 3e) há uma mistura de partículas com tendências esféricas e partículas com formas laminares. A síntese em sistema H por 30 min (Fig. 3f), por sua vez, também levou à formação de partículas com tendências esféricas, como é característico para a HAp [21], 2004). A síntese em sistema HM (Fig. 3g, 3h e 3i) levou à formação de, além das partículas com tendências esféricas, partículas laminares quando da síntese por 10 min

(Fig. 3g) e partículas semelha ntes a bastonetes quando da síntese por 20 min (Fig. 3h), o que pode indicar que é preciso um tempo maior de síntese para se possa alcançar maior organização do sistema.

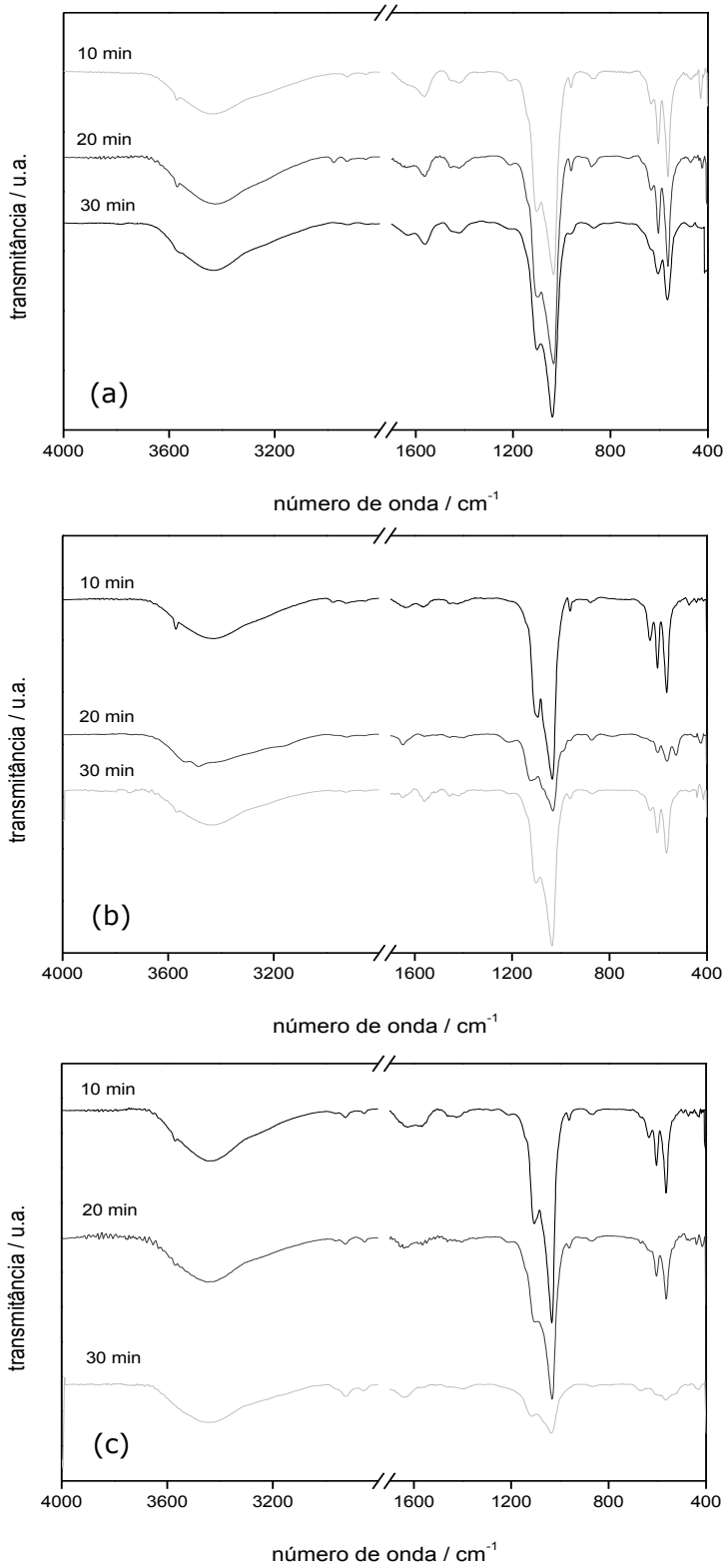

Figura 2. Espectros de infravermelho das amostras obtidas pela síntese da hidroxiapatita conduzida por 10, 20 e 30 min em (a) chapa aquecedora, (b) sistema hidrotermal e (c) sistema hidrotermal assistido por micro-ondas.

Ao comparar os resultados obtidos pelas análises de MEV com os resultados obtidos por DRX, nota-se que os materiais caracterizados por esta técnica como sendo formados por uma única fase, a HAp, apresentam, na microscopia eletrônica, uma tendência a morfologia esférica, em especial para os materiais sintetizados em chapa aquecedora, em sistema H por 30 min e sistema HM por 20 e 30 min. A morfologia não uniforme apresentada pelos materiais sintetizados em sistema H por 10 e 20 min (Fig. 3d e 3e) deve-se à mistura presente nesses materiais (brushita, monetita e HAp).

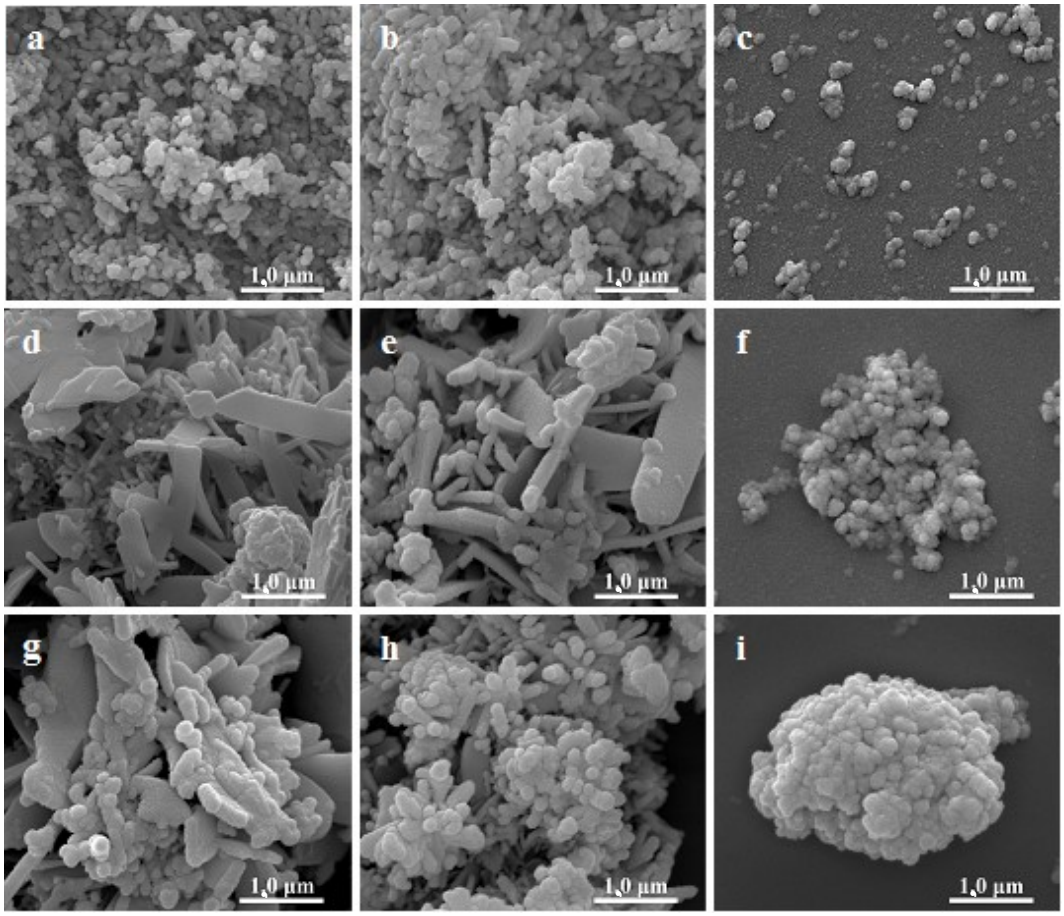

Figura 3. Micrografias obtidas para os materiais sintetizados em chapa aquecedora por (a) 10, (b) 20 e (c) 30 min; em sistema hidrotermal por (d) 10, (e) 20 e (f) 30 min; e, em sistema hidrotermal assistido por micro-ondas por (g) 10, (h) 20 e (i) 30 min.

4. CONCLUSÕES

Os resultados apresentados e analisados no presente trabalho indicaram que é possível sintetizar HAp por diferentes processos de síntese. No entanto vale ressaltar que a síntese em chapa aquecedora é a que gera materiais com menor tamanho médio de cristalito, independente do tempo de síntese (10, 20 ou 30 min). Ressalta-se também que nesse tipo de síntese, os materiais mais cristalinos foram obtidos a partir da síntese por 20 min.

O sistema hidrotermal só possibilitou a formação da HAp em 30 min de síntese, sendo que tempos menores geraram misturas de HAp com brushita e monetita, fosfatos de cálcio que possuem menor razão molar Ca/P e, portanto, são mais solúveis.

O sistema hidrotermal assistido por micro-ondas gerou partículas com tamanho médio de cristalito maior, além de apresentar morfologia irregular quando das sínteses por 10 e 20 min, destacando-se uma maior cristalinidade para o material sintetizado por 30 min, já que o difratograma desse material apresenta picos mais intensos e mais bem definidos.

Dessa forma pode-se perceber que

metodologias tradicionais de síntese podem gerar HAp com boas propriedades cristalinas e morfológicas, comparáveis as HAp obtidas em sistemas mais modernos como o sistema assistido por micro-ondas, que tem recebido grande atenção nos últimos tempos por ser amplamente divulgado como sendo capaz de gerar materiais com características mais refinadas.

5. AGRADECIMENTOS

Os autores agradecem a Fundação Araucária (15585/2010), NEMAN Pronex Fundação Araucária/CNPq (17378/2009), CNPq RHAE e CAPES pelo apoio financeiro. Aos laboratórios de Microscopia Eletrônica; Microanálise e de Difração de Raios X e Laboratório de Espectroscopia da UEL onde foram realizadas as análises de caracterização. A autora L. N. Cividatti agradece ao suporte oferecido pela UTFPR-Londrina.

6. REFERÊNCIAS E NOTAS

[1] Zhou, H.; Lee, J. *Acta Biomater.* **2011**, *7*, 2769. [CrossRef]

[2] Iyyappan, E.; Wilson, P. *Ceram Int.* **2013**, *39*, 771. [CrossRef]

[3] Hench, L. L. *J. Am. Ceram. Soc.* **1991**, *74*, 1487. [CrossRef]

[4] Karampas, I. A.; Kontoyannis, C. G. *Vib. Spectrosc.* **2013**, *64*, 126. [CrossRef]

[5] Beheri, H. H.; Mohamed, K. R; El-Bassyouni, G. T. *Mater. Des.* **2013**, *44*,461. [CrossRef]

[6] Chang, C.; Peng, N.; He, M.; Teramoto, Y.; Nishio, Y.; Zhang, L. *Carbohyd. Polym.* **2013**, *91*, 7. [CrossRef]

[7] Yu, C.; Chang, J.; Lee, Y.; Lin, Y.; Wu, M.; Yang, M.; Chien, C. *Mater. Lett.* **2013**, *93*, 133. [CrossRef]

[8] Kumar, T. S. S.; Manjubala, I.; Gunasekaran, J. *Biomaterials.* **2000**, *21*, 1623. [CrossRef]

[9] Kweh, S. W. K.; Khor, K. A.; Cheang, P. J. *Mater. Process. Tech.* **1999**, *89*, 373. [CrossRef]

[10] Lim, G. K.; Wang, J.; Ng, S. C.; Gan, L. M. *Mater. Lett.* **1996**, *28*, 431. [CrossRef]

[11] Santos, M. H.; Oliveira, M.; Souza, L. P. F., Mansur, H. M., Vasconcelos, W. L. *Mater. Res.* **2004**, *7*, 625. [CrossRef]

[12] Afshar, A.; Ggorbani, M.; Ehsani, N.; Saeri, M. R.; Sorrell, C. C. *Mater. Des.* **2003**, *24*, 197. [CrossRef]

[13] Pires, J.; Carvalho, A. P.; Pereira, P. R.; Carvalho, M. B. *React. Kinet. Catal. Lett.* **1998**, *65*, 9. [CrossRef]

[14] Chemat, F.; Poux, M.; Berlan, J. *J. Chem. Soc., Perkin Trans. 2.* **1994**, *12*, 2597. [CrossRef]

[15] Suryanarayana, C.; Norton, M. G. X-Ray Diffraction: A Practical Approach. New York: Plenum Press, 1998.

[16] Gubicza, J.; Nauyoks, S.; Balogh, L.; Labar, J.; Zerda, T. W.; Ungár, T. *J. Mater. Res.* **2007**, *22*, 1314. [CrossRef]

[17] Nakamoto, K. Infrared and Raman Spectra of Inorganic and Coordination Compounds, 6th ed. New Jersey: John Wiley & Sons, 2009.

[18] Han, J. K.; Song, H. Y.; Saito, F.; Lee, B. T. *Mater. Chem. Phys.* **2006**, *99*, 235. [CrossRef]

[19] Vaidya, S. N.; Karunakaran, C.; Pande, B. M.; Gupta, N. M.; Iyer, R. K.; Karweer, S. B. *J. Mater. Sci.* **1997**, *32*, 3213. [CrossRef]

[20] Stuerga, D. A. C.; Gaillard, P. *J. Microwave Power.* **1996**, *31*, 101.

[21] Welzel, T.; Zaika, W. M.; Epple, M. *Chem. Commun.* **2004**, *10*, 1204. [CrossRef]

Orbital: The Electronic Journal of Chemistry
journal homepage: www.orbital.ufms.br
ISSN 1984-6428

| Vol 6 | | No. 1 | | January-March 2014 |

Full Paper

Photocatalytic Degradation of Malachite Green Using Nano-sized cerium-iron Oxide

K. L. Ameta[a*], Neema Papnai[a] and Rakshit Ameta[b]

[a]*Department of Chemistry, Faculty of Arts, Science and Commerce, Mody Institute of Technology and Science, Lakshmangarh-332311, Rajasthan, India.*
[b]*Department of Chemistry, Pacific College of Basic & Applied Sciences, PAHER University, Udaipur 313024, Rajasthan, India.*

Article history: Received: 06 December 2013; revised: 13 January 2014; accepted: 26 January 2014. Available online: 02 April 2014.

Abstract: Nano-sized cerium-iron oxide nanoparticles has been synthesized, characterized and explored as an efficient photocatalyst for the photocatalytic degradation of malachite green. The effects of different variables on degradation of dye were optimized such as the pH of the dye solution, dye concentration, amount of photocatalyst and light intensity. About 91% degradation of dye of 2×10^{-5} M concentration was observed after 2 hours at 8.5 pH and 600 Wm^{-2} light intensity. The reason for the high catalytic activity of the synthesized nanoparticles is ascribed to the high surface area which determines the active sites of the catalyst and accelerates the photocatalytic degradation.

Keywords: cerium-iron oxide; nanoparticles; photocatalyst; photodegradation; malachite green

1. INTRODUCTION

Photocatalysis has emerged as a probable solution to some of the worldwide problems like energy crisis, environmental pollution, waste water treatment, etc. Extensive researches in the field of photocatalysis have revealed various fascinating applications of photocatalytic reactions and semiconductor photocatalysts [1, 2]. In this process a photoactive material is required to initiate the catalytic reaction. Semiconductor particulate system provides low cost and convenient way of treating several undesirable chemicals [3, 4].

A lot of work has been done on various photocatalytic materials such as TiO_2, ZnS, ZnO, WO_3, V_2O_5, CdS, etc. [5-10] but very less attention is being given to the mixed oxide nanoparticles. The mixed oxide particle has the ability to obtain structures in combination with the properties that neither individual oxide possesses [11].

Ceria has recently been attracting much attention in the oxidative catalysis research due to its high oxygen storage capacity [12] and redox properties [13]. Cerium compounds has been used in applications like optical coating and fuel cells [14], various industrial heterogeneous catalysts and in automotive Three-Way Converters (TWC) [15] because of its high ultraviolet absorbance [16], high oxygen ion mobility [17] and its multiple valence states [18]. Wide spread use of cerium compounds in industrial applications is spurred by its large abundance on earth's crust more than that of copper [19, 20]. However, work that shows the potential use of ceria with other metal oxide in degradation of dyes is scarce in literature.

In this study, the removal of malachite green dye with cerium-iron oxide ($CeFeO_3$) was investigated. $CeFeO_3$ nanoparticles were synthesized and characterization of the synthesized oxide was carried out. The kinetics of the absorption process was evaluated to study the absorption mechanism of the dye molecules.

2. MATERIAL AND METHODS

Materials

*Corresponding author. E-mail: klameta77@hotmail.com

Chemicals and reagents

Cerium (III) nitrate hexahydrate, iron (III) nitrate nonahydrate, sodium hydroxide, sulphuric acid and doubly distilled water were used to conduct the experiments. These were purchased from Sigma-Aldrich Chemicals Pvt. Ltd. India, SD Fine, CDH and Merck, India. All the chemicals and reagents used were of analytical grade and used without further purification.

Dye

Malachite green ($C_{23}H_{25}N_2Cl$), dye which is used for dyeing cloth and leather and as a histological stain was procured from CDH, India. The molecular weight of malachite green is 364.90 g/mol and maximum wavelength is 620 nm. The chemical structure of the dye is shown in Fig. 1.

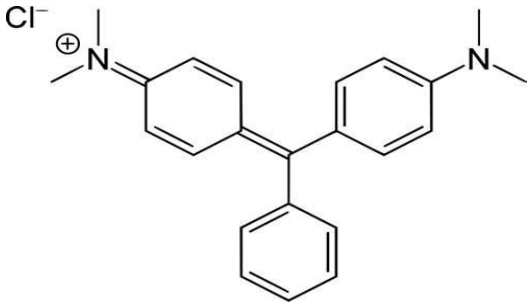

Figure 1. Chemical structure of Malachite green.

Methods

Synthesis of cerium-iron oxide ($CeFeO_3$) nanoparticles

The synthesis of mixed cerium iron oxide was achieved by co-precipitation method. The mixed oxide was prepared by adding aqueous solution of 1M NaOH drop-wise to the aqueous solution of 0.1M of both $Ce(NO_3)_3.6H_2O$ and $Fe(NO_3)_3.9H_2O$ with concurrent vigorous stirring. The pH of the mixed solution was adjusted at different pH in alkaline range but at 10 pH complete precipitation was observed so the pH was maintained at 10. After 4 hours of continuous stirring, the precipitate was filtered and repeatedly washed with deionized water. The residue was dried in an oven at 110ºC overnight and then grounded in acetone with mortar and pestle. The powder received was then calcined at 500ºC for 4 hours under static air in muffle furnace.

Characterization of the synthesized nanoparticles

X-ray powder diffraction study was performed to establish the phase purity and crystallinity of the prepared bimetal oxide by X-ray diffractometer. The nanoparticles size was determined by the Scherrer equation.

Photocatalytic degradation of dye

A stock solution of malachite green of 1.0×10^{-3} M concentration was prepared by dissolving 0.365 g of malachite green in 1000 mL of doubly distilled water. The absorption maximum of the dye was determined with the help of a spectrophotometer (Systronics Model 106). Photocatalytic degradation of malachite green was studied by taking 50 mL reaction mixture which contains 2.0×10^{-5} M of malachite green and 0.05 g of $CeFeO_3$. The reaction mixture was exposed to light. For irradiation purpose, 200 W tungsten lamp (Philips) was used. The intensity of light was measured by solar power meter (TENMARS Model TM 207). A water filter was used to cut off thermal radiation. The pH of the solution was measured by a digital pH meter (Systronics Model 324). The desired pH of the solution was adjusted by the addition of 0.1N sodium hydroxide and 0.1N hydrochloric acid solutions. To measure the degradation of dye, optical density was taken at regular time intervals.

3. RESULTS AND DISCUSSION

Characterization of the synthesized nanoparticles

The XRD pattern for $CeFeO_3$ is shown in Fig. 2. Graph has been plotted between intensity (cycles per second) and 2θ values (in degrees). The nanoparticles size was 23.28 nm as determined by Scherrer equation.

Photocatalytic degradation of dye

A 2.0 mL of the solution was taken out from the reaction mixture at regular time intervals and absorbance was measured spectrophotometrically at λ_{max} 620 nm. It was observed that the absorbance of the solution decreases with increasing time intervals showing thereby that the concentration of the dye decreases with increasing time of exposure. A plot of 2 + log O.D. versus time was linear and follows first

order kinetics. The rate constant was determined by using the expression, k = 2.303 × slope.

The typical run for dye degradation is given in Table 1 and graphically represented in Fig. 3.

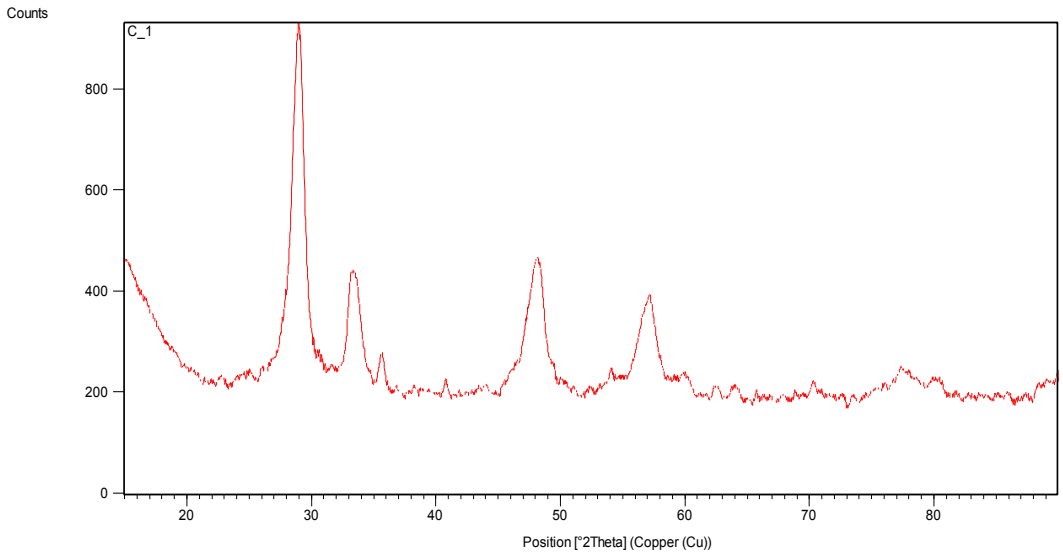

Figure 2. Powder X-ray Diffraction pattern of $CeFeO_3$.

Table 1. A typical run of malachite green dye using $CeFeO_3$. [(a)]

Time (min.)	Optical Density (O.D.)	2 + log O.D.
0	1.1479	2.0599
20	0.685	1.8357
40	0.413	1.616
60	0.277	1.4425
80	0.192	1.2833
100	0.123	1.0899
120	0.095	0.9777

$k = 3.45 \times 10^{-4}\ s^{-1}$

(a) Reaction Conditions: Dye concentration = 2.0×10^{-5} M, Light intensity = 600 Wm^{-2}, $CeFeO_3$ = 0.05 g in 50 mL dye solution, pH = 8.5.

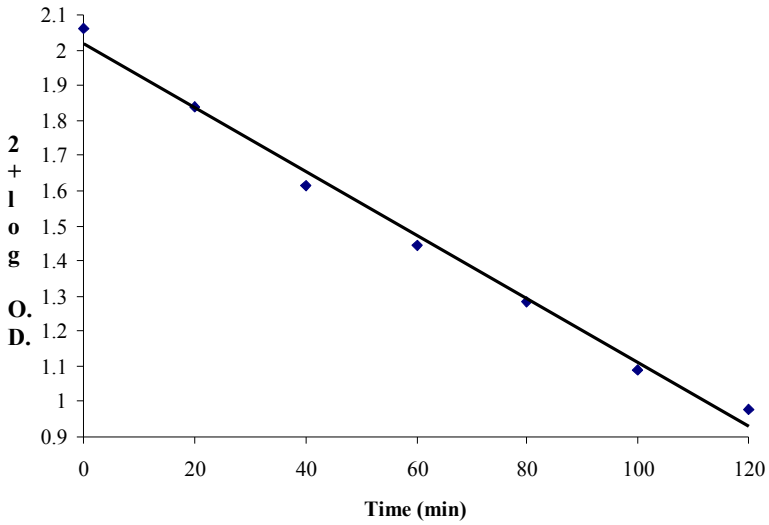

Figure 3. Plot of 2 + log O.D. verses time for a typical run.

Effect of different variables on photocatalytic degradation of dye

Effect of pH

The pH of the solution is likely to affect the degradation of dye and hence, the effect of pH on the rate of degradation of the dye was investigated in the pH range 6 to 10. The results are reported in Table 2. As observed, the rate of reaction increased with increasing pH of the solution up to pH 8.5. However, a further increase in pH of solution resulted in decreased reaction rate. An increase in the rate of photocatalytic degradation of malachite green with increase in pH may be due to generation of more •OH radicals, which are produced from the reaction between $^{-}$OH ions and hole (h^{+}) of the semiconductor. Above pH 8.5, a decrease in the rate of photocatalytic degradation of the dye was observed, which may be due to the fact that cationic form of malachite green converts in its neutral form, which faces no attraction towards the negatively charged semiconductor surface due to absorption of $^{-}$OH ions.

Table 2. Effect of pH on degradation of malachite green. [(a)]

pH	k × 10^4 s^{-1}
6.0	0.26
6.5	0.42
7.0	0.71
7.5	1.61
8.0	2.76
8.5	**3.45**
9.0	2.52
9.5	2.17
10.0	1.76

[(a)] Reaction Conditions: Dye Concentration = 2.0×10^{-5} M, Light intensity = 600 Wm^{-2}, $CeFeO_3$ = 0.05 g in 50 mL dye solution.

Effect of dye concentration

The effect of dye concentration on the rate of the reaction of photocatalytic degradation was studied by taking different concentrations of dye. The results are reported in Table 3. It has been observed that the rate of photocatalytic degradation increases with an increase in the concentration of the dye up to 2.0×10^{-5} M. Further increasing in the concentration of dye, the rate of photocatalytic bleaching decreases. It may be due to the fact that as the concentration of dye was increased, more dye molecules were available for excitation and energy transfer and, hence an increase in the rate was observed but on further increase of dye concentration, dye starts acting as a filter for the incident light and will not permit the light intensity to reach the semiconductor surface and as a result rate decreases.

Table 3. Effect of dye concentration on degradation of malachite green. [(a)]

[Malachite green] × 10^5 M	k × 10^4 s^{-1}
1.5	3.19
2.0	**3.45**
2.5	2.78
3.0	2.25
3.5	1.84
4.0	1.62
4.5	1.33

[(a)] Reaction Conditions: $CeFeO_3$ = 0.05 g in 50 mL dye solution, pH = 8.5, Light intensity = 600 Wm^{-2}.

Effect of amount of $CeFeO_3$

The amount of $CeFeO_3$ is also likely to affect the rate of photocatalytic degradation of dyes and therefore, different amounts of $CeFeO_3$ were used. The results are reported in Table 4. These results showed that an increase in catalyst amount from 0.01 g to 0.05 g increased the photodegradation efficiency, as the exposed surface area of the semiconductor also increases and after that the further increase in catalyst above 0.05 g has negligible effect on the photodegradation efficiency.

Table 4. Effect of amount of $CeFeO_3$ on degradation of malachite green. [(a)]

$CeFeO_3$ (g/ 50 mL dye solution)	k × 10^4 s^{-1}
0.01	1.59
0.02	2.09
0.03	2.37
0.04	2.99
0.05	**3.45**
0.06	3.13
0.07	3.02

[(a)] Reaction Conditions: Dye Concentration = 2.0×10^{-5} M, Light intensity = 600 Wm^{-2}, pH = 8.5.

Effect of light intensity

The effect of light intensity on the rate of the reaction was also observed and the observations are summarized in Table 5. It has been observed that on increasing the intensity of light up to 600Wm^{-2}, the rate of reaction also increases because on increasing the intensity, the number of photons striking per unit

area of reaction mixture will also increase. This will result in a corresponding increase in the rate of degradation of malachite green. Small decrease in the rate on further increasing light intensity may be due to some thermal or side reactions.

Table 5. Effect of light intensity on degradation of malachite green.

Light intensity (Wm^{-2})	$k \times 10^4\ s^{-1}$
200	1.89
300	1.99
400	2.07
500	2.58
600	**3.45**
700	3.01
800	2.78

[(a)] Reaction Conditions: Dye Concentration = 2.0×10^{-5} M, $CeFeO_3$ = 0.05 g in 50 mL dye solution, pH = 8.5.

Mechanism

On the basis of these observations, a tentative mechanism for photocatalytic degradation of malachite green may be proposed as –

$$^1MG_0 \xrightarrow{h\nu} {}^1MG_1 \quad \text{.... (1)}$$

$$^1MG_1 \xrightarrow{ISC} {}^3MG_1 \quad \text{.... (2)}$$

$$SC \xrightarrow{h\nu} e^-(CB) + h^+(VB) \quad \text{.... (3)}$$

$$e^- + O_2 \longrightarrow O_2^{\bullet-} \quad \text{.... (4)}$$

$$O_2^{\bullet-} + {}^3MG_1 \longrightarrow \text{Leuco MG} \quad \text{.... (5)}$$

$$Leuco\ MG \longrightarrow \text{Products} \quad \text{.... (6)}$$

Malachite green (MG) absorbs radiations of suitable wavelength and gives rise to its first excited singlet state. Then it undergoes intersystem crossing (ISC) to give the triplet state of the dye. On the other hand, the semiconducting $CeFeO_3$ (SC) also utilizes the radiant energy to excite its electron from valence band to the conduction band. This electron will be abstracted by oxygen molecule (dissolved oxygen) generating superoxide anion radical ($O_2^{\bullet-}$). This anion radical will reduce the dye malachite green to its leuco form, which may ultimately degrade to products. It was also confirmed that this degradation proceeds through reduction and not oxidation as the rate of degradation was not affected appreciably in presence of hydroxyl radical scavenger (2-propanol).

4. CONCLUSION

The synthesized bimetal oxide presented a pure phase and the crystal size in nanometric scale. Results indicate that cerium-iron oxide can be employed for the degradation of malachite green dye. The absorption kinetics of the dye followed the pseudo-first order model. The absorption process was found to be controlled by both the external surface and the interparticle diffusion with surface diffusion at the earlier stage followed by interparticle diffusion at the later stage. Experimental results showed that various variables such as the pH of the reaction mixture, concentration of dye, light intensity and amount of semiconductor had their effect on dye degradation.

5. ACKNOWLEDMENTS

The authors are thankful to the Department of Science & Technology (DST, Rajasthan Government, India) for sanctioning the student project for Ph.D. and SAIF Chandigarh, India for the instrumental facility.

6. REFERENCE AND NOTES

[1] Yogo, K.; Ishikawa, M. *Catal. Surv. JPN* **2000**, *4,* 83. [CrossRef]

[2] Pradhan, G. K.; Parida, K. M. *Int. J. Eng. Sci. Tech.* **2010**, *2,* 53.

[3] Ibhadon, A.O.; Fitzpatrick, P. *Catalysts* **2013**, *3*, 189. [CrossRef]

[4] Beydoun, D.; Amal, R.; Low, G.; McEvoy, S. *J. Nanopartic. Res.* **1999**, *1*, 439. [CrossRef]

[5] Epling, G. A.; Lin, C. *Chemosphere* **2002**, *46,* 561. [CrossRef]

[6] Wang, C.; Ao, Y.; Wang, P.; Zhang, S.; Qian, J.; Hou, J. *Appl. Surf. Sci.* **2010**, *256,* 4125. [CrossRef]

[7] Tan, T.K.; Khiew, P.S.; Chiu, W.S.; Radiman, S.; Abd-Shukor, R.; Huang, N.M.; Lim, H.N. *World Acad. Sci. Eng. Tech.* **2011**, *55*, 791.

[8] Neppolian, B.; Choi, H.C.; Sakthivel, S.; Arabindoo, B.; Murugesan, V. *J. Hazard. Mater.* **2002**, *B89*, 303. [CrossRef]

[9] Li, B.; Xu, Y.; Rong, G.; Jing, M.; Xie, Y. *Nanotechnology* **2006**, *17,* 2560. [CrossRef]

[10] Ma, L. L.; Sun, H. Z.; Zhang, Y. G.; Lin, Y. L.; Li, J. L; Wang, E.; Yu, Y.; Tan, M.; Wang, J. B. *Nanotechnology* **2008**, *19*, 115709. [CrossRef]

[11] Fang, J.; Xu, L.; Zhang, Z.; Yuan, Y.; Cao, S.; Wang, Z.; Yin,L.; Liao, Y.; Xue,C. *Appl. Mater. Interfaces* **2013**, *5,* 8088. [CrossRef]

[12] Campbell, C. T.; Peden, C. H. F. *Science* **2005**, *309*, 713. [CrossRef]

[13] Dong, F.; Suda, A.; Tanabe, T.; Sobukawa, H. Y. N.; Shinjoh, H.; Sugiura, M.; Descorme, C.; Duprez, D. *Catal. Today* **2004a**, *90,* 223. [CrossRef]

[14] Murray, E. P.; Tsai T.; Barnett, S. A. *Nature* **1999**, *400*, 649. [CrossRef]

[15] Mai, H.; Mengfei, L.; Ping, F. *J. Rare Earth.* **2006**, *24*, 188. [CrossRef]

[16] Maestro, P.; Huguenin, D. *J. Alloys Compd.* **1995**, *225*, 520. [CrossRef]

[17] Nolan, M.; Fearon, J. E.; Watson, G. W. *Solid State Ionics* **2006**, *177*, 3069. [CrossRef]

[18] Deshpande, S.; Patil, S.; Kuchibhatla, S.V.; Seal, S. *Appl. Phys. Lett.* **2005**, 87. [CrossRef]

[19] Hickey, N.; Arneodo Larochette, P.; Gentilini, C.; Sordelli, L.; Olivi, L.; Polizzi, S.; Montini, T.; Fornasiero, P.; Pasquato, L.; Graziani, M. *Chem. Mater.* **2007**, *19*, 650. [CrossRef]

[20] Lide, D. R. *CRC Handbook of Chemistry and Physics: CRC, 88th edn*, 2007.

Orbital: The Electronic Journal of Chemistry
journal homepage: www.orbital.ufms.br
ISSN 1984-6428

| Vol 6 | | No. 1 | | January-March 2014 |

Full Paper

Synthesis and Antimicrobial Study of Some Methyl 4-*O*-palmitoyl-α-L-rhamnopyranoside Derivatives

Mohammed M. Matin*

Organic Research Laboratory, Department of Chemistry, University of Chittagong, Chittagong-4331, Bangladesh.

Article history: Received: 31 December 2013; revised: 09 March 2014; accepted: 11 March 2014. Available online: 02 April 2014.

Abstract: 4-*O*-Palmitoylation of methyl *α*-L-rhamnopyranoside (**2**) was carried out via blocking-deblocking technique. Methyl *α*-L-rhamnopyranoside (**2**) was first converted into 2,3-*O*-isopropylidene derivative (**5**) which on palmitoylation followed by deacetonation gave the desired 4-*O*-palmitoylrhamnopyranoside (**7**) in good yield. A number of 2,3-di-*O*-acyl derivatives of **7** were also prepared to get newer rhamnopyranosides (**8**-**14**) of biological importance. All the rhamnopyranosides (**2**, **5**-**14**) were employed as test chemicals for *in vitro* antibacterial and antifungal functionality test against ten human pathogenic bacteria and four fungi, respectively. The study revealed that some of the tested rhamnopyranoside derivatives showed excellent antimicrobial functionalities as compared to the standard antibiotic.

Keywords: methyl α-L-rhamnopyranoside; palmitoylation; antimicrobial activities; structure activity relationship

1. INTRODUCTION

L-Rhamnose is an important member of the monosaccharide series [1]. Rhamnolipids comprise one of the most important classes of biosurfactants and exhibit diverse biological functions [2]. For the above reasons, the total synthesis of rhamnolipids has attracted considerable attention [3]. Several oligosaccharides have been isolated from plants which contain L-rhamnose with aglycon moiety at C-4 position [4] e.g. Kaempferol 3,7-di-*O*-α-L-rhamnopyranoside (**1**) was isolated from *Consolida armeniaca*. Recently, Gohar *et al*. [5] isolated new 3-*O*-acyl-α-L-rhamnopyranoside flavonol glycoside named ceratoside for the first time from *Ceratonia siliqua L.* seeds. Ceratoside showed significant antioxidant activity comparable to that of most common antioxidant ascorbic acid and could be used as a potential source for natural antioxidants. In the last few decades, syntheses of several oligosaccharides containing rhamnose have been accomplished from natural products by hydrolysis [6]. Tsai *et al*. [7] reported the synthesis and crystallographic structure of phenyl 2,3,4-tri-*O*-acetyl-1-thio-α-L-rhamnopyranoside which acts as a glycosyl donor.

Acylation of monosaccharide derivatives is of growing importance in the field of synthetic carbohydrate chemistry because of its usefulness for providing newer derivatives of biological importance [8]. For example, the human pathogens *M. tuberculosis* and *M. avium* produce sulfated glycolipids and recently it was shown that the core region of glycopeptidolipids could be selectively sulfated at position C-2 of 3,4-di-*O*-methyl-L-rhamnose [9]. Due to the role of rhamnose as mediator of cell-cell and host-pathogen interactions, Liptak *et al*. [10] have reported the synthesis of 4-*O*-sulfonic acid (**3**) of rhamnopyranoside **2**.

Our previous projects on selective acylation and antimicrobial evaluation of rhamnopyranosides revealed that selective decanoylation of methyl α-L-rhamnopyranoside (**2**) using dibutyltin oxide method gave methyl 3-*O*-decanoyl-α-L-rhamnopyranoside (**4**) which exhibited higher antimicrobial activity than that of the standard antibiotic [11]. We have been interested to extend studies by the introduction of acyl group (i.e. palmitoyl group as aglycon moiety) at position C-4 instead of position C-3 of methyl α-L-

*Corresponding author. E-mail: mahbubchem@cu.ac.bd

rhamnopyranoside (**2**). This may provide important information about positional effects of the acyl group in its role as antimicrobial functionality.

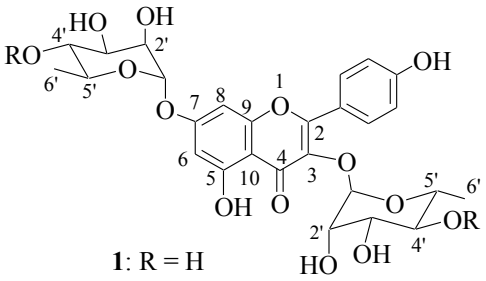

1: R = H

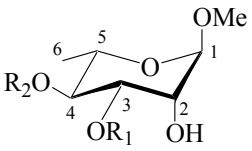

2: $R_1 = R_2 = H$
3: $R_1 = H$; $R_2 = SO_3Na$
4: $R_1 = CH_3(CH_2)_8CO$; $R_2 = H$

2. MATERIAL AND METHODS

General experimental procedure

Melting points (mp) were determined on an electrothermal melting point apparatus and are uncorrected. Evaporations were performed under diminished pressure on a Büchi rotary evaporator. IR spectra were recorded on a FTIR spectrophotometer (Shimadzu, IR Prestige-21) using KBr and $CHCl_3$ technique. Thin layer chromatography (TLC) was performed on Kieselgel GF_{254} and visualization was accomplished by spraying the plates with 1% H_2SO_4 followed by heating the plates at 150-200 °C until coloration took place. Column chromatography was carried out with silica gel (100-200 mesh). ^1H (400 MHz) and ^{13}C (100 MHz) NMR spectra were recorded using $CDCl_3$ as a solvent. Chemical shifts were reported in δ unit (ppm) with reference to TMS as an internal standard and *J* values are given in Hz. The assignments of the signals were confirmed by decoupling and DEPT experiments. All reagents used were commercially available (Aldrich) and were used as received unless otherwise specified.

Synthesis

Methyl α-L-rhamnopyranoside (2): The title compound (**2**) was prepared from L-rhamnose (Merck) and anhydrous methanol with Amberlite IR 120 (H^+) ion exchange resin in 82% yield as a crystalline solid, mp 109-110 °C (Lit. mp 108-109 °C) [12].

Methyl 2,3-O-isopropylidene-α-L-rhamnopyranoside (5): To a solution of methyl α-L-rhamnopyranoside (**2**) (2.0 g, 11.235 mmol) in 2,2-Dimethoxypropane (DMP, 30 mL) was added *p*-toluenesulfonic acid (*p*-TSA, catalytic) at room temperature with stirring. Stirring was continued for 2 h when excess DMP was removed under reduced pressure, water (5 mL) was added to the reaction mixture, extracted with dichloromethane (3×15 mL) and concentrated successively. The residue thus obtained on chromatography with *n*-hexane/ethyl acetate (9.3/0.7) afforded (**5**) (2.403 g, 98%) as a colorless thick liquid.

R_f = 0.51 (*n*-hexane/ethyl acetate = 9.3/0.7). IR ($CHCl_3$): 3420-3300 (br) (OH), 1370 cm^{-1} [$C(CH_3)_2$]. ^1H NMR (400 MHz, $CDCl_3$): δ 4.80 (1H, s, H-1), 4.07 (1H, d, *J* = 5.8 Hz, H-2), 4.01 (1H, dd [apparent t], *J* = 6.9 and 5.8 Hz, H-3), 3.50-3.60 (1H, m, H-5), 3.33 (3H, s, *O*-CH_3), 3.28-3.33 (1H, m, H-4), 3.09-3.14 (1H, br s, exchange with D_2O, O*H*), 1.47 (3H, s, CH_3), 1.30 (3H, s, CH_3), 1.24 (3H, d, *J* = 6.2 Hz, 6-CH_3). ^{13}C NMR (100 MHz, $CDCl_3$): δ 109.4 [*C*$(CH_3)_2$], 98.0 (C-1), 78.4 (C-4), 75.7 (C-3), 74.3 (C-2), 65.6 (C-5), 54.8 (*O*-*C*H_3), 27.9, 26.0 [C(*C*$H_3)_2$], 17.4 (C-6).

Methyl 2,3-O-isopropylidene-4-O-palmitoyl-α-L-rhamnopyranoside (6): Palmitoyl chloride (3.48 g, 15.945 mmol) was added to a stirred solution of the monoacetonide **5** (2.3 g, 10.54 mmol) in anhydrous pyridine (8 mL) at 0 °C followed by addition of 4-dimethylaminopyridine (DMAP, catalytic). The reaction mixture was stirred at room temperature for 12 h, treated with cold water (2 mL) and extracted with chloroform (3×10 mL). Usual work-up and chromatography (elution with *n*-hexane/ethyl acetate = 18/1) afforded the title compound **6** (4.62 g, 96%) as a pale-yellow needles, mp 40-41 °C.

R_f = 0.5 (*n*-hexane/ethyl acetate = 9.3/0.7). IR (KBr): 1730 (CO), 1372 cm^{-1} [$C(CH_3)_2$]. ^1H NMR (400 MHz, $CDCl_3$): δ 4.88 (1H, s, H-1), 4.85 (1H, dd, *J* = 10.0 and 7.0 Hz, H-4), 4.10-4.15 (2H, m, H-2 and H-3), 3.67-3.71 (1H, m, H-5), 3.37 (3H, s, *O*-CH_3), 2.28-2.37 [2H, m, $CH_3(CH_2)_{13}CH_2CO$], 1.58-1.63 [2H, m, $CH_3(CH_2)_{12}CH_2CH_2CO$], 1.55 (3H, s, C$H_3$), 1.33 (3H, s, C$H_3$), 1.19-1.29 [24H, m, $CH_3(CH_2)_{12}CH_2CH_2CO$],

1.15 (3H, d, J = 6.3 Hz, 6-CH_3), 0.89 [3H, t, J = 6.6 Hz, CH_3(CH$_2$)$_{14}$CO]. ^{13}C NMR (100 MHz, CDCl$_3$): δ 173.0 [CH$_3$(CH$_2$)$_{14}$*C*O], 109.8 [*C*(CH$_3$)$_2$], 98.1 (C-1), 76.0 (C-4), 75.6 (C-3), 74.2 (C-2), 64.0 (C-5), 54.0 (*O*-*C*H$_3$), 34.4, 32.0, 29.7, 29.6, 29.4, 29.3 (×5), 29.2, 29.1, 24.9, 22.7 [CH$_3$(*C*H$_2$)$_{14}$CO], 27.7, 26.4 [C(*C*H$_3$)$_2$], 17.0 (C-6), 14.1 [*C*H$_3$(CH$_2$)$_{14}$CO].

Methyl 4-O-palmitoyl-α-L-rhamnopyranoside (7): 4-*O*-Palmitoate **6** (4.5 g, 9.854 mmol) was gently dissolved in glacial acetic acid (25 mL) at room temperature. The solution was slowly warmed to 40 °C and stirred at this temperature for 18 h. After completion of the reaction, acetic acid was evaporated in *vacuum* and co-evaporated with toluene (3×3 mL) to remove traces of acetic acid. The residue thus obtained on chromatography with *n*-hexane/ethyl acetate (2/1) afforded **7** (3.57 g, 87%) as yellow solid, mp 53-54 °C.

R_f = 0.45 (*n*-hexane/ethyl acetate = 1/1). IR (KBr): 3480-3400 (br) (OH), 1735 cm^{-1} (CO). ^{1}H NMR (400 MHz, CDCl$_3$): δ 4.80 (1H, t, J = 9.6 Hz, H-4), 4.68 (1H, s, H-1), 3.90 (1H, d, J = 3.3 Hz, H-2), 3.81 (1H, dd, J = 9.6 and 3.3 Hz, H-3), 3.70-3.78 (1H, m, H-5), 3.35 (3H, s, *O*-CH_3), 2.93-3.22 (2H, br s, exchange with D$_2$O, 2×O*H*), 2.33 [2H, t, J = 7.3 Hz, CH$_3$(CH$_2$)$_{13}$CH_2CO], 1.50-1.63 [2H, m, CH$_3$(CH$_2$)$_{12}$CH_2CH$_2$CO], 1.20-1.33 [24H, m, CH$_3$(CH_2)$_{12}$CH$_2$CH$_2$CO], 1.18 (3H, d, J = 6.3 Hz, 6-CH_3), 0.86 [3H, t, J = 6.5 Hz, CH_3(CH$_2$)$_{14}$CO]. ^{13}C NMR (100 MHz, CDCl$_3$): δ 174.9 [CH$_3$(CH$_2$)$_{14}$*C*O], 100.5 (C-1), 75.1 (C-4), 70.9, 70.2 (C-2/C-3), 65.5 (C-5), 55.0 (*O*-*C*H$_3$), 34.5, 31.9, 29.7 (×4), 29.6, 29.5, 29.4, 29.3, 29.2, 29.1, 24.9, 22.6 [CH$_3$(*C*H$_2$)$_{14}$CO], 17.4 (C-6), 14.1 [*C*H$_3$(CH$_2$)$_{14}$CO].

General procedure for 2,3-di-O-acylation of palmitoate 7: To a solution of the 2,3-dihydroxy compound **7** (0.4 g) in anhydrous pyridine (1 mL) was added 2.2 molar equivalent acyl halide at 0 °C followed by addition of catalytic amount of DMAP. The reaction mixture was allowed to attain room temperature and stirring was continued for 10-16 h. A few pieces of ice was added to the reaction mixture to decompose unreacted (excess) acylating agent and extracted with dichloromethane (DCM) (3×5 mL). The DCM layer was washed successively with 5% hydrochloric acid, saturated aqueous sodium hydrogen carbonate solution and brine. The DCM layer was dried and concentrated under reduced pressure. The residue thus obtained on column chromatography (*n*-hexane/ethyl acetate) gave the corresponding 2,3-di-*O*-acyl-4-*O*-palmitoate.

Methyl 2,3-di-O-acetyl-4-O-palmitoyl-α-L-rhamnopyranoside (8): Obtained as a semi-solid, 98%.

R_f = 0.51 (*n*-hexane/ethyl acetate = 8.5/1.5). ^{1}H NMR (400 MHz, CDCl$_3$): δ 5.26 (1H, dd, J = 10.1 and 3.3 Hz, H-3), 5.21 (1H, d, J = 3.3 Hz, H-2), 5.06 (1H, t, J = 9.9 Hz, H-4), 4.60 (1H, s, H-1), 3.78-3.87 (1H, m, H-5), 3.36 (3H, s, *O*-CH_3), 2.25 [2H, t, J = 7.4 Hz, CH$_3$(CH$_2$)$_{13}$CH_2CO], 2.12 (3H, s, COCH_3), 1.95 (3H, s, COCH_3), 1.51-1.60 [2H, m, CH$_3$(CH$_2$)$_{12}$CH_2CH$_2$CO], 1.20-1.29 [24H, br s, CH$_3$(CH_2)$_{12}$CH$_2$CH$_2$CO], 1.20 (3H, d, J = 6.5 Hz, 6-CH_3), 0.86 [3H, t, J = 6.6 Hz, CH_3(CH$_2$)$_{14}$CO]. ^{13}C NMR (100 MHz, CDCl$_3$): δ 172.8 [CH$_3$(CH$_2$)$_{14}$*C*O], 170.1, 169.9 (CH$_3$*C*O), 98.5 (C-1), 70.7, 69.8, 69.1 (C-2/C-3/C-4), 66.2 (C-5), 55.1 (*O*-*C*H$_3$), 34.3, 31.9, 29.7 (×5), 29.4, 29.3 (×2), 29.2, 29.1, 25.0, 22.7 [CH$_3$(*C*H$_2$)$_{14}$CO], 20.9, 20.6 (*C*H$_3$CO), 17.4 (C-6), 14.0 [*C*H$_3$(CH$_2$)$_{14}$CO].

Methyl 2,3-di-O-methanesulfonyl-4-O-palmitoyl-α-L-rhamnopyranoside (9): Appeared as needles, mp 57-58 °C, 92%.

R_f = 0.50 (*n*-hexane/ethyl acetate = 8.8/1.2). ^{1}H NMR (400 MHz, CDCl$_3$): δ 5.06 (1H, t, J = 9.8 Hz, H-4), 5.03 (1H, dd, J = 9.8 and 2.6 Hz, H-3), 4.98 (1H, d, J = 2.6 Hz, H-2), 4.83 (1H, s, H-1), 3.78-3.88 (1H, m, H-5), 3.39 (3H, s, *O*-CH_3), 3.15 (3H, s, SO$_2$CH_3), 3.04 (3H, s, SO$_2$CH_3), 2.33 [2H, t, J = 7.4 Hz, CH$_3$(CH$_2$)$_{13}$CH_2CO], 1.56-1.66 [2H, m, CH$_3$(CH$_2$)$_{12}$CH_2CH$_2$CO], 1.15-1.39 [27H, br s, CH$_3$(CH_2)$_{12}$CH$_2$CH$_2$CO and 6-CH_3], 0.85 [3H, t, J = 6.7 Hz, CH_3(CH$_2$)$_{14}$CO]. ^{13}C NMR (100 MHz, CDCl$_3$): δ 172.5 [CH$_3$(CH$_2$)$_{14}$*C*O], 98.5 (C-1), 78.0, 74.5, 69.6 (C-2/C-3/C-4), 66.5 (C-5), 55.4 (*O*-*C*H$_3$), 38.7 (SO$_2$*C*H$_3$), 38.6 (SO$_2$*C*H$_3$), 34.1, 31.9, 30.2, 29.7 (×4), 29.6, 29.4, 29.3, 29.2, 29.1, 24.7, 22.7 [CH$_3$(*C*H$_2$)$_{14}$CO], 17.3 (C-6), 14.1 [*C*H$_3$(CH$_2$)$_{14}$CO].

Methyl 2,3-di-O-pivaloyl-4-O-palmitoyl-α-L-rhamnopyranoside (10): Isolated as a thick syrup, 88%.

R_f = 0.51 (*n*-hexane/ethyl acetate = (9.2/0.8). ^{1}H NMR (400 MHz, CDCl$_3$): δ 5.27 (1H, dd, J = 10.1 and 3.0 Hz, H-3), 5.17 (1H, d, J = 3.0 Hz, H-2), 5.11 (1H, t, J = 9.9 Hz, H-4), 4.56 (1H, s, H-1), 3.82-3.88 (1H, m, H-5), 3.36 (3H, s, *O*-CH_3), 2.18-2.27 [2H, m, CH$_3$(CH$_2$)$_{12}$CH$_2$CH_2CO], 1.51-1.58 [2H, m, CH$_3$(CH$_2$)$_{12}$CH_2CH$_2$CO], 1.19-1.32 [33H, br s, CH$_3$(CH_2)$_{12}$CH$_2$CH$_2$CO and C(CH_3)$_3$], 1.19 (3H, d, J = 6.3 Hz, 6-CH_3), 1.08 [9H, s, C(CH_3)$_3$], 0.85 [3H, t, J = 6.6 Hz, CH_3(CH$_2$)$_{14}$CO]. ^{13}C NMR (100 MHz,

$CDCl_3$): δ 177.1 [2×*C*OC$(CH_3)_3$], 172.6 [$CH_3(CH_2)_{14}$*C*O], 98.5 (C-1), 70.9, 69.7, 69.2 (C-2/C-3/C-4), 66.4 (C-5), 55.0 (*O*-*C*H_3), 38.9, 38.7 [2×*C*$(CH_3)_3$], 27.1 (×3) [C(*C*$H_3)_3$], 27.0 (×3) [C(*C*$H_3)_3$], 34.2, 31.9, 29.6, 29.5, 29.4, 29.3, 29.2, 29.1, 27.1 (×2), 27.0 (×2), 24.8, 22.7 [CH_3(*C*$H_2)_{14}$CO], 17.5 (C-6), 14.0 [*C*$H_3(CH_2)_8$CO].

Methyl 2,3-di-O-octanoyl-4-O-palmitoyl-α-L-rhamnopyranoside (11): Colorless liquid, 90%.

R_f = 0. 52(*n*-hexane/ethyl acetate = 9/1). ^{1}H NMR (400 MHz, $CDCl_3$): δ 5.25 (1H, dd, *J* = 10.0 and 3.1 Hz, H-3), 5.21 (1H, d, *J* = 3.1 Hz, H-2), 5.07 (1H, t, *J* = 10.0 Hz, H-4), 4.58 (1H, s, H-1), 3.78-3.87 (1H, m, H-5), 3.37 (3H, s, *O*-C*H*$_3$), 2.18-2.35 [6H, br m, $CH_3(CH_2)_{13}CH_2CO$ and 2 $CH_3(CH_2)_5CH_2CO$], 1.43-1.61 [6H, br m, $CH_3(CH_2)_{12}CH_2CH_2CO$ and 2×$CH_3(CH_2)_4CH_2CH_2CO$], 1.20-1.32 [40H, br m, $CH_3(CH_2)_{12}CH_2CH_2CO$ and 2×$CH_3(CH_2)_4CH_2CH_2CO$], 1.18 (3H, d, *J* = 6.4 Hz, 6-C*H*$_3$), 0.81-0.88 [9H, m, C*H*$_3(CH_2)_{14}$CO and 2×C*H*$_3(CH_2)_6$CO].

Methyl 2,3-di-O-decanoyl-4-O-palmitoyl-α-L-rhamnopyranoside (12): Thick oil, 89%.

R_f = 0.50 (*n*-hexane/ethyl acetate = 9/1). ^{1}H NMR (400 MHz, $CDCl_3$): δ 5.27 (1H, dd, *J* = 10.0 and 3.3 Hz, H-3), 5.23 (1H, d, *J* = 3.3 Hz, H-2), 5.06 (1H, t, *J* = 10.0 Hz, H-4), 4.59 (1H, s, H-1), 3.79-3.86 (1H, m, H-5), 3.36 (3H, s, *O*-C*H*$_3$), 2.37 [2H, t, *J* = 7.3 Hz, $CH_3(CH_2)_{13}CH_2CO$], 2.21-2.30 [2H, m, $CH_3(CH_2)_7CH_2CO$], 2.12-2.18 [2H, m, $CH_3(CH_2)_7CH_2CO$], 1.45-1.66 [6H, br m, $CH_3(CH_2)_{12}CH_2CH_2CO$ and 2×$CH_3(CH_2)_6CH_2CH_2CO$], 1.21-1.31 [48H, br m, $CH_3(CH_2)_{12}CH_2CH_2CO$ and 2×$CH_3(CH_2)_6CH_2CH_2CO$], 1.20 (3H, d, *J* = 6.3 Hz, 6-C*H*$_3$), 0.86 [9H, t, *J* = 6.3 Hz, C*H*$_3(CH_2)_{14}$CO and 2×C*H*$_3(CH_2)_8$CO].

Methyl 2,3-di-O-(2-chlorobenzoyl)-4-O-palmitoyl-α-L-rhamnopyranoside (13): Thick oil, 83%.

R_f = 0.45 (*n*-hexane/ethyl acetate = 8.8/1.2). ^{1}H NMR (400 MHz, $CDCl_3$): δ 7.85 (1H, d, *J* = 8.0 Hz, Ar-*H*), 7.75 (1H, d, *J* = 8.0 Hz, Ar-*H*), 7.29-7.42 (5H, br m, Ar-*H*), 7.19-7.25 (1H, m, Ar-*H*), 5.69 (1H, dd, *J* = 10.0 and 3.2 Hz, H-3), 5.63 (1H, d, *J* = 3.2 Hz, H-2), 5.38 (1H, t, *J* = 9.9 Hz, H-4), 4.85 (1H, s, H-1), 3.93-4.02 (1H, m, H-5), 3.45 (3H, s, *O*-C*H*$_3$), 2.25 [2H, t, *J* = 7.4 Hz, $CH_3(CH_2)_{13}CH_2CO$], 1.40-1.52 [2H, m, $CH_3(CH_2)_{12}CH_2CH_2CO$], 1.27 (3H, d, *J* = 6.7 Hz, 6-C*H*$_3$), 1.11-1.22 [24H, m, $CH_3(CH_2)_{12}CH_2CH_2CO$], 0.86 [3H, t, *J* = 6.5 Hz, C*H*$_3(CH_2)_{14}$CO]. ^{13}C NMR (100 MHz, $CDCl_3$): δ 172.9 [$CH_3(CH_2)_{14}$*C*O], 164.6, 164.2 (2-Cl.C_6H_4*C*O), 134.0, 133.3, 132.9, 132.8, 131.7, 131.3, 131.1, 130.9, 129.1, 128.8, 126.6, 126.5 (Ar-*C*), 98.4 (C-1), 71.0, 70.9, 70.2 (C-2/C-3/C-4), 66.5 (C-5), 55.3 (*O*-*C*H_3), 34.2, 31.9, 29.7 (×5), 29.6, 29.4, 29.3, 29.2, 29.0, 24.8, 22.7 [CH_3(*C*$H_2)_{14}$CO], 17.5 (C-6), 14.1 [*C*$H_3(CH_2)_{14}$CO].

Methyl 2,3-di-O-(4-chlorobenzoyl)-4-O-palmitoyl-α-L-rhamnopyranoside (14): Oil, 85%.

R_f = 0.47 (*n*-hexane/ethyl acetate = 9/1). ^{1}H NMR (400 MHz, $CDCl_3$): δ 8.05 (2H, d, *J* = 8.0 Hz, Ar-*H*), 7.99 (2H, d, *J* = 8.0 Hz, Ar-*H*), 7.49 (2H, d, *J* = 7.8 Hz, Ar-*H*), 7.42 (2H, d, *J* = 7.8 Hz, Ar-*H*), 5.44 (1H, d, *J* = 2.9 Hz, H-2), 5.37 (1H, dd, *J* = 9.6 and 2.8 Hz, H-3), 5.18 (1H, t, *J* = 9.6 Hz, H-4), 4.75 (1H, s, H-1), 3.89-3.95 (1H, m, H-5), 3.44 (3H, s, *O*-C*H*$_3$), 2.24-2.30 [2H, m, $CH_3(CH_2)_{13}CH_2CO$], 1.55-1.62 [2H, m, $CH_3(CH_2)_{12}CH_2CH_2CO$], 1.21-1.33 [24H, br s, $CH_3(CH_2)_{12}CH_2CH_2CO$], 1.20 [3H, d, *J* = 6.4 Hz, 6-C*H*$_3$], 0.86 [3H, t, *J* = 6.3 Hz, C*H*$_3(CH_2)_{14}$CO].

Antimicrobial evaluation

Evaluation of chemicals against bacteria: Four Gram-positive bacteria viz *Bacillus cereus* BTCC 19, *Bacillus megaterium* BTCC 18, *Bacillus subtilis* BTCC 17 and *Staphylococcus aureus* ATCC 6538 and six Gram-negative bacteria viz. *Escherichia coli* ATCC 25922, *INABAET* (*vibrio*) AE 14748, *Pseudomonas species*, *Salmonella paratyphi* AE 14613, *Salmonella typhi* AE 14612 and *Shigella dysenteriae* AE 14369 were used to study *in vitro* antibacterial activities of the synthesized rhamnopyranoside derivatives (2, 5-14). For the detection of antibacterial activities, the disc diffusion method [13] was followed. Chloroform ($CHCl_3$) was used as a solvent for test chemicals and a 2% solution of the compound was used in the investigation. Proper control was maintained with chloroform without chemicals. Mueller-Hinton (agar and broth) medium was used for culture of bacteria. All the results were compared with the standard antibacterial antibiotic ampicillin (50 µg/disc, Beximco Pharmaceuticals Ltd., Bangladesh).

Evaluation of chemicals against fungi: The antifungal activities of the synthesized palmitoylated derivatives (2, 5-14) were investigated against four plant pathogenic fungi viz. *Alternaria alternata* (Fr)

Kedissler, Curvularia lunata (Wakker Boedijin), *Fusarium equiseti* (Corda) *Sacc. and Macrophomina phaseolina* (Maubl) Ashby. The investigation was based on food poisoning technique [14]. Sabouraud (agar and broth) medium was used for culture of fungi. The results were compared with standard antifungal antibiotic nystatin (100 µg/mL medium, Beximco Pharmaceuticals Ltd., Bangladesh).

3. RESULTS AND DISCUSSION

Synthesis of 4-*O*-palmitoylrhamnopyranoside 7

The present study mainly describes the selective 4-*O*-palmitoylation of methyl α-L-rhamnopyranoside (2). Dibutyltin oxide method in this regard was found to be unsuccessful and furnished the 3-*O*-acyl derivatives only [11]. Thus, blocking-deblocking technique was employed successfully for the 4-*O*-palmitoylation of rhamnopyranoside 2. Initially, methyl α-L-rhamnopyranoside (2) was prepared from L-(+)-rhamnose according to the literature procedure [12] (Scheme 1). Reaction of 2 with excess DMP in the presence of *p*-TSA (cat.) afforded a product in 98% yield as a colourless thick liquid. In its IR spectrum, stretching bands at 3420-3300 (br) and 1370 cm^{-1} were due to hydroxyl and isopropylidene groups, respectively. In the ^1H NMR spectrum, two three-proton singlets at δ 1.47 and 1.30 and in the ^{13}C NMR spectrum, three carbon signals at δ 109.4 (CMe_2), 27.9 and 26.0 (CMe_2) were indicative of the presence of one acetonide group in the molecule. The acetonide protection was formed between *cis*-vicinal 2,3-diol positions of 2 and the similar formation was observed by Liptak et al. [10].

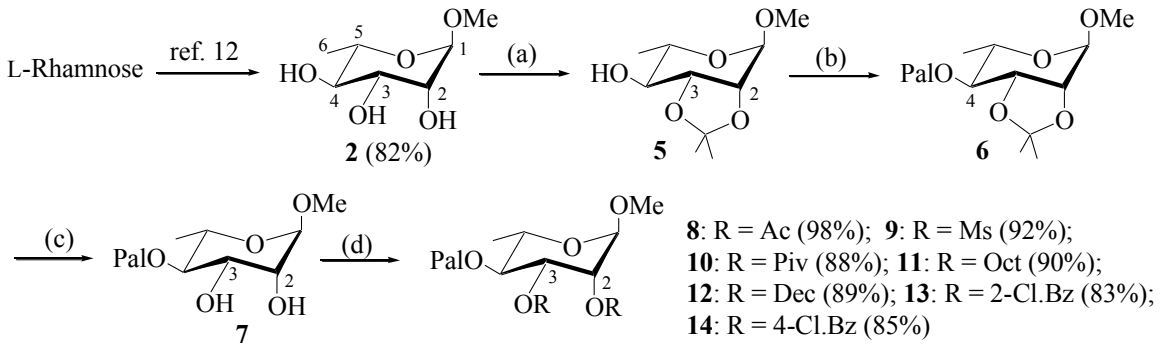

Scheme 1. *Reagents and conditions*: (a) DMP, *p*-TSA, rt, 2 h, 98%; (b) PalCl, pyridine, DMAP, 0 ºC-rt, 12 h, 96%; (c) AcOH, 40 ºC, 18 h, 87%; (d) RCOCl, pyridine, DMAP, 0 ºC-rt, 12 h.

The monoacetonide **5**, having free hydroxyl group at C-4 position, on palmitoylation with palmitoyl chloride in pyridine afforded a compound as needles (Scheme 1). IR spectrum of the compound showed the presence of a carbonyl-stretching band at 1730 cm^{-1} and absence of hydroxyl stretching band. In the ^1H NMR spectrum, two two-proton multiplets at δ 2.28-2.37 and 1.58-1.63, a twenty four-proton multiplet at δ 1.19-1.29 and a three-proton triplet at δ 0.89 were indicative of the presence of one palmitoyloxy group in the molecule. In addition, the downfield shift of H-4 (~ δ 4.85) as compared to the precursor compound **5** (δ 3.28-3.33 ppm) confirmed the attachment of the palmitoyloxy group at position C-4. The rest of the ^1H and ^{13}C NMR spectra were in complete accord with the structure assigned as methyl 2,3-*O*-isopropylidene-4-*O*-palmitoyl-α-L rhamnopyranoside (**6**).

In the subsequent step, removal of the isopropylidene functionality was conducted by stirring 4-*O*-palmitoate **6** with glacial acetic acid at 40 °C for 18 h to give a yellow solid. In its IR spectrum, the presence of a new broad band at 3480-3400 cm^{-1} corresponding to hydroxyl region was indicative for the removal of isopropylidene moiety in the molecule. This fact was also confirmed by observing the absence of methyl protons and carbons corresponding to isopropylidene group in its both ^1H and ^{13}C NMR spectra. In the ^1H NMR spectrum, a broad two-proton singlet (exchanged with D_2O) at δ 2.93-3.22 was due to the presence of two hydroxyl groups. Thus, the structure of the compound was assigned as methyl 4-*O*-palmitoyl-α- L-rhamnopyranoside (**7**).

Synthesis of 2,3-di-*O*-acyl derivatives of palmitoate 7

To confirm the structure of palmitoate **7** as well as to get newer derivatives of biological importance seven 2,3-di-*O*-acyl derivatives (**8-14**) containing various groups (e.g. acetyl, methanesulfonyl, pivaloyl, octanoyl, decanoyl, 2-chlorobenzoyl and 4-chlorobenzoyl, as shown in Scheme 1, were prepared. Thus, treatment of diol **7** with acetic anhydride in pyridine provided a compound in 98% yield. In its ^{1}H NMR spectrum, two three-proton singlets at δ 2.12 and 1.95 corresponding to two methyl groups and in the ^{13}C NMR spectrum two carbonyl signals at 170.1 and 169.9 clearly indicated the attachment of two acetyloxy groups in the molecule. Thus, the structure was assigned as methyl 2,3-di-*O*-acetyl-4-*O*-palmitoyl-α-L-rhamnopyranoside (**8**).

In the next step, mesylation of **7** with methanesulfonyl chloride in pyridine gave needles in 92% yield. In its ^{1}H NMR spectrum, two three-proton singlets at δ 3.15 and 3.04 clearly indicated the attachment of two mesyloxy groups in the molecule. The reasonable down field shift of H-2 (δ 4.98) and H-3 (δ 5.03) protons as compared to that of compound **7** confirmed the attachment of two mesyloxy groups at position C-2 and C-3. The rest of the ^{1}H NMR spectrum and ^{13}C NMR spectrum were in complete agreement with the structure accorded as methyl 2,3-di-*O*-methanesulfonyl-4-*O*-palmitoyl-α-L-rhamnopyranoside (**9**).

Similarly, 4-*O*-palmitoate **7** was converted to 2,3-di-*O*-pivaloate (**10**), 2,3-di-*O*-octanoate (**11**), 2,3-di-O-decanoate (**12**), 2,3-di-O-(2-chlorobenzoate) (**13**) and 2,3-di-*O*-(4-chlorobenzoate) (**14**) in reasonably high yields (Scheme 1). These compounds (**10-14**) were characterized by spectroscopic analysis and comparing the structure with that of diacetate **8**.

Conformational study of the L-rhamnopyranosides (2, 5-14)

Methyl α-L-rhamnopyranoside (**2**) is well known to exist in $^{1}C_{4}$ conformation [15]. However, in case of compounds **5-14**, the presence of acyl group(s) and/or isopropylidene functionality at 2,3 position increases the bulk in the molecule. Therefore, it was thought to derive the conformations of **5-14** using ^{1}H NMR spectral data. The coupling constants determined from the 400 MHz ^{1}H NMR spectra in $CDCl_3$ of **5-14** are shown in Table 1.

Table 1. Coupling constants of compounds **5-14.**

Compound no.	coupling constants (Hz)		
	$J_{2,3}$	$J_{3,4}$	$J_{4,5}$
5	5.8	6.9	--
6	--	10.0	7.0
7	3.3	9.6	9.6
8	3.3	10.1	9.9
9	2.6	9.8	9.8
10	3.0	10.1	9.9
11	3.1	10.0	10.0
12	3.3	10.0	10.0
13	3.2	10.0	9.9
14	2.9	9.6	9.6

In case of **7**, appearance of a distinct triplet for H-4 at δ 4.80 ($J_{4,3}$ = $J_{4,5}$ = 9.6 Hz) and a doublet of doublet for H-3 at δ 3.81 ($J_{3,4}$ = 9.6 and $J_{3,2}$ = 3.3 Hz) were informative. The large coupling constants ($J_{4,3}$ = $J_{4,5}$ = 9.6 Hz) for the H-4 axial proton requires *trans*-diaxial relationship with H-3 and H-5 protons. This clearly requires H-3 and H-5 protons to be axial. Again, the small coupling constant between H-3 and H-2 protons requires *cis* axial-equatorial relationship. As H-3 is axially oriented, H-2 must be present in equatorial position. These observation confirmed that 4-*O*-palmitoate **7** exist in $^{1}C_{4}$ conformation with C-5 substituent (–CH_3) equatorially oriented [(*5S*) configuration].

In one step earlier compound **6**, the relative stereochemistry of the substituents at C-2, C-3 is *cis* and C-3, C-4 is *trans* and the same stereochemistry is retained in the product **7** formation. But rhamnopyranoside **6** showed a doublet of doublet for H-4 at δ 4.85 ($J_{4,3}$ = 10.0 and $J_{4,5}$ = 7.0 Hz). The

smaller coupling constant between H-4 and H-5 ($J_{4,5}$ = 7.0 Hz) than the expected value ($J_{4,5}$ = ~10.0 Hz) was due the presence of a five-membered isopropylidene ring fused to the six-membered rhamnopyranoside ring. This clearly indicates the slight distortion of the pyranose ring from regular $^1C_4$ conformation as shown in the Figure 1. Similar distortion of the pyranose ring from regular $^1C_4$ conformation was also observed for compound **5**. It was evident from the Table 1 that coupling constants of compounds **8-14** were in good agreement with regular $^1C_4$ conformation with C-5 substituent (–CH_3) equatorially oriented [(*5S*) configuration].

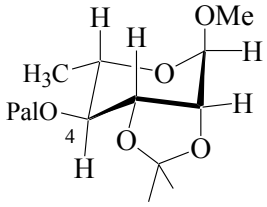

6

Slight distortion in $^1C_4$ conformation

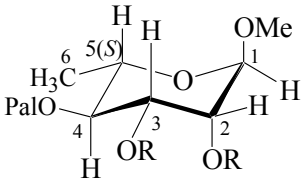

Regular $^1C_4$ conformation

7: R = H; **8**: R = Ac;
9: R = Ms; **10**: R = Piv;
11: R = Oct; **12**: R = Dec;
13: R = 2-Cl.Bz;
14: R = 4-Cl.Bz.

Figure 1.

Antimicrobial activities

The results of the *in vitro* inhibition zone against the selected Gram-positive bacteria due to the effect of the rhamnopyranosides (**2**, **5-14**) are mentioned in Table 2. It was observed from Table 2 that the tested chemicals are less effective against these Gram-positive organisms. Only 2,3-di-*O*-octanoate **11** exhibited considerable inhibition against these pathogens. Inhibition zone against the selected Gram-negative bacteria due to the effect of the chemicals (**2**, **5-14**) are presented in Table 3. Like Gram-positive organisms, these rhamnopyranosides didn't show considerable inhibition against the tested Gram-negative pathogens. Although 4-*O*-palmitoyl-2,3-di-*O*-octanoate **11** was found to be more effective against these Gram-negative pathogens.

Table 2. Inhibition against Gram-positive organisms by the rhamnopyranosides.

Compound no.	Diameter of zone of inhibition in mm (50 µg.dw/disc)			
	Bacillus cereus	***Bacillus megaterium***	***Bacillus subtilis***	***Staphylococcus aureus***
2	NF	NF	NF	NF
5	7	6	NF	6
6	7	4	8	NF
7	NF	5	5	8
8	7	7	6	NF
9	5	6	8	NF
10	NF	4	5	8
11	*23	17	*25	*20
12	5	NF	8	4
13	NF	6	8	6
14	8	NF	7	4
****Ampicillin**	*22	*19	*25	*21

NB. NF indicates not found, dw means dry weight,
"**" indicates standard antibiotic, "*" shows good inhibition.

Table 3. Inhibition against Gram-negative organisms by the rhamnopyranosides.

Compound no.	Diameter of zone of inhibition in mm (50 µg.dw/disc)					
	Escherichia coli	*INABAET (vibrio)*	*Pseomodomonas species*	*Salmonella paratyphi*	*Salmonella typhi*	*Shigella dysenteriae*
2	NF	NF	NF	NF	NF	NF
5	8	9	6	6	6	7
6	NF	NF	6	7	6	8
7	NF	6	NF	7	5	5
8	8	7	4	9	NF	8
9	NF	NF	6	7	6	7
10	NF	9	9	NF	NF	NF
11	*21	*26	*21	*20	*19	14
12	8	NF	NF	7	9	5
13	10	NF	8	9	6	6
14	7	9	5	NF	8	NF
**Ampicillin	*25	*24	17	*35	13	*35

NB. NF indicates not found, dw means dry weight,
"**" indicates standard antibiotic, "*" shows good inhibition.

Structure activity relationship (SAR)

It was evident from Table 2-4 that incorporation of palmitoyl group increased the antimicrobial potentiality of rhamnopyranoside **2**. Again, these acylated rhamnopyranoside derivatives (**2, 5-14**) were more active against fungal pathogens than that of bacterial organisms. An important observation was that, compounds **5** and **6** showed poorer toxicity than that of compounds **7-14** against these pathogens. This is probably due to the slight distortion in $^{1}C_{4}$ conformation of **5** and **6**. While compounds **7-14** having regular $^{1}C_{4}$ conformation showed much better antimicrobial potentiality. Again, compounds **2**, **5**, **6** and **7** contain more hydroxyl groups than that of compounds **8-14**. Compounds **8-14** having fewer or no hydroxyl groups showed much better antimicrobial potentiality. Here the hydrophobicity of the molecules increased gradually from compound **5**, **7** to **8-14**. The hydrophobicity of materials is an important parameter with respect to such bioactivity as toxicity or alteration of membrane integrity, because it is directly related to membrane permeation [16]. Hunt also proposed that the potency of aliphatic alcohols is directly related to their lipid solubility through the hydrophobic interaction between alkyl chains from alcohols and lipid regions in the membrane [17]. We believe that a similar hydrophobic interaction might occur between the acyl chains of glucofuranoses accumulated in the lipid like nature of the bacteria membranes. As a consequence of their hydrophobic interaction, bacteria lose their membrane permeability, ultimately causing death of the bacteria [16-18].

It was observed from Table 2-4 that 4-*O*-palmitoyl-2,3-di-*O*-octanoate **11** exhibited excellent activity against both bacterial and fungal pathogens which was, in some cases, higher than that of the standard antibiotics. This led us to conclude that incorporation of 4-*O*-palmitoyl group in rhamnopyranoside frame work along with 2,3-di-*O*-octanoyl group increased the antimicrobial potentiality of the rhamnopyranoside **2**.

4. CONCLUSION

Thus, we have successfully synthesized methyl 4-*O*-palmitoyl-α-L-rhamnopyranoside (**7**) in reasonably good yield from methyl α-L-rhamnopyranoside (**2**) via blocking-deblocking technique. A number of 2,3-di-*O*-acyl substituted derivatives (**8-14**) of **7** were also prepared for biological evaluation. All the rhamnopyranosides (**2**, **5-14**) were employed as test chemicals for in vitro antibacterial and antifungal functionality test. The structure activity relationship (SAR) study revealed that incorporation of 4-*O*-palmitoyl group in rhamnopyranoside frame work along with 2,3-di-*O*-octanoyl group increased the antimicrobial potentiality of the rhamnopyranoside 2.

5. ACKNOWLEDGMENTS

The author highly acknowledges the financial support from Bangladesh University Grants Commission (UGC, 2010-2011). The author is also indebted to Dr. M.S. Rahman and Mr. D.C. Debnath, University of Chittagong for screening antimicrobial activities.

6. REFERENCES AND NOTES

[1] Schaffer, R. In: The Carbohydrates (vol. 1A, 2nd edn). Pigman W.; Horton, D., Eds, New York: Academic Press, 1972, pp 69-111.

[2] Lang, S.; Wullbrandt, D. *Appl. Microbiol. Biotechnol*. **1999**, *51*, 22. [CrossRef]

[3] Bauer, J.; Brandenburg, K.; Zahringer, U.; Rademann, J. *Chem. Eur. J.* **2006**, *12*, 7116. [CrossRef]

[4] Kucukislamoglu, M.; Yayli, N.; Senturk, H. B.; Genc, H. *Turk J. Chem*. **2000**, *24*, 191.

[5] Gohar, A.; Gedara, S. R.; Baraka, H. N. *J. Med. Plants Res*. **2009**, *3*, 424.

[6] Qin,L.; Ming, L.; Mabry, T. J.; Dixon, R. A. *Phytochemistry* **1994**, *36*, 229. [CrossRef]

[7] Tsai, Y. F.; Yang, J. T.; Chen, J. D.; Lin, C. H. *Acta Cryst. E* **2007**, *63*, 3772. [CrossRef]

[8] Andary, C.; Wylde, R.; Laffite, C.; Privat, G.; Winternitz, F. *Phytochemistry* **1982**, *21*, 1123. [CrossRef]

[9] Marin, L. M. L.; Laneelle, M. A.; Prome, D.; Laneelle, G.; Prome, J. C.; Daffe, M. *Biochemistry* **1992**, *31*, 11106. [CrossRef]

[10] Lazar, L.; Csavas, M.; Borbas, A.; Gyemant, G.; Liptak, A. *Arkivoc* **2004**, *vii*, 196. [CrossRef]

[11] Kabir, A. K. M. S.; Matin, M. M.; Hossain, A. *J. Bangladesh Chem. Soc.* 2003, 16, 85.

[12] Haines, A. H. *Carbohydr. Res*. **1969**, *10*, 466. [CrossRef]

[13] Bauer, A. W.; Kirby, W. M. M.; Sherris, J. C.; Turck, M. *Am. J. Clin. Pathol*. **1966**, *45*, 493.

[14] Grover R. K.; Moore, J. D. *Phytopathol*. **1962**, *52*, 876.

[15] Liptak, A.; Fugedi, P.; Nanasi, P. *Carbohydr. Res*. **1978**, *65*, 209. [CrossRef]

[16] Kim, Y. M.; Farrah, S.; Baney, R. H. *Int. J. Antimicrob. Agents* **2007**, *29*, 217. [CrossRef]

[17] Hunt, W. A. *Adv. Exp. Med. Biol.* **1975**, *56*, 95. [CrossRef]

[18] Judge, V.; Narasimhan, B.; Ahuja, M.; Sriram, D.; Yogeeswari, P.; Clercq, E. D.; Pannecouque, C.; Balzarini, J. *Med. Chem*. **2013**, *9*, 53. [CrossRef].

Orbital: The Electronic Journal of Chemistry
journal homepage: www.orbital.ufms.br
ISSN 1984-6428

| Vol 6 | | No. 1 | | January-March 2014 |

Full Paper

Determinação de Chumbo em Águas de Abastecimento Utilizando Filmes de Bismuto Crescidos *in situ* Sobre Eletrodos de Pasta de Carbono

Sarah P. Monteiro, Leandro A. R. Ribeiro, Wilson T. Fonseca, Regina M. Takeuchi, André L. Santos*

Faculdade de Ciências Integradas do Pontal – Universidade Federal de Uberlândia, Rua 20, 1600, Tupã. 38304-402 Ituiutaba-MG, Brasil.

Article history: Received: 23 February 2014; revised: 12 March 2014; accepted: 15 March 2014. Available online: 02 April 2014.

Abstract: In this work, bismuth films were electrodeposited in situ onto carbon paste electrodes (CPEs) and they were used for lead determination in tap water samples by anodic stripping square wave voltammetry. The analytical performance of CPEs prepared with different binder agents was compared. It was observed that CPEs prepared with solid paraffin as binder agent provided the best results. All parameters of the analytical method were optimized and the best conditions obtained were: acetate buffer 0.1 mol L^{-1} (pH=4.75) as supporting electrolyte; pre-concentration time of 240 s and electrodepositing potential of -1.2 V vs. $Ag/AgCl/KCl_{sat}$. The best Bi^{3+} concentration was 2.0 µmol L^{-1}. At these optimized conditions, analytical curves were constructed and two linear regions were obtained: 25 to 100 nmol L^{-1} and 250 to 1000 nmol L^{-1}. Detection limits (LD) corresponding to these linear ranges were, respectively, 5.77 and 52.3 nmol L^{-1}. Recovery experiments were performed in tap water samples and recovery percentages close to 100 % were always obtained although the best results were obtained for samples spiked with 250 nmol L^{-1} of Pb^{2+}.

Keywords: carbon paste electrodes; bismuth film; lead; anodic stripping voltammetry; tap water

1. INTRODUÇÃO

A contaminação ambiental por metais pesados tem gerado preocupações em toda comunidade científica e na sociedade em geral. Esta preocupação se justifica pelo fato destes contaminantes serem substâncias não biodegradáveis, bioacumulativas e altamente tóxicas. Dentre os metais pesados, o chumbo se destaca por ser um poluente metálico abundante e perigoso na forma de cátions ou quando ligados a cadeias carbônicas curtas [1]. O chumbo é um metal bastante versátil, sendo empregado em baterias automotivas, tintas, agrotóxicos, como componente de ligas para solda, etc. Assim, este metal acumula os dois fatores primordiais para exercer forte ação poluente: toxicidade e abundância, esta última garantida pela intensa utilização do chumbo pela sociedade moderna. A principal forma de introdução do chumbo no ambiente é via contaminação de corpos d'água por atividades antropogênicas tais como: despejo de efluentes municipais, atividades de metalurgia e mineração, lixiviação de agrotóxicos, etc. Assim, o chumbo é uma das espécies cujo teor em água potável é regulamentado pela legislação brasileira. O Ministério da Saúde regulamenta, por meio da Portaria 2914 de 12/12/2011 [2], a quantidade máxima de chumbo permitida em água potável em 0,01 mg L^{-1} (48,3 nmol L^{-1}).

Neste contexto, verifica-se a necessidade de métodos analíticos altamente sensíveis e capazes de quantificar chumbo em baixíssimas concentrações com elevada confiabilidade. Esses métodos, além de contribuir para o controle de qualidade e preservação dos recursos hídricos podem ainda auxiliar no entendimento da propagação do chumbo no ambiente além de serem úteis para a identificação de fontes poluidoras. A espectroscopia de absorção atômica (AAS) e a espectrometria de massas com plasma indutivamente acoplado (ICP-MS) são técnicas analíticas amplamente empregadas para quantificar metais pesados com elevada precisão e sensibilidade. Apesar do sucesso destas técnicas para a análise de metais pesados em água, o elevado custo instrumental

*Corresponding author. E-mail: alsantos@pontal.ufu.br

e a necessidade de mão de obra extremamente especializada constituem sérias limitações, principalmente considerando a implementação em análises de rotina. Diante destas limitações, as técnicas eletroanalíticas apresentam-se como uma alternativa promissora para a quantificação de metais pesados em águas naturais, pois oferecem elevada sensibilidade com baixos limites de detecção, excelente precisão associado ao uso de uma instrumentação de custo relativamente baixo.

Dentre as técnicas eletroanalíticas, sem dúvida alguma, as técnicas voltamétricas de redissolução são as mais sensíveis para a quantificação de íons metálicos. Dentre as características vantajosas destas técnicas destacam-se: limites de detecção extremamente baixos (10^{-10} a 10^{-12} mol L^{-1}), capacidade multielementar e de especiação, além de maior seletividade, pois o analito pode ser seletivamente pré-concentrado na superfície do eletrodo. As técnicas voltamétricas de redissolução têm sido empregadas com êxito para a quantificação de metais pesados em diversas amostras, dentre as quais pode-se citar: etanol combustível [4,5]; gasolina [6,7], águas naturais e de abastecimento [8-12], suco de frutas [13], bebidas alcoólicas [14-18], etc. As contribuições das técnicas voltamétricas de redissolução combinadas ao uso de microeletrodos para quantificação de metais em amostras de água foram revisadas por Xie *et al* [3].

Vários tipos de eletrodos têm sido empregados como eletrodos de trabalho para a quantificação de íons metálicos por voltametria de redissolução. Um tipo de eletrodo que tem ocupado um lugar de destaque em eletroanálise, principalmente na eletroanálise de metais, são os eletrodos de pasta de carbono (CPEs). Esses eletrodos são constituídos por uma mistura entre pó de carbono e um líquido orgânico imiscível à água que tem a função de aglutinante, conferindo uma consistência pastosa ao eletrodo. O sucesso dos CPEs deve-se a uma série de características vantajosas apresentadas por esses eletrodos, tais como: baixo custo, facilidade de construção, manipulação e de modificação química, baixas correntes residuais, amplo intervalo útil de potencial, estabilidade química e possibilidade de modificação interna do material, permitindo que a renovação da superfície possa ser realizada de maneira rápida e simples. Os CPEs têm trazido avanços impressionantes tanto na eletroanálise de compostos orgânicos quanto inorgânicos, sendo este assunto abordado em alguns artigos de revisão [19,20]. Em 2008, completaram-se exatamente cinquenta anos desde que os CPEs foram introduzidos pelo Professor Ralph Norman Adams. Nesta oportunidade, Svancara e uma equipe de especialistas em eletroanálise e eletroquímica escreveram um artigo de revisão comemorativo [21]. Alguns autores deste grupo são também responsáveis pela mais completa revisão sobre os avanços do uso de CPEs em eletroanálise [22]. Em 2012, foi lançado um livro totalmente dedicado às contribuições dos CPEs à eletroanálise [23].

CPEs com desempenho analítico otimizado podem ser obtidos se estes eletrodos forem combinados com modificadores químicos capazes de modular as propriedades químicas da superfície eletródica, de modo a estabelecer interações químicas entre o eletrodo e o analito. Estas interações irão resultar em melhor seletividade ou sensibilidade ou ainda melhorar ambas. Um tipo de eletrodo quimicamente modificado que tem sido utilizado com sucesso na eletroanálise de metais são os eletrodos recobertos por filmes de bismuto (BiFE, do inglês *"Bismuth Film Electrodes"*). Os BiFEs combinam as propriedades vantajosas do mercúrio, tais como: elevado sobrepotencial para a redução de H^+ e elevada capacidade para a formação de ligas com baixa toxicidade, baixo custo e facilidade de preparação. A literatura apresenta alguns artigos de revisão sobre a utilização dos BIFEs em eletroanálise [24,25], bem como exemplos da aplicação destes eletrodos para a determinação de inúmeros íons metálicos em diferentes amostras [26-30].

Neste contexto, o objetivo deste trabalho é empregar CPEs recobertos com filmes de Bi visando a determinação de Pb^{2+} em amostras de água de abastecimento. Pretende-se, com isso, obter um eletrodo que apresente elevada detectabilidade para o Pb^{2+}, precisão e que, ao mesmo tempo, apresente baixo custo e seja de fácil construção, o que permitiria sua implementação em análises de rotina, mesmo em laboratórios de pequeno e médio porte.

2. MATERIAIS E MÉTODOS

Reagentes

Os padrões de Pb^{2+} utilizados neste trabalho foram preparados por diluição de uma solução padrão de Pb^{2+} para absorção atômica (Fluka Analytical). Uma solução estoque de 0,01 mol L^{-1} de Bi^{3+} foi preparada a partir da dissolução de $Bi(NO_3)_3.5H_2O$

(Impex) em uma solução 10 % de HNO_3 (Impex). Quatro diferentes eletrólitos de suporte foram estudados neste trabalho e todos os reagentes empregados no preparo destas soluções foram de pureza analítica, sendo utilizados sem qualquer procedimento de purificação. Todas as soluções aquosas empregadas neste trabalho foram preparadas com água ultrapura (ASTM tipo 1, com resistividade maior que 18 MΩ cm) produzida por um ultrapurificador da marca Megapurity®.

Para o preparo dos eletrodos de trabalho foram utilizados quatro diferentes de aglutinantes: parafina sólida (Synth), óleo mineral (Nujol®-Aldrich), borracha de silicone (Polystic®) e o adesivo bicomponente à base de resina epóxi (Araldite®). O pó de carbono usado para o preparo dos eletrodos foi de grau espectroscópico com diâmetro de partícula entre 1-2 µm da Merck.

Preparo dos eletrodos de trabalho

Prepararam-se quatro tipos de CPEs, utilizando diferentes aglutinantes. Os eletrodos preparados com Nujol®, Araldite® e borracha de silicone foram preparados adicionando-se a um béquer 20 % (m/m) de aglutinante e 80 % (m/m) de pó de carbono. Após a homogeneização completa dos componentes da pasta, cada uma foi introduzida em um suporte cilíndrico de Teflon®, contendo um êmbolo de cobre como contato elétrico. Para o preparo dos eletrodos contendo 20 % (m/m) de parafina sólida como aglutinante, adotou-se o seguinte procedimento: a parafina sólida foi fundida em banho aquecido a 65-70 ºC por 10 min. Em seguida, o pó de carbono foi adicionado e a mistura foi homogeneizada ainda em banho aquecido, para, posteriormente, ser inserida no suporte de Teflon®. Previamente à primeira utilização de cada eletrodo, estes foram polidos manualmente sobre papel impermeável até a obtenção de uma superfície lisa, uniforme e brilhante. Após o polimento, os eletrodos foram transferidos para a célula eletroquímica contendo apenas eletrólito de suporte e foram submetidos a 20 ciclos sucessivos de potencial entre -1,3 e +0,5 V *vs.* $Ag/AgCl/KCl_{sat}$ a 100 mV s^{-1}. O polimento e as sucessivas varreduras de potencial foram realizados a cada novo dia de trabalho ou ao final de cada estudo.

Instrumentação

Todas as medidas eletroquímicas foram efetuadas utilizando-se um potenciostato/galvanostato Autolab, modelo µAutolab III cuja interface e controle foram realizados pelo *software* GPES versão 4.9. A célula eletroquímica empregada foi uma célula de compartimento único contendo sempre 10 mL de solução e três eletrodos: o eletrodo de referência, um fio de Ag recoberto com AgCl e imerso em solução saturada de KCl ($Ag/AgCl_{sat}$), o eletrodo auxiliar constituído por um fio de platina enrolado em espiral, e os CPEs como eletrodo de trabalho. Todos os experimentos foram efetuados à temperatura ambiente.

3. RESULTADOS E DISCUSSÃO

Estudos Preliminares

Inicialmente, o efeito do Bi^{3+} sobre a resposta voltamétrica do Pb^{2+} foi avaliado, registrando-se voltamogramas de onda quadrada na ausência e na presença de Bi^{3+}. Estes voltamogramas foram registrados com um CPE preparado com parafina sólida como aglutinante e são apresentados na Figura 1.

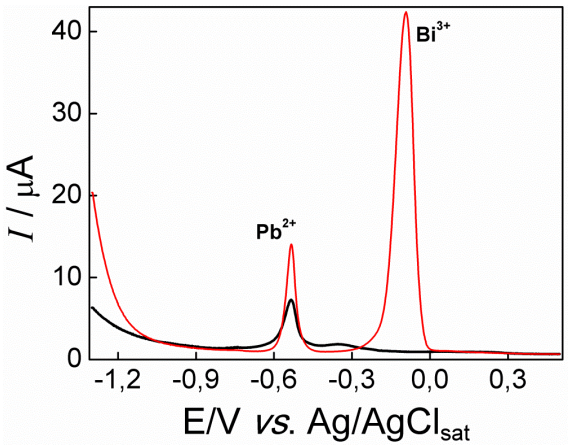

Figura 1. Voltamogramas de onda quadrada registrados na presença de 0,5 µmol L^{-1} de Pb^{2+} em tampão acetato 0,1 mol L^{-1}, pH 4,75. (—) Ausência de Bi^{3+}. (—) Presença de 5,0 µmol L^{-1} de Bi^{3+}. Potencial de eletrodeposição ($E_{eletrodeposição}$): -1,3 V; tempo de eletrodeposição ($t_{eletrodeposição}$): 180 s. Amplitude de pulso (ΔE): 25 mV; frequência (f): 25 Hz, incremento de varredura (ΔE_s): 2 mV.

A Figura 1 mostra que o Bi^{3+} intensificou consideravelmente o pico de redissolução anódica do chumbo (E_p = -0,53 V), aumentando, portanto, a detectabilidade para este metal. Este comportamento é consequência da formação de ligas entre o chumbo e

o bismuto, assim, o Pb^{2+} é depositado mais facilmente na superfície contendo bismuto do que sobre uma superfície contendo apenas carbono. Além disso, a presença do bismuto diminui a taxa de evolução de hidrogênio, diminuindo a competição deste processo com a eletrodeposição do Pb^{2+}. Estes fatores combinados garantem uma eletrodeposição mais eficiente do Pb^{2+}, levando ao aumento da detectabilidade observado na Figura 1. Esta Figura mostra, ainda, que a redissolução anódica do bismuto produz um pico em -0,1 V. Assim, o filme de bismuto pode ser removido da superfície do eletrodo a cada varredura, desde que se mantenha o potencial final suficientemente positivo. Visando garantir que o filme fosse completamente removido após cada medida, aplicou-se + 0,5 V durante 30 s após cada medida voltamétrica.

A resposta voltamétrica do Pb^{2+} sobre um filme de bismuto crescido sobre o CPE preparado com parafina sólida como aglutinante foi comparado à resposta fornecida por um filme de bismuto crescido sobre carbono vítreo, sendo os resultados obtidos apresentados na Figura 2.

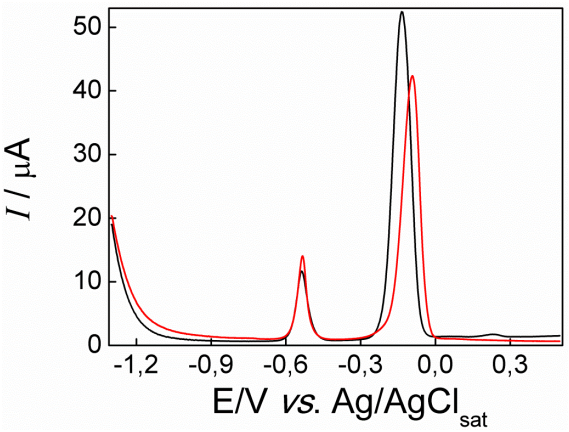

Figura 2. Voltamogramas de onda quadrada registrados na presença de 0,5 µmol L^{-1} de Pb^{2+} + 5 µmol L^{-1} Bi^{3+} em tampão acetato 0,1 mol L^{-1}, pH 4,75. (—) Eletrodo de carbono vítreo. (—) CPE. $E_{eletrodeposição}$: -1,3 V; $t_{eletrodeposição}$: 180 s. ΔE = 25 mV; f = 25 Hz, ΔE_s = 2 mV

A Figura 2 mostra que o sinal obtido para o Pb^{2+} foi praticamente o mesmo para os filmes crescidos sobre o CPE e sobre o eletrodo de carbono vítreo. Este resultado sugere que o material sobre o qual o filme de bismuto é crescido exerce um efeito secundário sobre o sinal do Pb^{2+} comparado ao o efeito promovido pelo Bi^{3+} (Figura 1). Apesar de não fornecer um ganho significativo de sinal em relação ao carbono vítreo, o CPE apresenta algumas vantagens, tais como: facilidade de preparo e, principalmente, baixo custo que o torna bastante atrativo para o desenvolvimento de um método voltamétrico prático e de baixo custo. Desta forma, todos os estudos subsequentes foram efetuados com os CPEs. É importante ressaltar que o crescimento de um filme de Bi sobre a superfície de um CPE faz com que uma de suas principais características atrativas, a possibilidade de modificação interna, não seja explorada. No entanto, a praticidade e o menor custo deste eletrodo em relação ao carbono vítreo, justificam seu uso ainda que limitado à uma modificação superficial.

Uma vez definido que o CPE seria o eletrodo sobre o qual os filmes de Bi seriam crescidos, avaliou-se o efeito do aglutinante sobre a resposta voltamétrica do Pb^{2+}. Os voltamogramas de onda quadrada obtidos nestes estudos são apresentados na Figura 3 A. A Figura 3 B, apresenta voltamogramas cíclicos em presença de $[Fe(CN)_6]^{3-}$ registrados com os diferentes CPEs preparados.

A Figura 3 A mostra claramente que o CPE preparado com parafina sólida como aglutinante apresenta a melhor resposta para o Pb^{2+}, além de fornecer picos voltamétricos mais intensos, verifica-se que este eletrodo apresenta também as menores correntes residuais. Baixas correntes residuais são altamente desejáveis, pois conduzem a baixos limites de detecção, os quais são necessários para a determinação de metais em amostras de água. A literatura tem mostrado que a parafina sólida produz CPEs com menores correntes residuais do que CPEs preparados com Nujol®, sendo este comportamento atribuído ao fato de o compósito preparado com parafina sólida ser mais rígido e mais compacto [12]. Uma vantagem adicional dos CPEs preparados com parafina sólida como aglutinante é que estes podem ter suas aplicações estendidas à matrizes com elevado teor de etanol, tais como etanol combustível [4] e cachaça [14], enquanto CPEs preparados com Nujol® são instáveis e sofrem desagregação neste tipo de amostra [4]. A Figura 3 B, mostra os voltamogramas cíclicos registrados com os diferentes CPEs em presença de $[Fe(CN)_6]^{3-}$. Verifica-se que os CPEs preparados com Nujol®, parafina sólida e borracha de silicone, apresentaram um excelente perfil voltamétrico em presença de $[Fe(CN)_6]^{3-}$. Esses resultados indicam que estes três CPEs funcionam perfeitamente e que, portanto, o pior desempenho para Pb^{2+} apresentado pelos CPEs preparados com Nujol®

e com borracha de silicone não pode ser atribuído a problemas de preparo destes eletrodos. Por outro lado, verificou-se que o CPE preparado com Araldite® não apresentou resposta voltamétrica satisfatória nem para o Pb^{2+} nem para o $[Fe(CN)_6]^{3-}$. As correntes residuais deste eletrodo foram muito maiores que as dos outros CPEs. Estes resultados demonstram que o procedimento adotado para o preparo do CPE com Araldite® não foi adequado e resultou em um eletrodo com elevada resistência elétrica, o que prejudica a transferência eletrônica entre a superfície eletródica e as espécies em solução. Isso acontece, pois o Araldite® utilizado apresenta tempo de cura de 10 min. Assim, ocorre o endurecimento do aglutinante antes que a pasta esteja bem homogeneizada, resultando em regiões pobres em pó de carbono e, portanto, com elevada resistência elétrica. Assim, esses resultados sugerem que para o preparo de um CPE com Araldite® como aglutinante, o melhor procedimento parece ser a diluição do aglutinante com ciclohexanona, conforme descrito por Silva *et al* [31]. O melhor desempenho dos CPEs preparados com parafina sólida pode ser atribuído ao fato desse CPE ser mais compacto, produzindo uma superfície mais uniforme e condutora sobre a qual os íons metálicos podem ser depositados mais eficientemente. Diante destes resultados, todos os estudos subsequentes foram efetuados empregando-se o CPE preparado com parafina sólida como aglutinante.

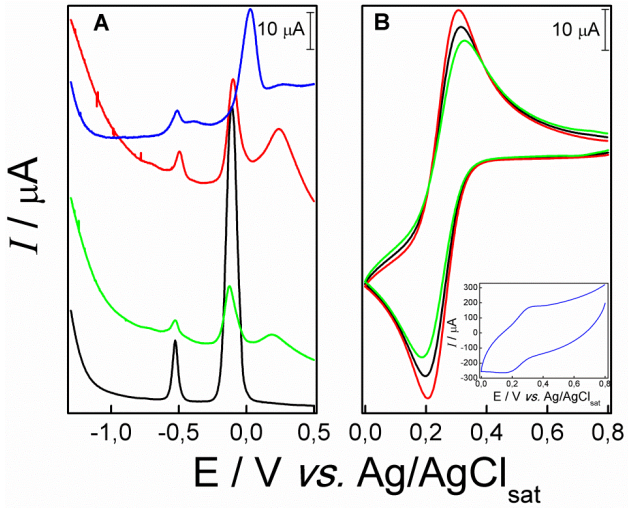

Figura 3. A) Voltamogramas de onda quadrada registrados na presença de 0,5 µmol L^{-1} de Pb^{2+} + 5 µmol L^{-1} Bi^{3+} em tampão acetato 0,1 mol L^{-1}, pH 4,75. $E_{eletrodeposição}$: -1,3 V; $t_{eletrodeposição}$: 180 s. ΔE = 25 mV; f = 25 Hz, ΔE_s = 2 mV. B) Voltamogramas cíclicos registrados em KCl 1,0 mol L^{-1} contendo 6,0 mmol L^{-1} de $[Fe(CN)_6]^{3-}$. (—) Parafina sólida. (—) Nujol®. (—) Borracha de silicone. (—) Araldite®.

Em seguida, o efeito do eletrólito de suporte sobre a resposta voltamétrica do Pb^{2+} foi avaliado, sendo os resultados obtidos apresentados na Figura 4.

A Figura 4 mostra que a maior intensidade de sinal foi obtida em KNO_3 0,1 mol L^{-1} porém, este foi o eletrólito de suporte que forneceu a pior repetitividade. Uma possível explicação para esta falta de repetitividade é que em KNO_3 não existe nenhum sistema tamponante. Sabe-se que a eletrodeposição de metais é fortemente influenciada pelo pH. Assim, em KNO_3, podem ocorrer variações locais de pH durante a eletrodeposição dos íons metálicos, pois esta ocorre concomitantemente à redução da água que gera H_2 e produz OH^- na região da interface eletrodo/solução. Essa variação de pH na região da interface é suficiente para comprometer a repetitividade das medidas. Em um meio tamponado, este efeito é minimizado, o que explica a melhor repetitividade obtida em tampão acetato 0,1 mol L^{-1}. Em 0,1 mol L^{-1} de HNO_3, obteve-se um baixo sinal para Pb^{2+}, o que pode ser explicado pela elevada concentração de H^+ o que favorece a evolução de H_2 e dificulta a eletrodeposição de Pb^{2+} e Bi^{3+}, conduzindo a uma baixa quantidade de metal eletrodepositado e a um pico de redissolução anódica de baixa intensidade. Em 0,1 mol L^{-1} de NaOH, os íons metálicos estão na forma de hidróxi-complexos solúveis, tais como: $[Pb(OH)_4]^{2-}$ e $[Bi(OH)_4]^-$ [32], os quais, aparentemente, estabilizam os metais na solução,

dificultando a eletrodeposição, conduzindo a baixos sinais de redissolução. Com base nestes resultados, os estudos subsequentes foram efetuados utilizando-se tampão acetato 0,1 mol L^{-1} como eletrólito de suporte.

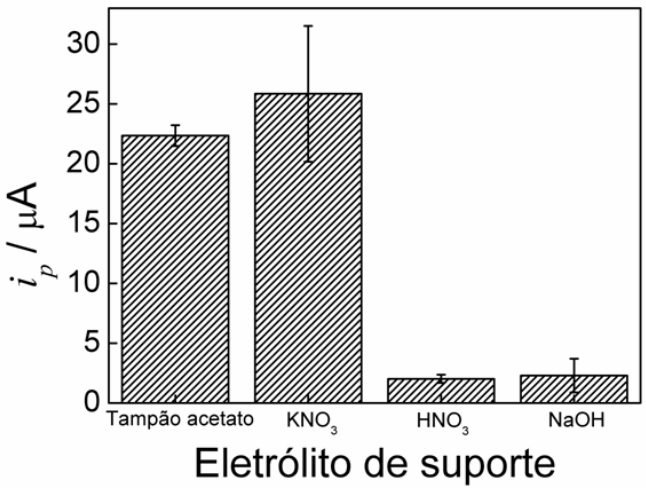

Figura 4. Correntes de pico para Pb^{2+} obtidas em diferentes eletrólitos de suporte. Voltamogramas de onda quadrada registrados em presença de 0,5 µmol L^{-1} de Pb^{2+} e 5,0 µmol L^{-1} de Bi^{3+}, nas seguintes condições: $E_{eletrodeposição}$: -1,3 V; $t_{eletrodeposição}$: 180 s. ΔE = 25 mV; f = 25 Hz, $ΔE_s$ = 2 mV. Concentração dos eletrólitos de suporte: 0,1 mol L^{-1}.

Estudos de otimização de parâmetros

Previamente à aplicação do método para a quantificação de Pb^{2+} em amostras de água de abastecimento, todos os parâmetros envolvidos no procedimento analítico foram submetidos a estudos de otimização. O primeiro parâmetro otimizado foi a concentração de Bi^{3+} na célula eletroquímica, sendo as correntes de pico para Pb^{2+} obtidas em diferentes concentrações de Bi^{3+} apresentadas na Figura 5.

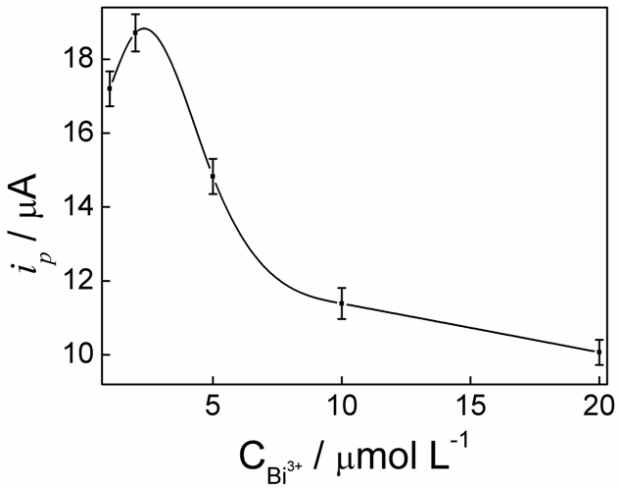

Figura 5. Variação da corrente de pico para Pb^{2+} em função da concentração de Bi^{3+}. Voltamogramas de onda quadrada registrados em tampão acetato 0,1 mol L^{-1} na presença de 0,5 µmol L^{-1} de Pb^{2+}, nas seguintes condições: $E_{eletrodeposição}$: -1,3 V; $t_{eletrodeposição}$: 120 s. ΔE = 25 mV; f = 25 Hz, $ΔE_s$ = 2 mV.

A Figura 5 mostra que o sinal voltamétrico para o Pb^{2+} aumenta até a concentração de Bi^{3+} de 2 µmol L^{-1}, a partir desta concentração, o sinal sofre uma queda acentuada. Este resultado é concordante

com a literatura que tem mostrado que a detectabilidade para o Pb^{2+} aumenta com o aumento da espessura do filme de bismuto até um certo limite, seguido por uma queda na sensibilidade para filmes mais espessos [33,34]. Uma possível explicação para este comportamento é que em condições nas quais a concentração de Bi^{3+} é muito maior que a de Pb^{2+}, a eletrodeposição de Bi^{3+} é favorecida em relação à de Pb^{2+}, o que leva a uma diminuição do sinal para este metal. Com base nos resultados apresentados na Figura 5, a concentração de Bi^{3+} de 2 µmol L^{-1} foi adotada nos experimentos posteriores. O próximo parâmetro otimizado foi o $E_{eletrodeposição}$. Foi verificado um aumento pronunciado do pico de redissolução anódica para o Pb^{2+} para valores de $E_{eletrodeposição}$ de até -1,2 V. Potenciais mais negativos não produziram aumentos significativos no sinal voltamétrico do Pb^{2+}, portanto, o potencial de eletrodeposição de -1,2 V foi o adotado como valor otimizado. O $t_{eletrodeposição}$ também foi otimizado e os valores de corrente de pico obtidos para o Pb^{2+} nos diferentes $t_{eletrodeposição}$ estudados são apresentados na Figura 6.

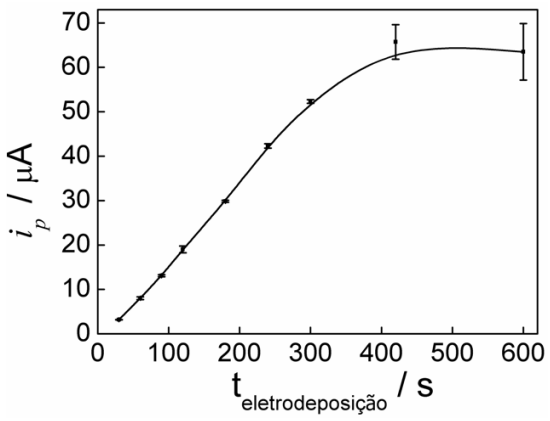

Figura 6. Variação da corrente de pico para Pb^{2+} em função do $t_{eletrodeposição}$. Voltamogramas de onda quadrada registrados em tampão acetato 0,1 mol L^{-1} na presença de 0,5 µmol L^{-1} de Pb^{2+} e de 2 µmol L^{-1} de Bi^{3+} nas seguintes condições: $E_{eletrodeposição}$: -1,2 V; ΔE = 25 mV; f = 25 Hz, ΔE_s = 2 mV.

A Figura 6 mostra um aumento significativo do sinal para tempos de eletrodeposição de até 420 s e, a partir deste valor, observa-se uma estabilização do sinal. Visando encontrar o melhor compromisso entre elevada sensibilidade e baixo tempo de análise, o $t_{eletrodeposição}$ de 240 s foi escolhido como valor otimizado. Finalmente, os parâmetros operacionais da técnica de voltametria de onda quadrada foram otimizados e os melhores valores foram: ΔE = 50 mV, f = 50 Hz e ΔE_s = 4 mV.

Curva analítica

Nas condições previamente otimizadas, foram registrados voltamogramas de onda quadrada em diferentes concentrações de Pb^{2+}, os quais foram utilizados para a construção de curvas analíticas. Os voltamogramas e as curvas analíticas obtidas são apresentados nas Figuras 7A e 7B.

Foram encontradas duas regiões nas quais a corrente de pico varia linearmente com a concentração de Pb^{2+}. A primeira região linear varia de 25 a 100 nmol L^{-1}, de acordo com a equação: $i_p(\mu A) = 0,37 + 0,08\ C_{Pb2+}(\text{nmol } L^{-1})$, com coeficiente de correlação linear (R) igual a 0,9976. A segunda região linear encontrada foi de 250 a 1000 nmol L^{-1}, de acordo com a equação: $i_p(\mu A) = -0,22 + 0,19\ C_{Pb2+}(\text{nmol } L^{-1})$, R = 0,9981. Para ambos os intervalos lineares, foram obtidos valores de R próximos a 1, demonstrando que ambas as curvas analíticas apresentam linearidade satisfatória. Foram determinados os limites de detecção (LD) para cada um dos intervalos lineares, através da equação: LD = $(3s_b/S)$, sendo s_b o desvio padrão obtido para o branco e S a sensibilidade, que é igual ao coeficiente angular da curva analítica. Os valores de LD encontrados para a primeira e segunda região linear foram: 5,77 e 52,3 nmol L^{-1}, respectivamente. O fato de serem obtidas duas regiões lineares pode ser explicado em termos da competição mútua entre Pb^{2+} e Bi^{3+} pela superfície do eletrodo. Em condições nas quais o Bi^{3+} está presente em concentrações maiores que o Pb^{2+}, a deposição de Bi^{3+} é favorecida, conduzindo a uma menor sensibilidade para o Pb^{2+}, fornecendo a primeira região linear com menor coeficiente angular. À

medida que a concentração de Pb^{2+} aumenta e torna-se comparável à concentração de Bi^{3+}, ocorre deposição de maiores quantidades relativas de Pb^{2+}, conduzindo a um aumento da sensibilidade para este metal, originando a segunda região linear com maior coeficiente angular.

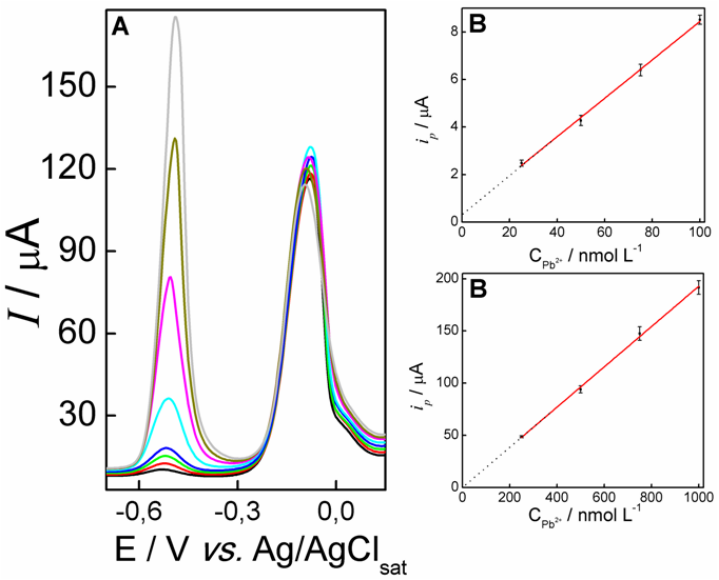

Figura 7. A) Voltamogramas de onda quadrada registrados em tampão acetato 0,1 mol L^{-1} (pH 4,75), contendo 2,0 µmol L^{-1} de Bi^{3+} e diferentes concentrações de Pb^{2+}. $E_{eletrodeposição}$ = -1,2 V; $t_{eletrodeposição}$ = 240s; ΔE = 50 mV; f = 50 Hz, $ΔE_s$ = 4 mV. (—) 25, (—) 50, (—) 75, (—) 100; (—) 250; (—) 500; (—) 750; (—) 1000 nmol L^{-1} de Pb^{2+}. B) Curvas analíticas.

Aplicação do método

O método desenvolvido foi empregado para a determinação de Pb^{2+} em amostras de água de torneira, para isto, os reagentes necessários para o preparo do tampão acetato foram adicionados diretamente à amostra evitando que esta sofresse diluição. Verificou-se que os voltamogramas de onda quadrada registrados nessas amostras não apresentaram o pico de redissolução anódica relativo ao Pb^{2+}. Este resultado indica que ou o Pb^{2+} está ausente nestas amostras ou está em concentrações abaixo do detectável pelo método proposto. Visando efetuar a validação do método desenvolvido, foram realizados estudos de adição e recuperação de Pb^{2+} nas amostras de água de torneira. As amostras foram enriquecidas com dois níveis de Pb^{2+}: 40 e 250 nmol L^{-1}, correspondendo, respectivamente, à primeira e à segunda região linear. O teor de Pb^{2+} nas amostras enriquecidas foi determinado em triplicata utilizando o método de adição de padrões. Os voltamogramas de onda quadrada e a curva de adição de padrão obtida para a amostra enriquecida com 40 nmol L^{-1} de Pb^{2+} são apresentados nas Figuras 8A e 8B.

A curva de adição de padrão foi linear de acordo com a equação: $i_p(\mu A)$ = 1,24 + 0,034 C_{Pb2+}(nmol L^{-1}) com R = 0,9981. Assim, constata-se que esta curva apresentou linearidade satisfatória, indicando que a mesma pode ser empregada para a determinação de Pb^{2+} nesta amostra. O teor de Pb^{2+} encontrado na amostra enriquecida foi de (36 ± 2) nmol L^{-1}, N=3; sendo este resultado expresso como (valor médio ± intervalo de confiança). Para a determinação do intervalo de confiança, utilizou-se grau de confiança de 95 % e dois graus de liberdade, situação na qual o parâmetro estatístico t assume o valor de 4,3 [35]. O teor de chumbo encontrado corresponde a uma porcentagem de recuperação de (91 ± 5) %. Uma vez que a concentração de Pb^{2+} adicionada na amostra não está contida no intervalo de confiança, constata-se que existem diferenças estatísticas entre o teor de Pb^{2+} adicionado e o recuperado. Portanto, pode-se concluir que a amostra analisada apresenta efeitos de matriz que não são completamente contornados pelo método de adição de padrão. A presença deste efeito de matriz pode ser confirmada pela comparação entre os coeficientes angulares da curva analítica e da curva de adição de padrão. Observou-se que o coeficiente angular da

curva de adição de padrão, construída em água de torneira, foi 0,034 μA nmol^{-1} L; enquanto o coeficiente angular da curva analítica, construída em água ultrapura, foi 0,081 μA nmol^{-1} L. A grande diferença entre os coeficientes angulares demonstra a perda de sensibilidade promovida pela amostra de água de torneira, que é uma consequência dos efeitos de matriz apresentados por esta amostra. Apesar da baixa porcentagem de recuperação, o valor de desvio padrão relativo (RSD) obtido foi de 2 % com um erro relativo de -10 %. Esses resultados indicam que o método proposto possui precisão satisfatória e que poderia, por exemplo, ser empregado para análises semiquantitativas de amostras de água de torneira.

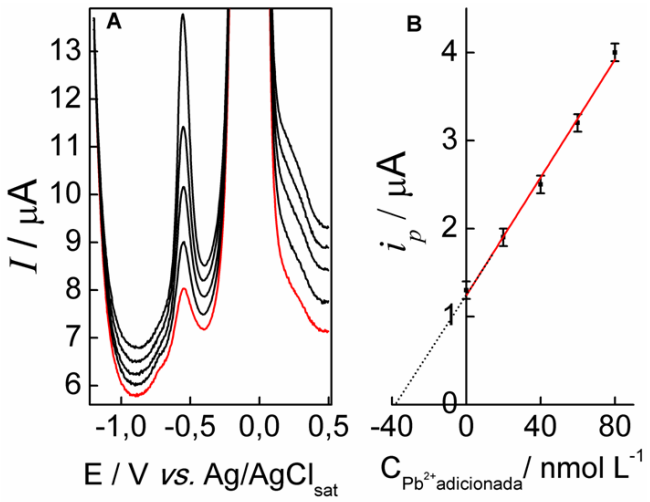

Figura 8. A) Voltamogramas de onda quadrada registrados na amostra de água de torneira enriquecida com 40 nmol L^{-1} de Pb^{2+} (—) e após sucessivas adições de 20 nmol L^{-1} de Pb^{2+} (—). Demais condições experimentais mantidas como na Figura 7A. B) Curva de adição de padrão.

Para avaliar se o método proposto é aplicável para a determinação de Pb^{2+} em águas contaminadas com maiores concentrações deste metal, outra amostra de água de torneira foi enriquecida com 250 nmol L^{-1} de Pb^{2+} sendo, posteriormente, submetida a estudos de adição e recuperação. Conforme mostra a Tabela 1, o teor de Pb^{2+} encontrado nesta amostra foi de (253 ± 12) nmol L^{-1} com 95 % de grau de confiança e dois graus de liberdade. Este resultado corresponde a uma porcentagem de recuperação de (102 ± 5) %.

Tabela 1. Resultados dos estudos de adição e recuperação em amostras de água de torneira.

Pb^{2+} adicionado/ nmol L^{-1}	Pb^{2+} recuperado*/ nmol L^{-1}	Erro relativo/ %	sd	RSD	% recuperada
40	36 ± 2	-10	0,72	2	91 ± 5
250	253 ± 12	+1,2	5,06	2	102 ± 5

*Valores expressos na forma (valor médio ± intervalo de confiança). Grau de confiança de 95 % e dois graus de liberdade, situação para qual t = 4,3 [35].

Para este nível de enriquecimento da amostra, não foram encontradas diferenças estatísticas entre o teor de Pb^{2+} adicionado e o recuperado. O erro relativo entre esses valores foi de 1,2 %, sendo o valor de RSD igual a 2 %. Estes resultados indicam que, para maiores concentrações de Pb^{2+}, o método desenvolvido fornece resultados mais precisos e exatos. Portanto, o método proposto pode ser empregado com êxito para a detecção de elevados níveis de contaminação de águas de abastecimento com Pb^{2+}.

4. CONCLUSÃO

Os resultados obtidos neste trabalho demonstraram que os filmes de bismuto crescidos *in situ* fornecem picos de redissolução anódica para o Pb^{2+} mais intensos do que os obtidos sobre um CPE não modificado. Verificou-se também que o uso de parafina sólida como aglutinante produz CPEs de melhor desempenho analítico para Pb^{2+} comparado aos CPEs preparados com Nujol® ou borracha de silicone como aglutinante. A superfície sobre a qual o filme de bismuto é crescido parece não afetar

significativamente a detectabilidade para o Pb^{2+}, sendo obtida praticamente a mesma intensidade de sinal tanto para filmes de bismuto crescidos sobre um CPE quanto para os crescidos sobre carbono vítreo. Isso é um fato interessante, pois permite que um CPE de custo significativamente inferior ao do carbono vítreo seja empregado para a determinação de Pb^{2+} sem perda de desempenho analítico. Finalmente, o método foi validado por meio de estudos de adição e recuperação em amostras de água de torneira. Verificou-se que foram obtidas porcentagens de recuperação próximas a 100 % para todas as amostras analisadas, embora os resultados mais confiáveis tenham sido obtidos para amostras enriquecidas com 250 nmol L^{-1} de Pb^{2+}.

5. AGRADECIMENTOS

Os autores agradecem à FAPEMIG (Proc.: APQ-00291-09, APQ-02497-12 e APQ-01557-13) pelo suporte financeiro. Wilson T. Fonseca agradece ao programa PIBIC/UFU/CNPq pela bolsa de iniciação científica concedida.

6. REFERÊNCIAS E NOTAS

[1] Baird, C; Cann, M. Química Ambiental, 4ª Ed. Porto Alegre: Bookman, 2011, Capítulo 15.

[2] Brasil, Ministério da Saúde, **Portaria nº 2914** de 12/12/2011. Disponível em: <http://www.comitepcj.sp.gov.br/download/Portaria_MS_2914-11.pdf>. Acesso em fevereiro de 2014.

[3] Xie, X. D.; Stueben, D.; Berner, Z. *Anal. Lett.* **2005**, *38*, 2281. [CrossRef]

[4] Takeuchi, R. M.; Santos, A. L.; Padilha, P. M.; Stradiotto, N. R. *Talanta* **2007**, *71*, 771. [CrossRef]

[5] Muñoz, R. A. A.; Angnes, L. *Microchem. J.* **2004**, *77*, 157. [CrossRef]

[6] Martiniano, L. C.; Almeida, J. M. S.; Cavalcante, G. H. R.; Marques, E. P.; Fonseca, T. C. O.; Paim, L. L.; Souza, A. G.; Stradiotto, N. R.; Aucelio, R. Q.; Marques, A. L. B. *Curr. Anal. Chem.* **2013**, *9*, 1. [CrossRef]

[7] Cardoso, W. S.; Fonseca, T. C. O.; Marques, A. L. B.; Marques, E. P. *J. Braz. Chem. Soc.* **2010**, *21*, 1733. [CrossRef]

[8] Oliveira, P. R.; Stradiotto, N. R.; Tanaka, A. A.; Bergamini, M. F. *Curr. Anal. Chem.* **2012**, *8*, 520. [CrossRef]

[9] Giacomino, A.; Abollino, O.; Lazzara, M.; Malandrino, M.; Mentasti, E. *Talanta* **2011**, *83*, 1428. [CrossRef]

[10] Cesarino, I.; Marino, G.; Matos, J. R.; Cavalheiro, E. T. G. *J. Braz. Chem. Soc.* **2007**, *18*, 810. [CrossRef]

[11] Arancibia, V.; Zúñiga, M.; Zúñiga, M. C.; Segura, R.; Esteban, M. *J. Braz. Chem. Soc.* **2010**, *21*, 255. [CrossRef]

[12] Silva, D. H.; Costa, D. A.; Takeuchi, R. M., Santos, A. L. *J. Braz. Chem. Soc.* **2011**, *22*, 1727. [CrossRef]

[13] El Mhammedi, M. A.; Achak, M.; Bakasse, M.; Chtaini, A. *Chemosphere* **2009**, *76*, 1130. [CrossRef]

[14] Costa, D. A.; Takeuchi, R. M.; Santos, A. L. *Int. J. Electrochem. Sci.* **2011**, *6*, 6410. [Link]

[15] Baldo, M. A.; Daniele, S. *Electroanalysis* **2006**, *18*, 633. [CrossRef]

[16] Clark, A. C.; Scollary, G. R. *Anal. Chim. Acta* **2000**, *413*, 25. [CrossRef]

[17] Stozhko, N. Y.; Kolyadina, L. I. *J. Anal. Chem.* **2005**, *60*, 901. [CrossRef]

[18] Gutierrez, C. A.; Hardcastle, J. L.; Ball, J. C.; Compton, R. G. *Analyst* **1999**, *124*, 1053. [CrossRef]

[19] Švancara, I.; Vytřas, K.; Barek, J.; Zima, J. *Crit. Rev. Anal. Chem.* **2001**, *31*, 311. [CrossRef]

[20] Zima, J.; Švancara, I.; Barek, J.; Vytřas, K.; *Crit. Rev. Anal. Chem.* **2009**, *39*, 204. [CrossRef]

[21] Švancara, I.; Vytřas, K.; Kalcher, K.; Walcarius, A.; Wang, J. *Electroanalysis* **2009**, *21*, 7. [CrossRef]

[22] Švancara, I.; Walcarius, A.; Kalcher, K.; Vytřas, K. *Cent. Eur. J. Chem.* **2009**, *7*, 598. [CrossRef]

[23] Švancara, I. Kalcher, K.; Walcarius, A.; Vytřas, K. Electroanalysis with Carbon Paste Electrodes, Boca Ratón: Taylor & Francis, 2012.

[24] Wang, J. *Electroanalysis* **2005**, *17*, 1341. [CrossRef]

[25] Švancara, I.; Prior, C.; Hocevar, S. B.; Wang, J. *Electroanalysis* **2010**, *22*, 1405. [CrossRef]

[26] Ion, I.; Ion, A. C. *Sens. Actuators, B* **2012**, *166-167,* 842. [CrossRef]

[27] Bi, Z.; Chapman, C. S.; Salaün, P.; Van Den Berg, C. M. G. *Electroanalysis* **2010**, *22,* 2897. [CrossRef]

[28] Nunes, L. M. S.; Faria, R. C. *Electroanalysis* **2008**, *20*, 2259. [CrossRef]

[29] Saturno, J.; Valera, D.; Carrero, H.; Fernández, L. *Sens. Actuators, B* **2011**, *159*, 92. [CrossRef]

[30] Kefala, G.; Economou, A.; Vougaropoulous, A.; Sofoniou, M. *Talanta* **2003**, *61*, 608. [CrossRef]

[31] Silva, R. A. B.; Rabelo, A. C.; Bottechia, O. L.; Muñoz, R. A.; Richter, E. M. *Quim. Nova* **2010**, *33*, 1398. [CrossRef]

[32] Salles, M. O.; Souza, A. P. R.; Naozuka, J.; Oliveira, P. V.; Bertotti, M. *Electroanalysis* **2009**, *21*, 1439. [CrossRef]

[33] Ping, J; Wu, J.; Ying, Y, Wang, M.; Liu, G.; Zhang, M. *J. Agric. Food Chem.* **2011**, *59*, 4418. [CrossRef]

[34] Li, D.; Jia, J.; Wang J. *Talanta* **2010**, *83*, 332. [CrossRef]

[35] Miller, J. N.; Miller, J. C. Estadística y Quimiometría para Química Analítica, 4ª Edición, Madrid: Prentice Hall, 2002.

Orbital: The Electronic Journal of Chemistry
journal homepage: www.orbital.ufms.br
ISSN 1984-6428

| Vol 6 | | No. 1 | | January-March 2014 |

Full Paper

Determinação do Número de Cetano de Blendas de Biodiesel/Diesel Utilizando Espectroscopia no Infravermelho Médio e Regressão Multivariada

Carla Felippi Chiella Ruschel[a*], Chun Te Huang[a], Dimitrios Samios[a], Marco Flôres Ferrão[a], Carlos Itsuo Yamamoto[b], Rubia Carla Barato Plocharski[b]

[a]*Instituto de Química, Universidade Federal do Rio Grande do Sul. Av. Bento Gonçalves, 9500. CEP: 91501-970. Porto Alegre, RS, Brasil.*
[b]*Departamento de Engenharia Química, Centro Politécnico, Universidade Federal do Paraná. CEP: 81531-980. Curitiba, PR, Brasil.*

Article history: Received: 04 October 2013; revised: 01 January 2014; accepted: 11 February 20145. Available online: 02 April 2014.

Abstract: The aim of this work is to determine the cetane number of biodiesel/diesel blends using mid-infrared spectroscopy coupled with multivariate regression. Thirty five samples were used into the calibration set and twenty for the prediction set. The partial least squares algorithms used were: by Interval (iPLS), by Backward Interval (biPLS) and by Synergy Intervals (siPLS). In the best iPLS model was selected the spectral range 1050-1500 cm^{-1} obtained with root mean square error of prediction (RMSEP) of 0.314 and determination coefficient (r^2) of 0.952 and root mean square error of cross-validation (RMSECV) of 0.728. For biPLS model the spectral range selected is a combination of several spectrum bands which showed a RMSEP of 0.353, r^2 of 0.960 and RMSECV of 0.664. The best model is the siPLS split the spectrum into 16 intervals and the combined spectral regions 1485-1277 cm^{-1} and 858-650 cm^{-1} presenting RMSECV = 0.642, RMSEP = 0.352 and r^2 = 0.962. The proposed methodology was adequate, with prediction errors less than 1%, being cleaner, faster and easy to perform.

Keywords: blends; biodiesel; diesel; cetane number; infrared; multivariate regression

1. INTRODUÇÃO

A avaliação de propriedades físico-químicas de um combustível fornece importantes informações a respeito da sua qualidade. O número de cetano, particularmente, está relacionado com a qualidade da combustão das misturas de óleo diesel sendo essencial na avaliação e garantia do desempenho energético do mesmo.

O número de cetano (NC), que é dado por um valor adimensional, representa a inflamabilidade do combustível, particularmente crítica, durante as condições de arranque a frio. Valores de números de cetano baixos levam a um longo tempo de atraso de ignição, ou seja, o tempo entre a injeção do combustível e o início da combustão. Consequentemente, quanto menor o NC, mais brusca é a fase de combustão da pré-mistura, conduzindo também a um maior ruído durante a combustão. Por outro lado, os números mais elevados de número de cetano promovem a rápida autoignição do combustível, e muitas vezes conduzem a uma redução das emissões de óxidos de nitrogênio (NOx), em particular quando o motor opera a baixa carga [1-3].

Especificações européias determinam um número de cetano de biocombustível de pelo menos 51, enquanto que nos EUA o limite mínimo de NC é mais baixo, 47. No Brasil ainda não foi estabelecido um valor mínimo para o número de cetano do biodiesel. Alguns autores ainda destacam a interdependência entre número de cetano e o grau de insaturação. O número de cetano diminui à medida que o número de insaturações aumenta, isto é, conforme a composição torna-se mais rica em ésteres de ácido linoleico e/ou linolênico. Em contraste, os ésteres altamente saturados, tais como os derivados de coco, dendê e sebo, por exemplo, apresentam os maiores valores de NC [4-6].

Esta propriedade pode ser obtida de três maneiras diferentes. Primeiramente é possível

*Corresponding author. E-mail: carlaruschel@gmail.com

calculá-la através de uma equação de quatro variáveis, que é maneira mais comum e utilizada, inclusive nos programas de monitoramento da qualidade dos combustíveis, a qual se nomeia índice de cetano. Porém este método referente à norma ASTM D4737 não foi desenvolvido a rigor para calcular o índice de cetano para blendas e sim somente para óleo diesel puro [7].

Esta propriedade pode então, ser verificada através do teste de qualidade de ignição ou *Ignition Quality Tester*– IQT, no qual se obtém o número de cetano derivado, nomeado desta forma por ser obtido por meio do teste realizado neste equipamento específico, que realiza a queima do combustível em uma câmara fechada. O IQT determina a qualidade da ignição de misturas de óleo diesel e biodiesel através da medição direta do atraso de ignição do combustível alimentado através de um bico injetor, em uma câmara de volume constante, com temperatura e pressão controladas automaticamente. Este método no Brasil tem sua metodologia regulada pela ANP (Agência Nacional de Petróleo, Gás Natural e Biocombustíveis) através da norma ASTM D 6890 - *Standard Test Method for Determination of Ignition Delay and Derived Cetane Number* (DCN) *of Diesel Fuel Oils by Combustion in a Constant Volume Chamber*. No entanto, apresenta algumas ressalvas, tais como: tempo de análise de 20 minutos e utilização de gases de arraste e combustão de alto custo [8].

Já o número de cetano propriamente dito é determinado quando se verifica esta propriedade, testando o combustível diretamente através de um motor, semelhante ao dos veículos comerciais, adequado para fins deste tipo de estudo, porém este teste tem alto custo de operação e necessita uma grande quantidade de amostra de combustível [9] enquanto as duas primeiras técnicas fazem, portanto, apenas boas aproximações do valor desta propriedade.

Esta característica é de extrema importância, uma vez que o número de cetano relaciona-se diretamente com a qualidade da queima do combustível. Deste modo, tem se tornado cada vez mais importante, pesquisas com metodologias alternativas mais rápidas, limpas e de menor custo para a determinação desta propriedade em diferentes misturas de biodiesel/diesel, uma vez que a tendência atual é de aumentar cada vez mais a quantidade de biodiesel presente no óleo diesel comercial.

Neste sentido, a espectroscopia no infravermelho médio (MIR) vem se mostrando como uma ótima alternativa em diferentes áreas pelas vantagens que apresenta em relação a outras técnicas analíticas, sendo que, entre elas, a mais relevante é a capacidade de análise de amostras tanto líquidas quanto sólidas sem requerer um pré-tratamento da amostra. Essa característica torna esta técnica especialmente interessante, por possibilitar uma análise direta e rápida dos produtos resultando em benefícios econômicos e ambientais nas mais diversas áreas de estudos, como a farmacêutica, ambiental, alimentícia etc. [10,11]. Sua utilidade tem sido comprovada também na caracterização de derivados do petróleo, como a gasolina e o diesel, especialmente quando associados a métodos multivariados de calibração, tais como PLS (*Partial Least Squares*) [12, 13], que são utilizados na construção de modelos de previsão da composição ou propriedades [14] e suas variações com algoritmos baseados na seleção de intervalos espectrais de maior seletividade, que podem ser amplamente empregados, como por exemplo iPLS (*Interval Partial Least Squares*), biPLS (*Backward Interval Partial Least Squares*) e siPLS (*Synergy Interval Partial Least Squares*) [10].

O método de mínimos quadrados parciais por intervalo (iPLS) seleciona as regiões espectrais, que contém as variáveis a fim de produzir os melhores modelos, retirando informações irrelevantes, diminuindo erros de predição, produzindo métodos de calibração mais robustos [15-18]. O espectro é dividido em intervalos menores, onde são construídos modelos de PLS com cada sub-região, com o número de variáveis latentes mais apropriado para cada intervalo [18, 19].

Para um modelo ser eficiente, ele deve ser capaz de descrever adequadamente as circunstâncias reais considerando preferencialmente todas as variações presentes. Neste método de calibração, algumas medidas são utilizadas para determinar o número adequado de variáveis latentes do modelo, como o cálculo do RMSECV (*Root Mean Square Error of Cross Validation*), através da equação 1.

$$RMSE = \sqrt{\frac{\sum_{i=1}^{n} \left(y_i - \hat{y}_i\right)^2}{n}} \qquad \text{(Eq. 1)}$$

Onde n é o número total de amostras de blendas de biodiesel/diesel utilizados, y_i é o valor do número de cetano medido através do teste de qualidade de ignição (método de referência) e $\hat{y}_i$ é o valor do número de cetano predito pelo modelo que utilizou os espectros de infravermelho juntamente com PLS e

suas variantes.

Os diferentes algoritmos PLS com seleção de variáveis, permitem relacionar subintervalos de espectros, pela construção de modelos por combinação ou exclusão de intervalos, pelos algoritmos denominado de regressão por mínimos quadrados parciais por sinergismo (siPLS) ou exclusão (biPLS), respectivamente [20, 21]. A combinação de intervalos que apresenta menor RMSECV, geralmente apresenta maior seletividade com a propriedade estudada, fornecendo melhores coeficientes de correlação e os menores erros de predição [18, 22, 23].

Neste sentido, o objetivo desta pesquisa foi avaliar o número de cetano de blendas de biodiesel/diesel através da espectroscopia no infravermelho médio juntamente com a análise multivariada por mínimos quadrados parciais, utilizando os algoritmos iPLS, biPLS e siPLS para a seleção do intervalo espectral.

2. MATERIAIS E MÉTODOS

Produção das blendas

Para este estudo foram produzidos diferentes tipos de biodiesel a partir de óleo de soja comercial, óleo residual de fritura e gordura vegetal hidrogenada com metanol ou etanol seguindo a metodologia TDSP [24]. O percentual de conversão do óleo/gordura em biodiesel foi calculado a partir dos respectivos espectros de ^{1}H-RMN das amostras de biodiesel [25].

No total foram preparadas 55 amostras das misturas em estudo a partir de óleo diesel S500 e dos diferentes tipos de biodiesel em várias proporções: 5, 10, 20, 50 e 75% de biodiesel, além do óleo diesel e do biodiesel puros. Os valores do número de cetano foram determinados segundo a norma ASTM D 6890 empregando um equipamento *Ignition Quality Tester LM (Advanced Engine Technology LTDA)*.

Obtenção dos espectros no infravermelho

A aquisição dos espectros das blendas de biodiesel/diesel foi realizada num espectrômetro de infravermelho médio modelo Spectrum 400 da marca Perkin Elmer, sendo utilizado um acessório de reflexão total atenuada horizontal (HATR) com cristal de seleneto de zinco (ZnSe). Para cada blenda, os espectros foram obtidos na faixa espectral compreendida entre 4000-650 cm^{-1}, sendo utilizada resolução de 4 cm^{-1}, 16 varreduras e realizado em duplicata. A partir das replicatas de cada amostra foram obtidos os espectros médios com os quais foram desenvolvidos os modelos de regressão multivariada.

Determinação do número de cetano pela metodologia ASTM D 6890

Para a obtenção do número de cetano é necessária uma filtração prévia das amostras por um filtro de 5 micrômetros de porosidade, acoplado a uma seringa de vidro para retirar qualquer resíduo sólido da amostra que possa entupir o bico injetor do equipamento. O volume de amostra necessário é de 40 mL, o tempo de cada análise é de 20 minutos e o resultado final é a média de 32 varreduras. O equipamento que realiza o teste de qualidade de ignição faz a completa combustão da mistura combustível sob condições controladas de temperatura e pressão. A qualidade de ignição do combustível tem uma relação inversa com o tempo de atraso da ignição e direta com o número de cetano derivado ou *derived cetane number* (DCN), um número adimensional que é o resultado final obtido em cada análise.

O tempo de atraso da ignição no IQT é medido pela diferença entre o tempo de injeção da amostra dentro da câmara e o tempo em que esta leva para explodir dentro da mesma. O cálculo do DCN é realizado através da equação 2, conforme a norma ASTM D 6890 e depende somente do valor do atraso de ignição [26].

$$DCN = 4{,}460 + \frac{186{,}6}{ID} \qquad \text{(Eq. 2)}$$

onde DCN = *Derived Cetane Number* ou Número de Cetano Derivado (adimensional) e ID = *Ignition Delay* ou Atraso de Ignição (milisegundos).

Construção dos modelos multivariados

Os dados de infravermelho foram modelados utilizando o software Matlab® e a ferramenta iPLSToolbox [15]. No total foram utilizadas 55 amostras, das quais foram selecionados 20 espectros de infravermelho dessas amostras, através do algoritmo de Kennard-Stone [27], para compor o conjunto de previsão e 35 espectros das amostras para o conjunto de calibração. Na fase de pré-

processamento destes dados, eles foram centrados na média.

3. RESULTADOS E DISCUSSÕES

A partir dos dados de RMN-^{1}H, foram obtidos os valores de rendimento da produção dos diferentes biodieseis, sendo para a rota metílica de 98%, 95% e 99%, respectivamente, para os óleos de soja, residual de fritura e da gordura vegetal hidrogenada; e para a rota etílica de 95%, 93% e 96%, respectivamente, para os óleos de soja, residual de fritura e da gordura vegetal hidrogenada [28].

Os resultados obtidos para o número de cetano das amostras das blendas de biodiesel/diesel, a partir do método de referência utilizando o equipamento IQT, variaram entre 45,57-57,20, para o conjunto de 55 amostras.

A partir dos espectros obtidos por infravermelho, de 4000 a 650 cm^{-1}, estes dados foram centrados na média, sendo os modelos iPLS, biPLS e siPLS construídos com 35 amostras para o conjunto de calibração e 20 amostras para o conjunto de previsão, totalizando 55 amostras.

Com base nos diferentes algoritmos utilizados (iPLS, biPLS e siPLS), subdividindo os espectros em 4, 8, 16, 32 e 64 intervalos, foram obtidos vários modelos cujos melhores resultados são apresentados na Tabela 1.

Tabela 1. Resultados obtidos para os melhores modelos iPLS, biPLS e siPLS utilizando os dados espectrais HATR-FTIR.

Modelo	Intervalo (s)	VL (s)[a]	RMSECV[b]	r^2(cv)[c]	RMSEP[d]
Global	Todos	5	0,772	0,947	0,318
iPLS4	4	3	0,695	0,956	0,495
iPLS8	7	5	0,728	0,953	0,314
iPLS16	15	4	0,849	0,935	0,532
iPLS32	26	4	0,818	0,939	0,488
iPLS64	22	4	0,882	0,929	0,488
biPLS4	1 4	3	0,695	0,956	0,505
biPLS8	1 2 7 8	3	0,695	0,956	0,505
biPLS16	1 2 4 8 9 10 12 13 14 16	5	0,688	0,956	0,422
biPLS32	11 13 22 23 26 32	4	0,664	0,960	0,353
biPLS64	24 28 30 35 49 51 64	4	0,612	0,966	0,375
si2PLS8	7 8	3	0,695	0,956	0,495
si2PLS16	13 16	3	0,642	0,962	0,353
si2PLS32	29 32	4	0,671	0,958	0,494
si2PLS64	49 52	5	0,663	0,960	0,344
si3PLS8	1 7 8	3	0,695	0,956	0,495
si3PLS16	1 13 16	3	0,642	0,962	0,353
si3PLS32	25 26 32	3	0,624	0,964	0,390
si3PLS64	19 21 48	8	0,589	0,968	0,502

[a] VL = número de variáveis latentes; [b] RMSECV = erro quadrático médio de validação cruzada; [c] r^2 (cv) = coeficiente de determinação; [d] RMSEP = erro quadrático médio de previsão

Dentre os modelos empregando a regressão multivariada destacaram-se os modelos i8PLS, bi32PLS e si2PLS16, sendo que os respectivos valores de RMSECV, RMSEP e coeficientes de correlação (r) estão apresentados na Tabela 1.

Considerando o melhor modelo obtido para o iPLS, tem-se na Figura 1 o espectro do modelo de iPLS dividido em 8 intervalos e seus respectivos erros

de validação cruzada para cada intervalo e para o modelo global (espectro inteiro). Observando esta figura pode-se verificar que a região apresentada no intervalo 7 possui um dos menores valores de erro e corresponde a região espectral na faixa de aproximadamente 1500 a 1050 cm^{-1}, onde são observadas sobreposição de bandas, além de picos na região de 1000 a 900 cm^{-1} referentes a deformação angular simétrica fora do plano de ligação C-H de olefinas. Picos em 1200 cm^{-1} referentes a deformação axial da ligação CC(=O)-O do éster, enquanto picos em torno de 1183 cm^{-1} podem ser relacionados a deformação axial assimétrica da ligação O-C-C. A região de 1300 a 900 cm^{-1} é conhecida como região de ‘‘impressão digital’’ do espectro que inclui várias bandas acopladas [29].

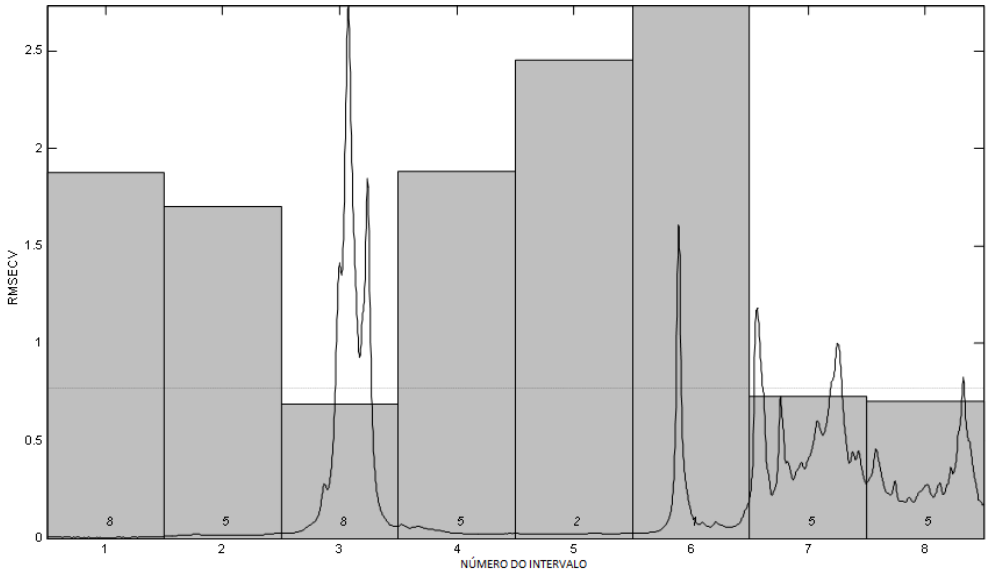

Figura 1. Valores de RMSECV para os intervalos (altura das barras) e para o modelo global (linha tracejada), Os números dentro das barras correspondem às Variáveis Latentes para cada intervalo.

Em recente artigo que utiliza dados de ATR-FTIR para determinar o número de cetano em 93 amostras de diesel da Croácia, os autores destacam que a região compreendida entre 1670-650 cm^{-1} apresentou menores erros de validação cruzada (RMSECV), porém os autores não apresentam resultados com previsão de amostras externas ao modelo [30]. Esta faixa espectral é concordante com os resultados obtidos para o iPLS na previsão do número de cetano para as blendas de biodiesel/diesel utilizadas no presente estudo.

Na Figura 2 são apresentados os valores de referência do número de cetano (obtidos por IQT) *versus* os valores previstos pelo modelo HATR-FTIR/PLS utilizando a mesma região do espectro indicada na Figura 1, obtendo RMSEP de 0,314; RMSECV de 0,728 e apresentando coeficiente de determinação r_{cv}^2 de 0,953. Para o melhor modelo biPLS, o espectro foi dividido em 32 intervalos sendo selecionados e combinados os intervalos 11 13 22 23 26 32 que resultam em menores valores de erro. As regiões destacadas na Figura 3 contêm sinais importantes como os estiramentos simétricos e assimétricos dos grupos CH_2 e CH_3 de 2950-2840 cm^{-1}, deformação angular simétrica do grupo CH_3 de 1390-1370 cm^{-1}, deformação angular assimétrica no plano do CH_2 de 725-720 cm^{-1}, presentes tanto no diesel quanto no biodiesel, além do estiramento da carbonila do éster em 1750-1725 cm^{-1}.

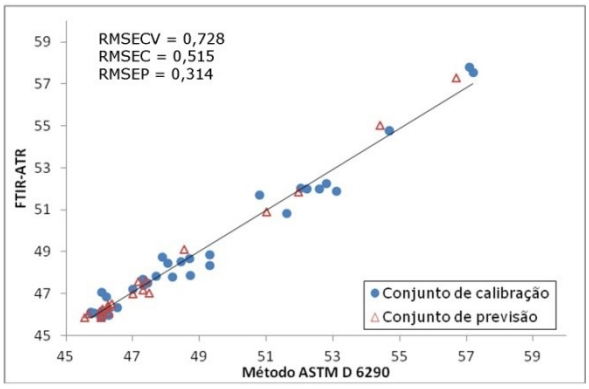

Figura 2. Valores de referência *versus* valores previstos para o número de cetano das blendas de biodiesel/diesel, para o modelo i8PLS usando a região espectral de 1500 a 1050 cm^{-1}.

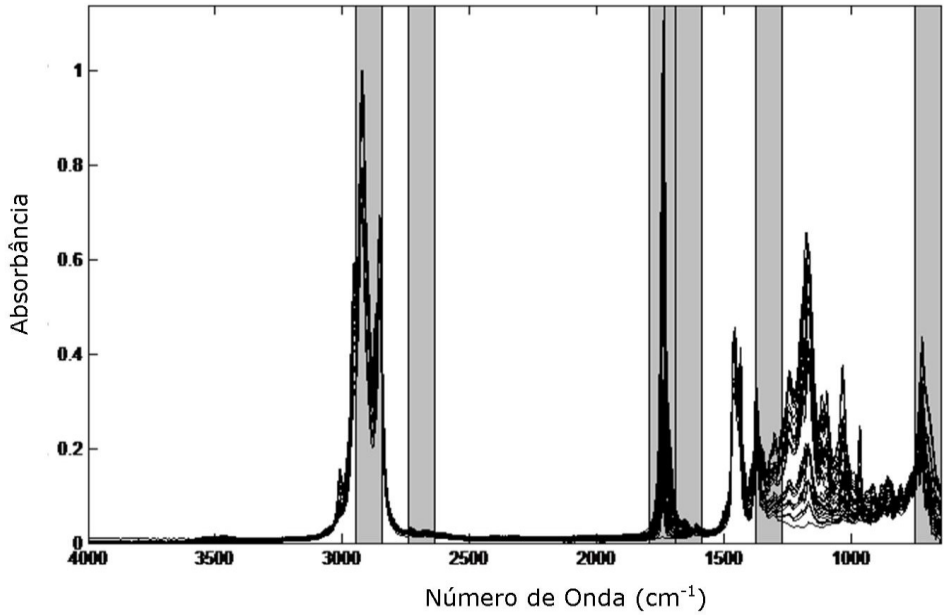

Figura 3. Regiões do espectro HATR-FTIR selecionadas pelo melhor modelo bi32PLS.

Na Figura 4 são apresentados os valores de referência do número de cetano (obtidos por IQT) *versus* os valores previstos pelo modelo HATR-FTIR/PLS utilizando as mesmas regiões do espectro mostradas na Figura 3, com valor de RMSEP de 0,353; RMSECV de 0,664 e apresentando coeficiente de determinação r_{cv}^2 de 0,960.

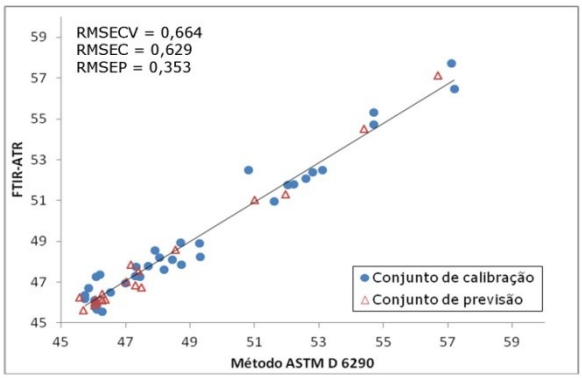

Figura 4. Valores de referência *versus* valores previstos para o número de cetano das blendas de biodiesel/diesel, para o modelo bi32PLS usando a combinação de várias regiões espectrais.

Considerando o melhor modelo obtido para o siPLS, tem-se na Figura 5 o espectro dividido em 16 intervalos combinados 2 a 2 e seus respectivos erros de validação cruzada para cada intervalo e para o modelo global (espectro inteiro). Observando a figura pode-se verificar que a combinação das regiões apresentadas nos intervalos 13 e 16, possuem o menor valor de erro e correspondem as regiões espectrais nas faixas de 1485-1277 cm^{-1} e 858-650 cm^{-1}, onde são observadas bandas de absorção atribuídas aos sinais dos hidrocarbonetos do diesel e a cadeia lateral dos ésteres (biodiesel).

Na Figura 6 são apresentados os valores de referência do número de cetano (obtidos por IQT) *versus* os valores previstos pelo modelo MID/PLS utilizando as mesmas regiões do espectro indicada na Figura 5, obtendo RMSEP de 0,353; RMSECV de 0,642 e apresentando coeficiente de determinação r_{cv}^2 de 0,962.

Apesar dos melhores modelos selecionados anteriormente apresentarem desempenho equivalente na previsão de amostras externas ao modelo (RMSEP), e estes semelhantes ao modelo global (sem seleção de variáveis), destaca-se o modelo siPLS dividido em 16 intervalos e agrupando-os em 2 intervalos, pois este utiliza somente 3 variáveis latentes. A redução do número de variáveis latentes, sem perda da exatidão, resulta em modelos com menor vulnerabilidade e maior robustez. Este modelo utilizou a combinação das regiões espectrais 1485-1277 cm^{-1} e 858-650 cm^{-1} que correspondem aos sinais dos hidrocarbonetos presentes no óleo diesel, bem como da cadeia lateral dos ésteres presentes no biodiesel, indicando a dependência desta propriedade tanto com o tamanho da cadeia quanto com a presença de ramificações.

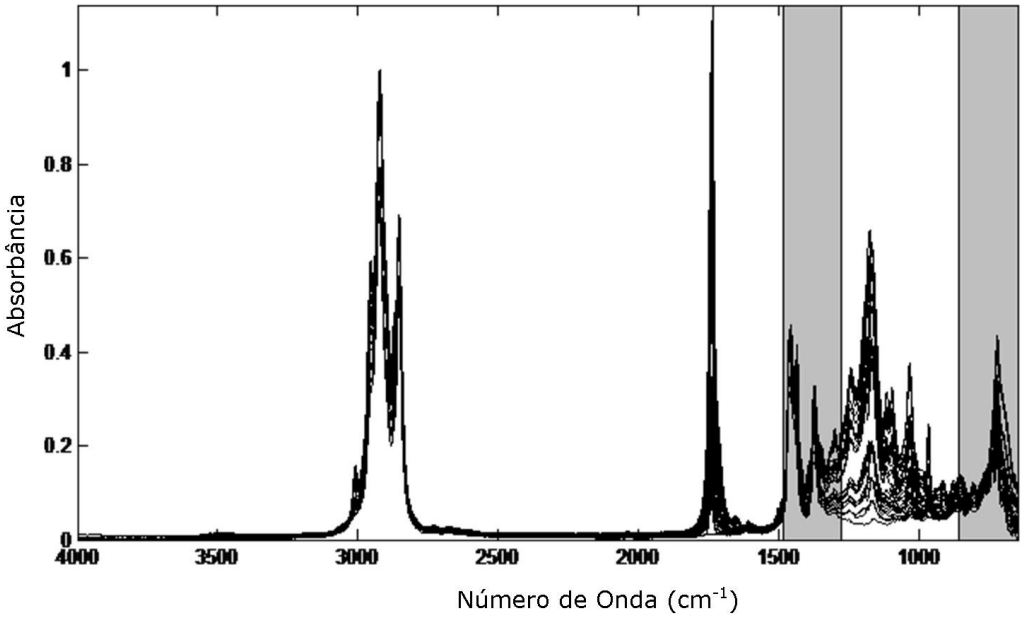

Figura 5. Regiões selecionadas pelo modelo si2PLS16: 1485-1277 cm^{-1} e 858-650 cm^{-1}.

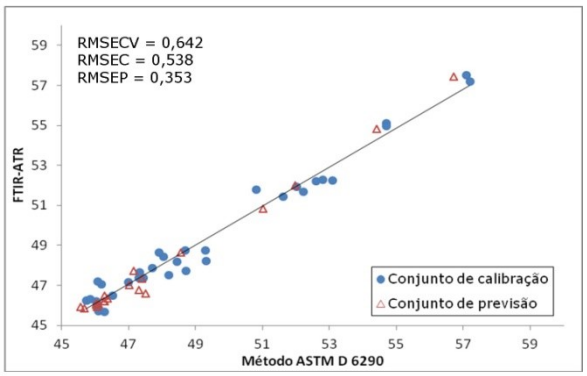

Figura 6. Valores de referência *versus* valores previstos para o número de cetano das blendas de biodiesel/diesel, para o melhor modelo si2PLS16 usando a combinação das regiões espectrais de 1485-1277 cm^{-1} e 858-650 cm^{-1}.

Além disso, a partir dos dados apresentados para os melhores modelos de calibração multivariada, pode-se observar que foi obtida uma ótima correlação entre os valores de referência, do número de cetano das amostras das blendas de biodiesel/diesel obtido por IQT conforme a norma ASTM D 6890 e os valores previstos pelos métodos aplicados neste estudo empregando tanto o iPLS dividindo o espectro em 8 intervalos, biPLS com 32 intervalos ou ainda o siPLS selecionando a combinação de 2 intervalos quando o espectro foi dividido em 16 partes.

4. CONCLUSÕES

A metodologia alternativa proposta neste trabalho, utilizando infravermelho (HATR/FTIR) e os algoritmos para seleção de regiões espectrais como iPLS, biPLS e siPLS, apresentou-se como uma ferramenta eficaz, limpa, rápida e de baixo custo para quantificar a propriedade número de cetano de blendas de biodiesel/diesel, com baixos erros de previsão. Portanto, este método possui diversas vantagens comparativamente a metodologia descrita na norma ASTM D 6890, podendo aprimorar o controle de qualidade dos combustíveis.

Todos os melhores modelos obtidos para cada algoritmo de seleção proporcionaram resultados satisfatórios, com potencialidade para aplicação em futuras metodologias inclusive na determinação de outros parâmetros de qualidade destas blendas. Além disto, destaca-se a possibilidade de aplicação desta metodologia para outros combustíveis, como etanol e gasolina.

5. AGRADECIMENTOS

Os autores agradecem ao CNPq pelo apoio financeiro, ao INCT-Bioanalítica, ao CECOM/UFRGS pelas análises de infravermelho e a REFAP pelo óleo diesel.

6. REFERÊNCIAS E NOTAS

[1] Giakoumis, E. G.; Rakopoulos, D.; Dimaratos, A. M.; Rakopoulos, D. C. *Proc. Inst. Mech. Eng. Pt. D J. Automobile Eng.* **2012**, *226*, 971. [CrossRef]

[2] Peterson, C. L.; Taberski, J. S.; Thompson, J. C.; Chase, C. L. *T. Am. Soc. Agr. Bio. Eng.* **2000**, *43*, 1371.

[3] Zhang, Y.; Boehman, A. L. *Energy Fuels* **2007**, *21*, 2003. [CrossRef]

[4] Hoekman, S. K.; Broch, A.; Robbins, C.; Ceniceros, E.; Natarajan, M. *Renew. Sust. Energ. Rev.* **2012**, *16*, 143. [CrossRef]

[5] Giakoumis, E. G.; *Rev. Renew. Energ.* **2013**, *50*, 858. [CrossRef]

[6] Lapuerta M.; Rodriguez-Fernandez J.; de Mora, E. F. *Energ. Policy* **2009**, *37*, 4337. [CrossRef]

[7] ASTM D4737 – 10 Standard Test Method for Calculated Cetane Index by Four Variable Equation 2010.

[8] ASTM D 6890 – 11b Standard Test Method for Determination of Ignition Delay and Derived Cetane Number (DCN) of Diesel Fuel Oils by Combustion in a Constant Volume Chamber 2011.

[9] ASTM D613 – 10a Standard Test Method for Cetane Number of Diesel Fuel Oil 2010.

[10] Xiaobo, Z.; Jiewen, Z.; Povey, M. J.W.; Holmes, M.; Hanpin, M. *Anal. Chim. Acta***2010,** *667*, 14. [CrossRef]

[11] Cramer, J. A.; Kramer, K. E.; Johnson, K. J.; Morris, R. E.; Rose-Pehrsson, S. L. *Chemometr. Intell. Lab.* **2008**, *92*, 13. [CrossRef]

[12] Pasquini, C.; Bueno, A. F. *Fuel* **2007**, *86*, 1927. [CrossRef]

[13] Fernandes, H. L.; Raimundo Jr, I. M.; Pasquini, C.; Rohwedder, J. J. R. *Talanta* **2008**, *75*, 804. [CrossRef]

[14] Brereton, R. G. Chemometrics: Data Analysis for the Laboratory and Chemical Plant, Chichester: John Wiley & Sons, 2003. [CrossRef]

[15] Norgaard, L.; Saudland, A.; Wagner, J.; Nielsen J. P.;
[27] de Tecnologia Química, Bloco A – LACAUT, Departamento de Engenharia Química, Universidade Federal do Paraná,2008. [Link]

[28] Kennard, R. W.; Stone, L. A. *Technometrics* **1969**, *11*, 137. [CrossRef]

[29] Guzatto, R.; Defferrari, D.; Reiznautt, Q. B.; Cadore, I. R.; Samios, D. *Fuel* **2012**, *92*, 197. [CrossRef]

Munck, L.; Engelsen, S. B. *Appl. Spectrosc.* **2000**, *54*, 413. [CrossRef]

[16] Parisotto, G.; Marques, M.; Hermes, A. L.; Flores, E. M. M.; Ferrão, M. F. *Orbital: Electron. J. Chem.* **2009**, *1*, 38. [Link]

[17] Ferrão, M. F.; Viera, M. D. S.; Pazos, R. E. P.; Fachini, D.; Gerbase, A.E.; Marder, L. *Fuel* **2011**, *90*, 701. [CrossRef]

[18] Müller, A. L. H.; Picoloto, R. S.; Mello, P. A.; Ferrão, M. F.; Dos Santos, M. F. P.; Guimarães, R. C. L.; Müller, E. I.; Flores, E. M. M. *Spectrochim. Acta A* **2012**, *89*, 82. [CrossRef]

[19] Müller, A. L. H.; Picoloto, R. S.; Ferrão, M. F.; Silva, F. E. B.; Müller, E. I.; Flores, E. M. M. *Drug Test. Anal.* **2012**, *4*, 500. [CrossRef]

[20] Munck, L.; Nielsen, J.P.; Moller, B.; Jacobsen, S.; Sondergaard, I.; Engelsen, S.B.; Norgaard, L.; Bro, R. *Anal. Chim. Acta***2001**, *446*, 169. [CrossRef]

[21] Francesquett, J. Z.; Viera, M. S.; Lovato, R. H.; Fachini, D.; Gerbase, A. E.; da Costa, A. B.; Ferrão, M. F. *Tecno-Lógica* **2010**, *14,* 87.

[22] Parisotto, G.; Ferrão, M. F.; Muller, A. L. H.; Müller, E. I.; Santos M. F. P.; Guimarães, R. C. L.; Dias, J. C. M.; Flores, E. M. M. *Energy & Fuels* **2010**, *24,* 5474. [CrossRef]

[23] Wu, D.; He, Y.; Nie, P.; Cao, F.; Bao, Y. *Anal. Chim. Acta* **2010**, *659*, 229. [CrossRef]

[24] Samios, D.; Pedrotti, F.; Nicolau, A.; Reiznautt, Q. B.; Martini, D. D.; Dalcin, F. M. *Fuel Process Technology* **2009**, *90*, 599. [CrossRef]

[25] Ruschel, C. F. C. Avaliação De Blendas De Óleo Diesel E Biodiesel Através Do Teste Da Qualidade De Ignição (IQT) [Master´s thesis] Porto Alegre, Brasil: Departamento de Química, Universidade Federal do Rio Grande do Sul, 2013. [Link]

[26] de Souza, T. Revisão da Equação de Cálculo de Índice de Cetano para as Características do Diesel Comercializado no Paraná [Master's thesis] Curitiba, Brasil: Centro Politécnico – Usinas Piloto

[30] Silverstein, R. M.; Webster, F. X.; Kiemle, D. Spectrometric Identification of Organic Compounds, New York: Wiley, 2004.

[31] Marinović, S.; Krištović, M.; Špehar, B.; Rukavina, V.; Jukić, A. *J. Anal. Chem.* **2012**, *67*, 939. [CrossRef]

Orbital: The Electronic Journal of Chemistry
journal homepage: www.orbital.ufms.br
ISSN 1984-6428

| Vol 6 | | No. 1 | | January-March 2014 |

Full Paper

Evaluation of Two Biosorbents in the Removal of Metal Ions in Aqueous Using a Pilot Scale Fixed-bed System

André G. Oliveira[a], Jefferson P. Ribeiro[b], Diego Q. Melo[a], Francisco W. Sousa[c], Vicente O. S. Neto[d], Giselle S. C. Raulino[b], Rivelino M. Cavalcante[e], Ronaldo F. Nascimento[a*]

[a]*Department of Analytical Chemistry and Physical Chemistry – Federal University of Ceará. Rua do Contorno, S/N Campus do Pici, Bl. 940 – CEP: 60451-970 – Fortaleza, CE – Brazil.*
[b]*Department of Hydraulic and Environmental Engineering – Federal University of Ceará. Rua do Contorno, S/N Campus do Pici, Bl. 713 – CEP: 60451-970 – Fortaleza – CE – Brazil.*
[c]*Federal Institute of Education, Science and Tecnology – Campus Crateús –Rua Lopes Vieira, s/n -CEP: 63700-000 – Crateús – CE – Brazil.*
[d]*Department of Chemistry – State University of Ceará. Rua Solon Medeiros, S/N – BR 020 – CEP: 63660-000 – Tauá – CE – Brazil.*
[e]*Institute of Marine Sciences, Federal University of Ceará. Av. Abolição,3207 – Meireles – CEP: 60165-081 – Fortaleza – CE – Brazil.*

Article history: Received: 25 April 2014; revised: 24 February 2014; accepted: 17 March 2014. Available online: 02 April 2014.

Abstract: The aim of the present work was to investigate the adsorption of toxic metal ions copper, nickel and zinc from aqueous solutions using low cost natural biomass (sugar cane bagasse and green coconut fiber) in pilot scale fixed-bed system. The Hydraulic retention time (HRT) was 229 minutes and the lowest adsorbent usage rate (AUR) found was 0.10 $g.L^{-1}$ for copper using green coconut fibers. The highest values of adsorption capacities founded were 1.417 and 2.772 $mg.g^{-1}$ of Cu(II) ions for sugarcane bagasse and green coconut fibers, respectively. The results showed that both sugarcane bagasse and green coconut fiber presented potential in the removal of metal ions copper, nickel and zinc ions from aqueous solution and the possible use in wastewater treatment station.

Keywords: multicolumn adsorption; toxic metal ions; wastewater

1. INTRODUCTION

Electroplating industries are considered one of the oldest, concentrating in areas of surface finishing and metal deposition [1]. However, these industries produce wastewater contaminated with toxic metals, becoming one of the most hazardous among chemical industries [2]. The contamination of water bodies by wastewater containing toxic metal ions is a worldwide environmental problem [3-5].

Toxic metal ions, known commonly as heavy metals, are classified as toxic materials due to their non-biodegradability and bioaccumulation tendency in living organisms. Its excessive amount cause health problem in animals, plants and humans [3]. In low concentration, these metal ions are essential to all living organisms [4]. However, these metals can cause various types of acute and chronic disease in humans like hemochromatosis, fever, lesions in the central nervous system, risk of lung cancer, etc., if ingested beyond the permissible levels [1-4, 6-7].

There are several technologies for removing toxic metal ions from wastewater: ion exchange, membrane separation, reverse osmosis, chemical precipitation, coagulation-flocculation, flotation and electrochemical treatment [2-3, 5-6, 8-9]. However, these methods have some disadvantages such as being costly, operation costs and high maintenance, ineffectiveness in removing traces of metal ions, and formation of polluted byproducts [3, 5-6].

In this context, adsorption is an attractive method because of its ease of operation and efficiency in removing toxic metal ions from wastewater [6]. Among the most used adsorbents the activated carbon stands, though in some cases their use becomes impractical due to its high cost [10]. With increasing

*Corresponding author. E-mail: ronaldo@ufc.br

environmental awareness and government policy rigidity, it became necessary to develop new ways to remove contaminants using low-cost methods [4]. Natural origin adsorbents have become an interesting alternative for removal of toxic metal ions using fixed-bed technology [3, 10-12].

The purpose of the study was to investigate the adsorption of toxic metal ions copper, nickel and zinc from aqueous solutions using sugar cane bagasse and green coconut fiber in fixed-bed system. The breakthrough curves were evaluated and Thomas and Yoon & Nelson models were applied to describe the dynamic performance of the adsorption process.

2. MATERIAL AND METHODS

Chemical and reagents

Standard solutions of metal ions composed of $Zn(NO_3)_2.6H_2O$, $Ni(NO_3)_2.6H_2O$ and $Cu(NO_3)_2.6H_2O$ were purchased from Merck (São Paulo, Brazil). The concentrations of ions were determined by atomic absorption spectrophotometry (AAS, GBC 933 plus model) in an air-acetylene flame.

Adsorbent preparation

Sugar cane bagasse and green coconut fibers were used as adsorbents, which were initially crushed, and the fractions corresponding to 20-150 mesh were used in the work. The mass of each adsorbent used was 1000 g.

Column studies

The column system, Figure 1, consist of 5 PVC columns (160 cm length and 5.4 cm I.D each) connected in series and a pump that provided a continue solution circulation through the columns system. Firstly, the columns were conditionated with deionized water and the flow rate of 80 $mL.min^{-1}$ was achieved. A volume of 50 L of multielement synthetic solution (pH = 5.0) was percolated and aliquots of 50 mL were collected at every 15 min at the exit of the column. The adsorption capacity was determined from breakthrough curves of multielement synthetic solutions of metal ions Cu(II), Ni(II) and Zn(II). The experiments with the adsorbent sugar cane bagasse were performed with the concentration of solution of 216 $mg.L^{-1}$ Cu(II), 60 $mg.L^{-1}$ Zn(II) and 7 $mg.L^{-1}$ Ni(II), whereas, the experiments with green coconut fiber were performed with the concentration of solution of 126 $mg.L^{-1}$ Cu(II), 42 $mg.L^{-1}$ Zn(II) and 6 $mg.L^{-1}$ Ni(II).

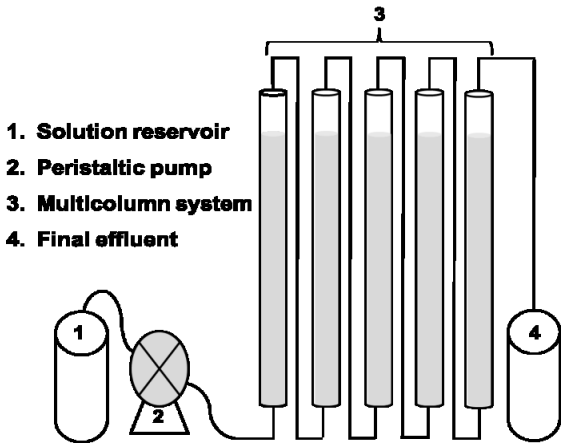

Figure 1. Schematic diagram of the experimental set up for a continuous process.

Designing of fixed bed biosorbent

A conventional fixed bed system is compound of a column where particles of biosorbent are placed in contact with the solution to be treated. The dynamic behavior and efficiency of a fixed-bed column are described in terms of effluent/influent (C/C_0) concentration versus time or volume of treated liquid, called breakthrough curve [10, 13].

In an ideal breakthrough curve it is assumed that removal of adsorbate is complete in the early stages of operation. Usually the breakthrough point (C_b) is the point at that the concentration of adsorbate effluent the column is 5% of the initial concentration (C_0) and the exhaustion point (C_x), around 90% of C_0 [14]. The primary adsorption zone (PAZ) or mass transfer zone (MTZ) in the fixed bed adsorber develops between the section of the column that is saturated with adsorbate and section that still contains no saturated biosorbent. It is represented by the portion of the curve between C_x and C_b which is assumed to have a constant length or depth, δ. This zone moves through the column in the flow direction at a certain speed, and when reaches the end of column, the concentration of adsorbate in the effluent begins to increase gradually. The column is operational until the MTZ reaches the end of the column and effluent is practically free adsorbate [14-17].

Some parameters that characterize the PAZ are described by [14, 17, 18] and were determinate in this work according to them. These parameters are listed

below: Total time to establish the PAZ (t_x), Time necessary to move the PAZ along the column (t_δ), Length of PAZ (δ), Time necessary for the formation of PAZ (t_f), Fractional capacity of biosorbent (F), Percentage of saturation in the column (%S).

The maximum adsorption capacity of biosorbent is given by equation 1 [15]:

$$q_{exp} = \frac{C_0 * F_m}{m_s} \int_{t=0}^{t=x} \left(1 - \frac{C}{C_0}\right) dt \qquad \text{eq. 1}$$

where q is the maximum adsorption capacity (mg g^{-1}); Co is the initial concentration of solution; C is the concentration of adsorbate at certain volume; m_s the mass of biosorbent (g); F_m is the volumetric flow (L min^{-1}) and t the time (min.).

Column adsorption models

Several models can be used to calculate kinetic constants and maximum adsorption capacities of a column. In this work, are used the Thomas and Yoon-Nelson models.

Thomas model

This model assumes a fixed bed behavior with continuous flow and uses the Langmuir isotherm for equilibrium and reaction kinetics second order reversible [19, 20]. It is applicable for conditions of favorable and unfavorable adsorption. The Thomas model can be expressed as a function of volume of effluent and in function of time [21, 22], equations 2 and 3.

$$\frac{C_e}{C_o} = \frac{1}{1 + e^{\left[\frac{k_{TH} q_o m}{F} - k_{TH} C_o t\right]}} \qquad \text{eq. 2}$$

The linearized form is described as

$$\ln\left(\frac{C_o}{C_e} - 1\right) = \frac{k_{TH} q_o m}{F} - k_{TH} C_o t \qquad \text{eq. 3}$$

where C_e is the effluent concentration (mg.L^{-1}), C_0 the influent concentration (mg.L^{-1}), F the flow rate (mL.min^{-1}), V the effluent volume (mL), m the mass of the adsorbent (g) and t the time (min), k_{TH} (L.mg^{-1}.min^{-1}) and q_{TH} (mg.g^{-1}) are the adsorption kinetic rate constant and the maximum adsorption capacity of the column, respectively. The constants (k_{TH}, q_{TH}) can be determined from the plot of ln(C_e/C_0) against t.

Yoon & Nelson Model

Yoon & Nelson [23] developed a relatively simple model, related to adsorption of gases with respect to activated carbon. This model not only is simpler than other designs and does not require detailed data relating to the characteristics of the solute, the type of adsorbent and physical properties of the bed. The nonlinear equation for this model is expressed as:

$$\frac{C_e}{C_o} = \frac{1}{1 + \exp[k_{YN}(\tau - t)]} \qquad \text{eq. 4}$$

The linearized equation of Yoon-Nelson is described as following:

$$t = \tau + \frac{1}{k_{YN}} \ln\left(\frac{C_e}{C_o - C_e}\right) \qquad \text{eq. 5}$$

where Ce and Co are the effluent and influent concentrations (mg.L^{-1}) at a given time *t* and *t*=0, K_{YN}(L.min^{-1}) is the Yoon-Nelson constant, τ (min) is the time required for 50% adsorbate breakthrough. From a linear plot of ln(C_0/Ce–C_0) against time t, values of K_{YN} and τ were determined from the intercept and slope of the plot.

3. RESULTS AND DISCUSSION

Characterization of adsorbent bed

Physical properties of the column bed containing the adsorbent are shown in Table.

Table 1. Physical parameters of the column bed containing the adsorbent.

Properties	Fixed Bed
Column diameter (d_L) (cm)	5.4
Total Bed height (cm)	800
Total area of the column (cm^2)	13610.58
Volume of the empty column (V_L) (cm^3)	18312.48
Mass of adsorbent in the column (g)	1000

Breakthrough curves

The breakthrough curves for studied ions using sugarcane bagasse and green coconut fibers are shown in Figure 2(a) and (b), respectively. It can be seen that breakthrough occurred rapidly for the three metal ions studied. At Figure 2(b) can be seen that copper didn't reach saturation, indicating a great affinity by green coconut fibers and this metal ions. The concentration of metal ions in synthetic solutions were with the

intent of simulate an effluent of an electroplating industry. The higher concentration of copper than nickel and zinc ions may have led to this greater uptake efficiency of copper, instead of nickel and zinc. This concentration gradient favors a higher adsorption of the higher concentration adsorbates in relation to other presents in solution. Sousa et al. [10] studying metal ions uptake using green coconut shell powder in a column system founded the same results.

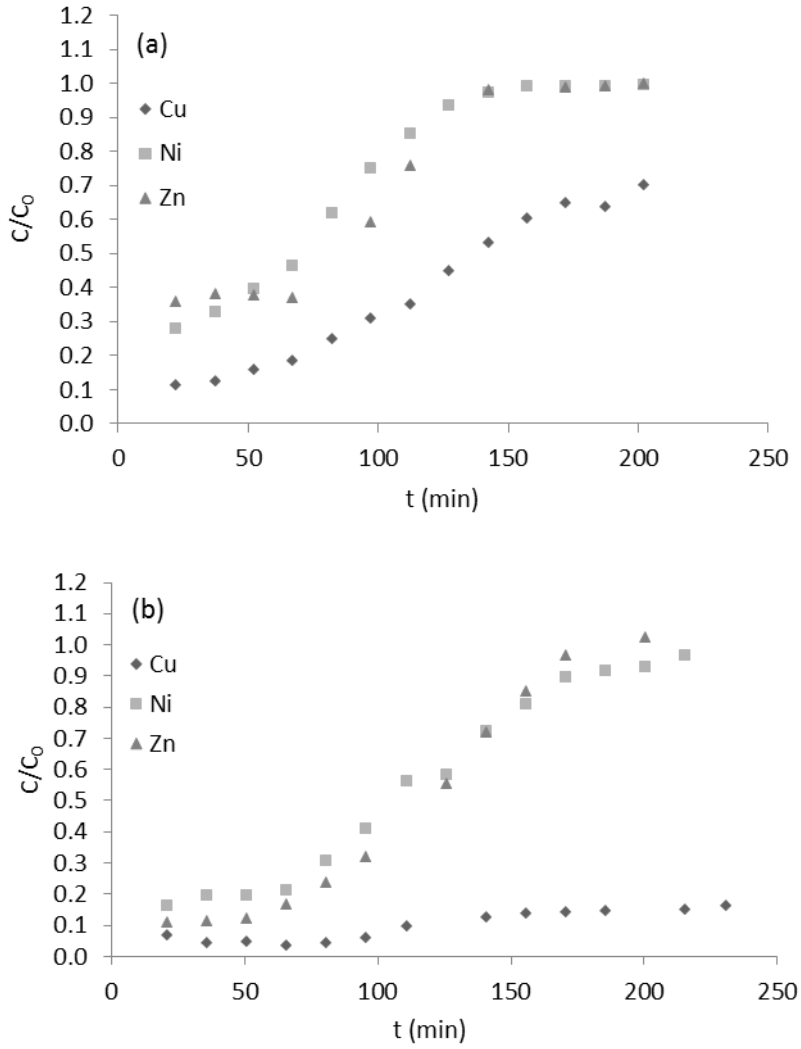

Figure 2. Breakthrough curves for (a) sugarcane bagasse and (b) green coconut fiber. Conditions: pH = 5, mass of adsorbent = 1 kg, flow rate=80 mL.min^{-1}.

Hydraulic retention time (HRT) is a typical parameter of design and operation for columns. Large residence times can lead to a decrease in the contaminant removal while shorter times do not allow an effective contact interaction to occur between the sorbent and sorbate [15, 24]. HRT is given by the ratio between the volume of the column and the flow rate. HRT for studied system was 229 min. Another important parameter is the adsorbent usage rate (AUR) that is the ratio between the weight of biosorbent in the column and the amount of liquid passed into the column at the time breakthrough occurs [15]. AUR gives information about the amount of adsorbent needed to treat a fixed volume of solution. Table 2 shows the breakthrough and exhaustion times, HRT, adsorbent usage rate and adsorption capacity obtained according equation 1.

As can be seen on Table 2, AUR was the same for the three metal ions studies as breakthrough time was the same either. That results means that only 0.57 g of adsorbent are needed to treat 1 L of contaminated solution for sugarcane bagasse and 0.62 g.L^{-1} for

green coconut fibers, exception for copper where AUR was 0.1 $g.L^{-1}$. The low values of AUR are due to the high bed height of the column, leading to a high HRT and high removal of metal ions. This parameter is an important concept in case of industry applies.

Table 2. Breakthrough times (t_b), exhaustion times (t_x), adsorbent usage rate and adsorption capacities (when $C/C_0 = 0.5$) obtained from breakthrough curves of sugarcane bagasse and green coconut fibers (Figure 1).

Adsorbent	Metal ion	t_b(min.)	t_x(min.)	AUR($g.L^{-1}$)	$q_{exp.}$ ($mg.g^{-1}$)
Sugarcane Bagasse	Cu (II)	22	202	0.57	1.417
	Ni (II)	22	127	0.57	0.029
	Zn (II)	22	142	0.57	0.286
Green Coconut Fibers	Cu (II)	140	>250	0.10	2.772
	Ni (II)	20	185	0.62	0.032
	Zn (II)	20	170	0.62	0.248

Table 3 presents the parameters t_x, t_δ, t_f, F, δ and percentage saturation (%S) of the column obtained from the breakthrough curves of Figure 2(a) – (b). The results show that the total time to establish the primary adsorption zone (t_x) was maximum for copper for both adsorbents used. The time required to move adsorption zone through the column (t_δ) was between 105 – 360 min. The time to form the primary adsorption zone (t_f) was between 18 – 42 min for sugarcane bagasse and 14 – 170 min for green coconut fibers. The length of PAZ was between 782 - 993 cm for sugarcane bagasse and 769 – 873 cm for green coconut fiber. This parameter is related to the region in the breakthrough curve situated between breakthrough and exhaustion time. The values obtained for the three metal ions for both adsorbents studied were near or higher than the column length (800 cm) probably due to the breakthrough occurred most of the time at the first point collected.

Table 3. Parameters t_x, t_f, t_δ, F, δ and percentage saturation of column for sugarcane bagasse and green coconut fibers.

Adsorbent	Metal ion	Parameters					
		t_x (min)	t_δ (min)	f	t_f (min)	δ (cm)	%
Sugarcane Bagasse	Cu (II)	202.50	180.40	0.90	18.00	782.24	90.24
	Ni (II)	127.10	105.00	0.59	42.53	993.27	49.71
	Zn (II)	142.10	120.00	0.65	41.61	955.29	58.60
Green Coconut Fibers	Cu (II)	500.00	360.00	0.53	170.46	873.93	48.28
	Ni (II)	215.50	195.00	0.85	30.00	840.98	83.83
	Zn (II)	173.75	153.25	0.91	14.41	769.45	90.95

Fixed bed column modeling

The experimental data obtained were fitted to the most commonly used kinetic models for adsorption in a fixed bed, Thomas and Yan & Nelson models. Nonlinear regression analysis was performed. The sum of the squares of the errors (SSE) was examined for every experimental data set, and the parameters of K_{TH} and q_{TH}as well as k_{YN} and T were determined for the lowest error values in each case by adjusting and optimizing the functions themselves using the *solver* add-in for Microsoft Excel®.

The Figures 3 and 4 show a comparison of the curves obtained from experimental data and theoretical models predicted by Thomas and Yoon & Nelson. These figures show that the Thomas model can be considered as a more suitable kinetic model to describe Cu(II), Zn(II) and Ni(II) adsorption in a fixed bed column of sugarcane bagasse and green coconut fibers. However, at the initial stage of adsorption, a small deviation between the model prediction and the experimental data was observed, mainly for zinc by sugarcane bagasse. The Thomas model is widely used to evaluate the column performance. It can be used to predict the breakthrough curve and the maximum solute uptake by the adsorbent. These parameters are essential for a successful design of an adsorption column [25]. Yoon & Nelson model just fitted well the data obtained for nickel by sugarcane bagasse and for copper by green coconut shell fibers.

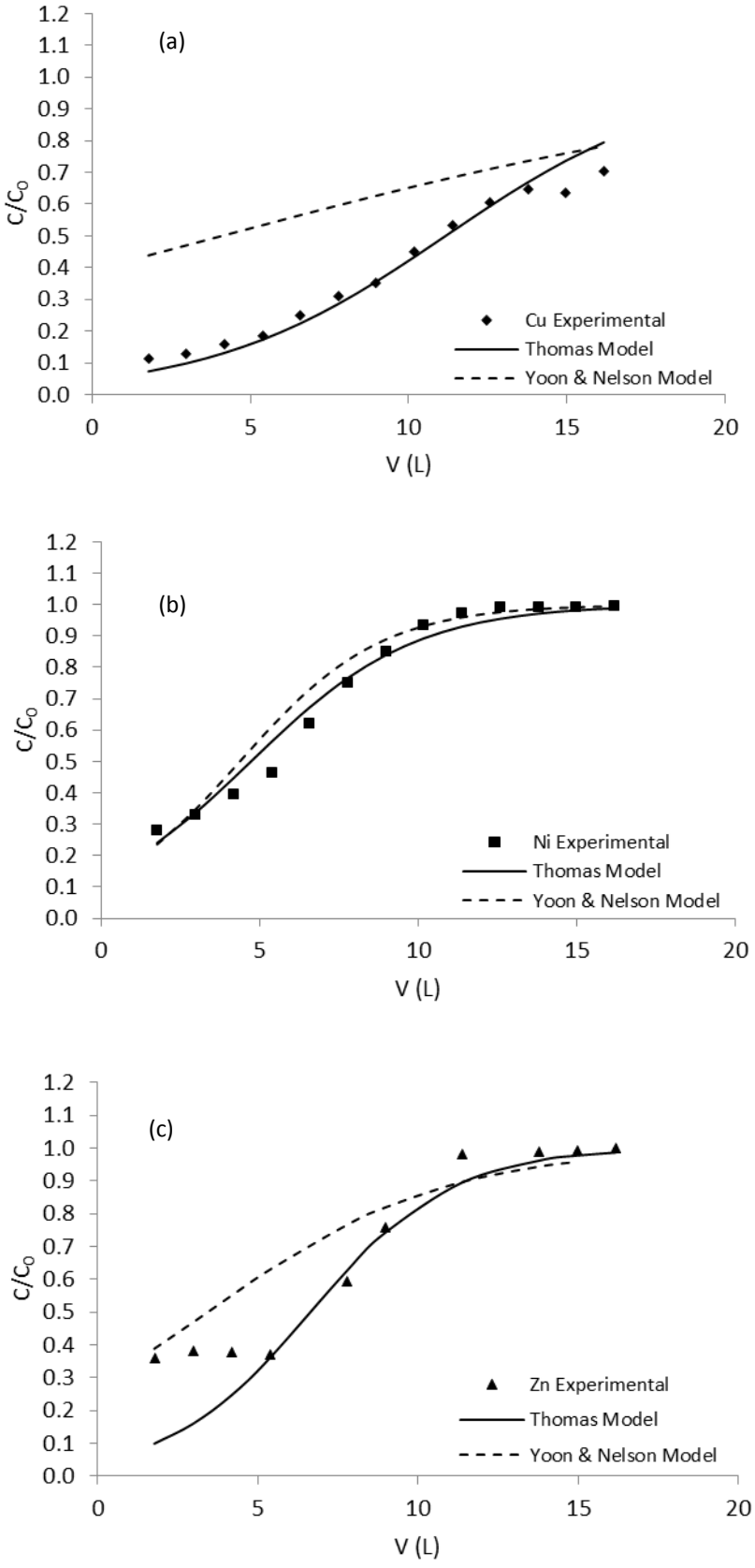

Figure 3. Comparison of the experimental and theoretical breakthrough curves obtained for (a) Cu(II), (b)Ni(II) and (c) Zn(II) by sugar cane bagasse

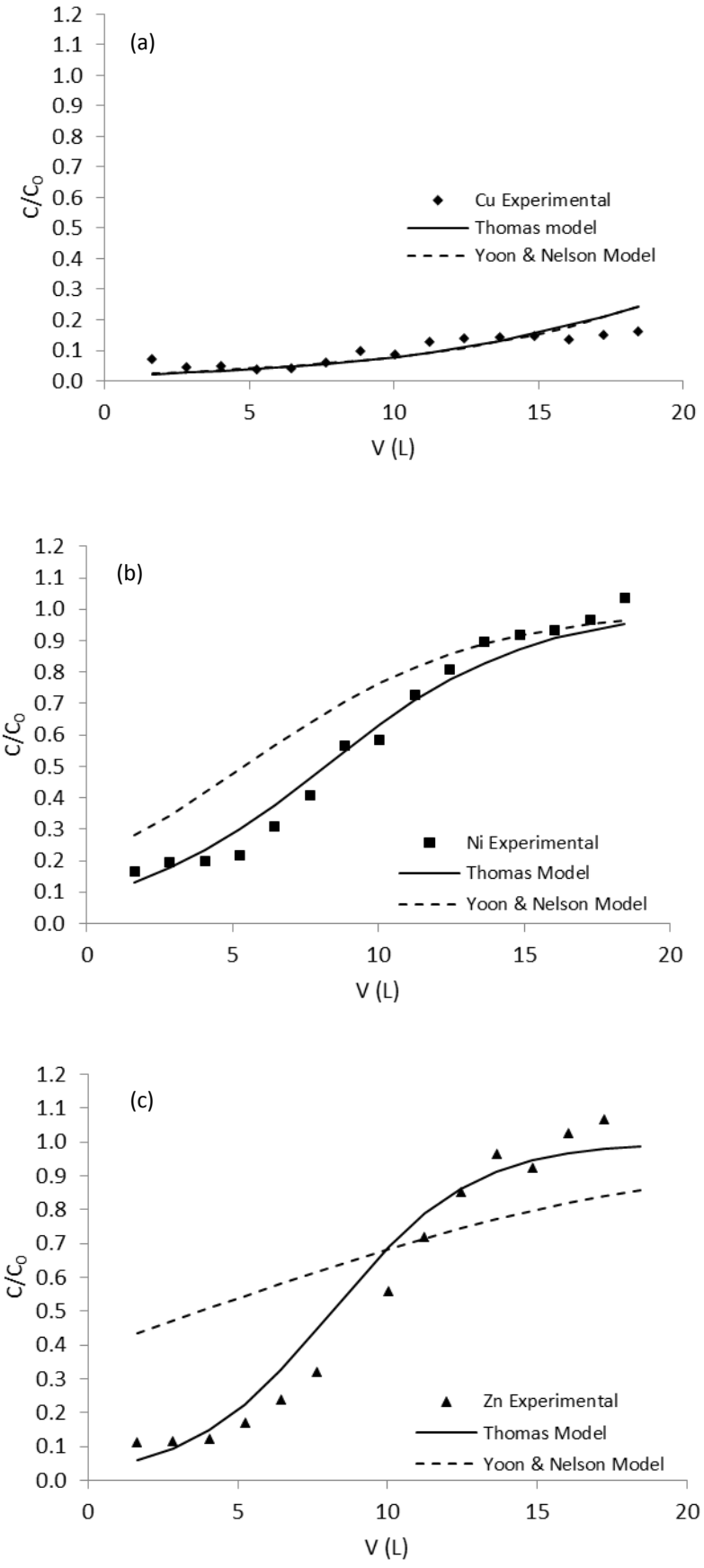

Figure 4. Comparison of the experimental and theoretical breakthrough curves obtained for (a) Cu(II), (b)Ni(II) and (c) Zn(II) by green coconut fiber.

Tables 4 and 5 shows the values of the parameters of each model for each metal ion studied, where it is found that the experimental data fitted well to the Thomas model, with low values of SSE, while the model of Yoon & Nelson showed high values of SSE reaching 8.87. The Thomas constant, k_{TH}, which characterizes the rate of transfer of metal ions from solution to the adsorbent, is related to the slope of the curve. The larger the slope is, the smaller the constant. The steeper the curve, the greater the constant is. In case of sugarcane bagasse, the constant value was lower for copper ion, as well as for green coconut fibers.

Comparing the adsorption capacities obtained by Thomas Model (Table 4 and 5) and the experimental results (Table 2), it can be seen that the values were close, especially for green coconut fibers. The q_{TH} for copper ions about 34 times larger than the zinc and nickel ions on sugarcane bagasse while for green coconut fibers it was 64 times than nickel and 9 times than zinc. In fact, the higher concentration of copper ions in solution favors adsorption. Obviously, other factors such as electronegativity, ionic radius, etc., may be involved. Therefore, the Thomas model can be considered as a suitable kinetic model to describe adsorption in a fixed bed. On the other hand, as Yoon & Nelson model didn't fitted well the data it was observed that the 50% breakthrough time (T) obtained from the model was different from the experimental.

Table 4. Calculated Parameters for Thomas and Yoon & Nelson Model from sugarcane bagasse.

Metal ions	Thomas Model			Yoon& Nelson Model			
	k_{TH}	q_{TH}	SSE	k_{YN}	T	T_{exp}	SSE
Cu(II)	9.9×10^{-2}	2.42	2.2×10^{-20}	8.4×10^{-3}	51.2	142.1	8.87
Ni(II)	2	0.07	4.0×10^{-18}	3.6×10^{-2}	54.6	72.1	1.3×10^{-1}
Zn(II)	2	0.07	5.7×10^{-1}	2.2×10^{-2}	42.9	97.1	3.36×10^{-1}

Table 5. Calculated Parameters for Thomas and Yoon & Nelson Model from green coconut fiber.

Metal Ions	Thomas Model			Yoon& Nelson Model			
	k_{TH}	q_{TH}	SSE	k_{YN}	T	T_{exp}	SSE
Cu (II)	1.0×10^{-1}	3.23	3.0×10^{-33}	1.0×10^{-2}	426.0	320.5	2.2×10^{-29}
Ni (II)	3.78	0.05	7.29×10^{-15}	2.0×10^{-2}	67.3	110.5	2.58
Zn (II)	8×10^{-1}	0.35	3.6×10^{-20}	9.8×10^{-3}	47.0	125.5	9.1×10^{-1}

4. CONCLUSION

The results indicated that the use of sugar cane bagasse and green coconut fibers as adsorbents of toxic metal ions in a fixed bed system is a feasible technology in wastewater treatment. The adsorbent usage rate was low for both materials studied, indicating a possible application in industry. Among the models applied, Thomas model fitted better the data than Yoon & Nelson model.

5. REFERENCES AND NOTES

[1] Ajmal, M.; Rao, R. A. K.; Ahmad, R.; Ahmad, J.; Rao, L. A. K. *J. Hazard. Mater.* **2001**, *B87*, 127. [CrossRef]

[2] Kurniawan, T. A.; Chan, G. Y. S.; Lo, W-H.; Babel, S. *Chem. Eng. J.* **2006**, *118*, 83. [CrossRef]

[3] Hasfalina, C. M.; Maryam, R. Z.; Luqman, C. A.; Rashid M. *APCBEE Procedia* **2012**, *3*, 255. [CrossRef]

[4] Kumara, R.; Bhatia, D.; Singh, R.; Rani, S.; Bishnoi, N. R. *Int. Biodeter. Biodegr.* **2011**, *65*, 1133. [CrossRef]

[5] Kumara, R.; Bhatia, D.; Singh, R.; Rani, S.; Bishnoi, N. R. *Int. Biodeter. Biodegr.* **2012**, *66*, 82. [CrossRef]

[6] Futalan, C. M.; Kan, C-C.; Dalida, M. L., Pascua, C.; Wan, M-W. *Carbohyd. Polym.* **2011**, *83*, 697. [CrossRef]

[7] Priya, P. G.; Basha, C. A.; Ramamurthi, V.; Begum, S. N.

J. Hazard. Mater. **2009**, *163*, 899. [CrossRef]

[8] Low, K. S.; Lee, C. K.; Leo, A. C. *Bioresource Technol.* **1995**, *51*, 227. [CrossRef]

[9] Sousa, F. W.; Sousa, M. J.; Oliveira, I. R. N.; Oliveira, A. G.; Cavalcante, R.M.; Fechine, P. B. A.; Neto, V. O. S.; Keukeleire, D.; Nascimento, R. F. *J. Environ. Manage.* **2009**, *90*, 3340. [CrossRef]

[10] Sousa, F. W.; Oliveira, A. G.; Ribeiro, J. P.; Rosa, M. F.; Keukeleire, D.; Nascimento, R. F. *J. Environ. Manage.* **2010**, *91*, 1634. [CrossRef]

[11] Malkoc, E.; Nuhoglu, Y. *J. Hazard. Mater.* **2006**, *B135*, 328. [CrossRef]

[12] Suksabye, P.; Thiravetyan, P.; Nakbanpote, W. *J. Hazard. Mater.* **2008**, *160*, 56. [CrossRef]

[13] Aksu, Z.; Gönen, F. *Sep. Purif. Technol.* **2006**, *49*, 205. [CrossRef]

[14] Gupta, V. K.; Srivastava, S. K; mohan, D.; sharma, S. *Waste manage.* **1997**, *17*, 517. [CrossRef]

[15] Cooney, D.O.; Adsorption Design for Wastewater Treatment. Boca Raton, Florida: CRC Press, 1999.

[16] Naja, G.; Volesky, B. *Environ. Sci. Technol.* **2006**, *40*, 3996. [CrossRef]

[17] Gupta, V. K.; Srivastava, S. K.; Tyagi, R. *Water res.* **2000**, *34*, 1543. [CrossRef]

[18] Kundu, S.; Gupta, A. K. *J. Colloid Interf. Sci.* **2005**, 290, 52. [CrossRef]

[19] Zhang, W.; Simanek, E.E. *Org. Lett.* **2000**, *2*, 843. [CrossRef]

[20] Markovska, L.; Meshko, V.; Noveski, V. *Korean J. Chem. Eng*. **2001**, *18*, 190. [CrossRef]

[21] Muhamad, H.; Doan, H.; Lohi, H. *Chem. Eng. J.* **2010**, *158*, 369. [CrossRef]

[22] Aksu, Z.; Gonen, F. *Process Biochem.* **2003**, *39*, 599. [CrossRef]

[23] Ipek, I. Y.; Kabay, N.; Yuksel, M.; *Desalination* **2013**, *310*, 151. [CrossRef]

[24] Ayoob, S.; Gupta, A. K.; Bhakat, P. B. *Sep. Purif. Technol.* **2007**, *52*, 430. [CrossRef]

[25] Shahbazia, A.; Younesi, H.; Badiei, A. *Chem. Eng. J.* **2011**, *168*, 505. [CrossRef]

Orbital: The Electronic Journal of Chemistry
journal homepage: www.orbital.ufms.br
ISSN 1984-6428

| Vol 6 | | No. 1 | | January-March 2014 |

Full Paper

Microwave-mediated Reduction of Selected Functional Groups Employing: *N,N*-Dimethylaniline.borane

S. Venkatesan Jaya kumar[a,*], S. Mothilal Krishna Ganesh[b]

[a]*Chemistry department, College of Natural Sciences, P.O.Box 378, Jimma University, Jimma, Ethiopia.*
[b]*Department of Computer Science & Engineering, St. Joseph University, Dar Es Salaam, Tanzania.*

Article history: Received: 07 May 2013; revised: 07 February 2014; accepted: 30 March 2014. Available online: 02 April 2014.

Abstract: *N,N*-Dimethylaniline.borane (DMANB) is a versatile reducing agent reduces a variety of functional groups under microwave irradiation (MWI) in very good yields with in short time. However, aliphatic and aromatic esters were not reduced under MWI (even after 25 minutes of irradiation). Besides these reducing properties the reagent displays chemoselectivity towards functional group and used in asymmetric synthesis. The combination of borane species from amine.borane with microwave irradiation provides a convenient and rapid method for reduction of functional groups.

Keywords: *DMANB; microwave irradiation; reduction; chemoselectivity*

1. INTRODUCTION

Over the decades, amine.borane complexes have gained wide applications in organic synthesis [1], dye industry as well as in various other industrial applications [2-5]. The utilization of these complexes was reported in H_2 storage fuel cells, due to its stability and high gravimetric content of hydrogen [6a, 6b]. The scope and uses of amine.borane in organic synthesis was limited because of stability [7a], lack of reactivity towards functional group [7b]. In order to activate the stable amine.borane complexes like triethylamine.borane, pyridine.borane high reaction temperature [9], addition of acetic acid [10], mineral acid [11] and lewis acid [12] are required. One set of amine.borane complexes derived from *N,N*-dialkyl anilines and *N,N* -dialkyl amines is significantly more reactive than most amine.boranes [1, 13, 4]. The steric effects and electronic property of the groups attached to nitrogen atom of amines influence their reducing property [1, 15a, 15b]. The main drawback from are their laborious synthesis [1], [7b, 17]. The procedure involves the alkylation of aniline or mono alkyl aniline, which is very delicate and time consuming. But diethyl aniline.borane complex is commercially available, properties are well documented [16]. Instead of aiming to prepare a new reactive amine.borane complex, we choose the novel technique like microwave irradiation, sonication to activate the moderately reactive amine.borane complexes towards the reduction of functional groups. On the other hand very few reports were available on the use of (DMANB) [8] as reducing agent as compared to *N,N*-diethyl aniline.borane [18]. Therefore, we intended to study the reduction potential of DMANB under microwave condition for the functional group reduction.

It has been well known that the activation of various chemical reactions by microwave irradiation is not only enhances the selectivity and product yield [19] but also shorten the reaction time, decreases the side products [20] and it is providing quite successful in the formation of a variety of carbon-heteroatom bonds [21]. By taking advantage of this efficient source of energy, compound libraries for lead generation and optimization can be assembled in a fraction of the time required by classical thermal methods [22]. Microwave-induced Organic Reaction Enhancement (MORE) chemistry has gained popularity as a non-conventional technique for rapid organic synthesis [23]. It can be termed as 'e-chemistry' because it is easy, effective, economical and eco-friendly and believed to be a step towards green chemistry. Furthermore, with the ease of recovery and recycling of *N,N*-dimethylaniline after the reaction makes amine.borane complex environmentally benign reagent.

*Corresponding author. E-mail: svjkumar70@gmail.com

We encouraged by the previous results [24] on hydroboration of alkenes to alcohols with DMANB under microwave irradiation and further expand its utility as a hydride source, we undertook a series of compounds for functional group reduction by DMNAB under microwave irradiation.

2. MATERIAL AND METHODS

All chemicals were purchased from Fluka and Aldrich. Melting point of compounds were measured using a differential scanning calorimeter (Shimadzu DSC-50) and are uncorrected. Liquid substrates were distilled prior to use. Proton nuclear magnetic resonance (^{1}H NMR) spectra were recorded using 400 MHz equipment, Bruker AVANCE. For ^{1}H NMR spectra, chemical shifts (δ) are referenced from TMS (0.00 ppm) and the samples were dissolved in an appropriate deuterated solvent. Carbon nuclear magnetic resonance (^{13}C NMR) spectra were recorded using a NMR spectrometer at 100 MHz. For ^{13}C NMR spectra, chemical shifts (δ) are given from reference signal of the deuterated solvent used. IR spectra were recorded on FTIR Shimadzu spectrometer. The mass spectra were recorded on EI-Shimadzu-GC-MS spectrometer. Elemental analyses were measured on a HERAEUS (CHNO, Rapid) analyzer.

Microwave specification

Microwave experiments were conducted using a CEM discover monomode oven operating at 2450MHz monitored by a PC computer and temperature was maintained at a constant value by power modulation (0-300W). Stirring was provided by an *in situ* magnetic stirrer. Reactions were performed under nitrogen atmosphere. Reaction conditions: power 300 Watts; ramp time 3min; hold time 10 min; stirring on; temperature 145 ^{o}C.

3. RESULTS AND DISCUSSION

Preparation and stability of DMANB complex:

The *N,N*-dimethyl aniline.borane complex was prepared by two methods [25, 26]. The complexing ability of amine towards borane was monitored by ^{11}B-NMR spectroscopy. This reagent could be maintained under nitrogen atmosphere and it is apparently stable indefinitely at room temperature. In ^{11}B NMR the amine.borane complex showed a peak at -4 ppm (decoupled) and -4 to -9 ppm (coupled).

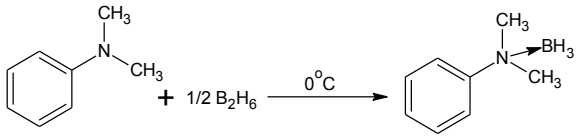

Encouraged by the results of our preliminary exploratory observations we undertook a study of the reduction of aldehydes, ketone, carboxylic acid, amide, ester, amino acid, Schiff base with DMANB under MWI. The results are summarized in Table 1.

The Aldehydes shown in entries 1, 13 and 14 from Table 1 were comfortably reduced to the corresponding alcohols by DMANB in a short period of time (4 minutes) under MWI and quantitative yields were obtained. 1:3 stoichiometry ratio was followed for the reduction. The halo aldehyde in entry 3 was reduced to the corresponding alcohol without affecting the halogen. Reduction of cyclohexanone is slow at room temperature (24 h with only 80% completion as shown by TLC and Gas-burette analysis), however under microwave irradiation the reduction was completed in just 5 minutes and a 96% yield of the corresponding alcohol was isolated (entry 5, Table 1). The same was observed in the case of acetophenone in 4 minutes (entry 4, Table 1).

Aliphatic and aromatic carboxylic acids (entries 1 and 13, Table 1) were readily reduced by DMANB to the corresponding alcohols in very good yields in a short period of time (5minutes). A one to one ratio of reagents was used since one hydride is utilized for acid hydrolysis and further two hydrides are required for the carbonyl reduction. Tandem reduction/hydroboration was observed with undecenoic acid and cinnamic acid (entries 8-9, Table 1) and a mixture of products was formed based on GC analysis (tandem reduction/hydroboration of carboxyl group and double bond; the reduction of carboxyl group alone and the hydroboration of double bond alone).

DMANB conveniently reduced amides to amines in very good yields within 6minutes under microwave irradiation. According to literature reports [8], the reduction of Benzamide, Acetanilide with *N,N*-diethyl aniline.borane requires 7-13hours under conventional methods. 1:2 stoichiometry ratio was followed for the reduction, because the reduced amine forms a complex with borane, hence excess borane needed to make the reduction convenient.

The reduction of amino acids [25, 26] is considered important transformation in organic synthesis, the amino alcohol obtained in this

transformation plays vital role in asymmetric synthesis [1] and peptide synthesis. In the present study the reduction of three amino acids were focused namely valine, proline and leucine (entries 14-16, Table 1). Amine.borane reagent conveniently reduces the amino acid to amino alcohol within 6 minutes in good yields. 1:2 stoichiometry ratio was followed, the specific rotation value $[\alpha]_D$ matches with the literature value [27].

Table 1. Reduction of representative functional groups with DMNAB complex.

Entry	Substrate	Time (min.)	Stoichiometry ratio (DMANB:Sub)	Product	Yield
1	Benzaldehyde	4	1:3	Benzyl alcohol	90
2	2-Fluoro-4-Bromo benzaldehyde	4	1:3	2-Fluoro-4-Bromo benzyl alcohol	1
3	*p*-Anisaldehyde	4	1:3	*p*-Anisyl alcohol	94
4	Acetophenone	4	1:2	*sec*-Phenethyl alcohol	98
5	Cyclohexanone	5	1:2	Cyclohexyl alcohol	96
6	Benzoic acid	6	1:1	Benzyl alcohol	93
7	Azealic acid	6	1:1 2:1	Diol	95
8	Undecenoic acid	6	1:1 & 2:1 1:2	Mixture of products	96 (crude)
9	Cinnamic acid	6	1:1 & 2:1 1:2	Mixture of products	95 (crude)
10	Benzamide	6	1:1	Benzyl amine	96
11	Acetanilide	6	1:1	*N*-Ethyl aniline	94
13	4-Bromo acetanilide	6	1:1	4-Bromo-*N*-Ethyl aniline	93
14	*L*-Valine	6	1:1	*L*-Valinol	95
15	*L*-Leucine	6	1:1	*L*-Leucinol	95
16	*L*-Proline	6	1:1	*L*-Prolinol	96
17	*n*-Butyl acetate	25	1:1 & 2:1	No reaction	
18	Ethyl benzoate	25	1:1 & 2:1	No reaction	
19	Methyl salicylate	25	1:1	No reaction	
20	Tyrosine methyl ester	25	1:1	No reaction	

The reduction of imine esters (Schiff base) to amine esters [17] in THF was facile with amine.borane under microwave irradiation within 4 minutes in good yields.

It is noteworthy to mention that the reagent DMANB did not reduce ester functionality up to 30 min of microwave irradiation. This observation led us further to the study on chemoselectivity aspects from reduction process.

Chemoselectivity studies

Encouraged by the results we under took a study of chemoselective reduction of 4-nitro benzaldehyde, nonomethyl hydrogen phthalate, 4-carbomethoxy acetanilide and imine esters with DMNAB. Reagent selectively reduces the aldehyde, acid, amide and imine functionality within 4-6 minutes under MWI condition and the ester group remains intact.

Table 2. Chemoselective reduction of selected functional groups with N, N-Dimethyl aniline.borane (DMANB).

Entry	Substrate	Time (min.)	Stoichiometry ratio (DMANB:Sub)	Product
1	*p*-Nitro benzaldehyde	4	1:3	*p*-Nitro benzyl alcohol
2	Monomethyl hydrogen phthalate	6	1:1	Methyl(2-hydroxy methyl) benzoate
3	4-Carbomethoxy acetanilide	6	1:1	4-Carbomethoxy-N-Ethyl aniline
4	*N*-[(4-chlorophenyl) methylene]aniline	4	1:1	*N*-(4-chlorobenzyl) aniline
5	Methyl 2-[(2-hydroxy phenyl)methylene] amino-3-methylbutanoate	4	1:1	Methyl 2-[(2-hydroxybenzyl) amino]-3-methylbutanoate
6	Ethyl-10-undecenoate	6	1:1	No reduction of ester group, hydroboration of double bond.

In the case of ethyl-10-undecenoate selective hydroboration of double bond was observed, further confirmed by corresponding signal in ^{11}B NMR at 75 ppm and supported by the oxidation of trialkyl boron species with NaOH / H_2O_2.

Experimental procedure for functional group reduction: [1, 7b, 13, 14, 25]

An oven dried, 50 mL flask fitted with a sidearm capped by a rubber septum (to permit introduction and removal of material with a hypodermic syringe) was equipped with microwave reflux condenser connected to a mercury bubbler by means of take-off adapter. DMANB in dry THF 10 mL (5.3M, 8.3 mmol) was added to the flask by syringe followed by compound in dry THF (5.00 mL, 6.25 mmol) slowly during 5 minutes under nitrogen atmosphere. The contents were stirred for about 4-6 minutes under microwave irradiation. At appropriate time intervals, samples were withdrawn and hydrolyzed using HCl (2M)-glycerol-water mixture, the hydrogen evolved was measured using the gasimeter. Progress of the reaction was cross checked by GC, TLC analysis. In a number of cases, the reduction was carried out as described above to establish yield and stoichiometry. However, the reaction mixtures were then worked up depends on nature of substrate and to isolate and characterize the reaction products.

With aldehydes, ketone, carboxylic acid and ester reaction mixture was quenched with HCl (3N, 10 mL) and product was extracted with ether. The combined ether extracts were washed with HCl 3N, water and brine and dried over anhydrous sodium sulphate, removal of solvent under vacuum gives crude product, which on purification by column chromatography yields pure product. In the case of amide, amino acid, imine, imine ester reaction mixture was quenched with potassium carbonate aqueous solution and product was extracted with ether. The crude product was obtained by simple acid/base manipulation, which was further purified by column chromatography, purity of the final product was obtained by HPLC method.

4. CONCLUSION

We have demonstrated the successful utilization of DMNAB towards the reduction of functional groups. Reagent DMANB has certain advantages over the currently available borane reagents such as borane.tetrahydrofuran (BTHF) and borane.dimethylsulfide (BMS). Pure DMANB is 1) quite concentrated at 5.6M, 2) thermally stable, 3) convenient and comfortable to handle, 4) environment friendly, not disagreeable odour, 5) DMANB makes available all three hydrides for the reduction. In comparison with conventional methods microwave technique is a novel and efficient method to activate the DMANB complex towards the reduction of functional groups. Studies on the stoichiometry, applications and limitations of this methodology are undergoing and will be reported in due course.

5. ACKNOWLEDMENTS

We express gratitude to our respected Rev. Fr. Dr. Arulraj Founder, DMI Group of Institutions, East Africa & India, Dr. T. X. A. Ananth, Director (International Operations), DMI group of Institutions, Mr.Ignatius Herman, Director (Academic), DMI

group of Institutions, also we acknowledge the support provided by Rev. Sr. Fatima Mary, Vice Principal (Administration), and Mr. N. Ressel Raj, Vice Principal (Academic), DMI. St. Joseph University, Tanzania.

6. REFERENCE AND NOTES

[1] Kanth, J. V. B. *Aldrichim. Acta* **2002**, *35*, 57.

[2] Lane, C. F. *Aldrichim. Acta* **1973**, *6*, 51.

[3] Masui, M.; Shiorii, T. *Tetrahedron Lett.* **1998**, *39*, 5199. [CrossRef]

[4] Akahoshi, H. *US patent.*1987, 4, 642,161.

[5] a) Mallory, G,O.; Hajdu, J. B. (eds.) Electroless plating, Fundamentals and Applications, *Am. electroplaters and surface finishers society*, Orlando, Florida, **1990**; b) Meller, A.; In: Gmelin Handbook of Inorganic and Organometallic Chemistry, Springer: Berlin, **1992**; 4th Supplement, Vol. 3, 1.

[6] a) Follet, M. *Chem. Ind.* **1986**, *1*, 123; b) Lane, C.F.; N-B-H Survey, *Contract # DE-FC36-05GO 15060* Northern Arizona University, **2006**.

[7] a) Hutchins, R. O.; Learn, K.; Nazer, B.; Pytiewski, D.; Pelter, A. *Organic preparations and procedures Int.* **1984**, *16*, 335; b) Brown, H. C.; Kanth, J. V. B.; Dalvi, P. V.; Zaidlewicz, M. *J. Org. Chem.* **1999**, *64*, 6263.[CrossRef]

[8] Brown, H. C.; Murray, L. T. *Inorg.chem.* **1984**, *23*, 2746. [CrossRef]

[9] Barnes, R. P.; Graham, J. H.; Taylor, M. D. *J. Org. Chem.* **1958**, *23*,1561. [CrossRef]

[10] Kelly, H. C.; Giusto, M. B.; Marchelli, F. R. *J. Am. Chem. Soc.* **1994**, *59*, 6470.

[11] Wuts, P. G. M.; Cabaj, J. E.; Havens, J. L. *J. Org. Chem.* **1994**, *59*, 6470. [CrossRef]

[12] Periasamy, M.; Kanth, J. V. B.; Prasad, A. S. B.*Tetrahedron* **1994**, *50*, 6411. [CrossRef]

[13] Brown, H.C.; Zaidlewicz, M.; Dalvi, P. V. *Organometallics* **1998**, *17*, 4202. [CrossRef]

[14] Brown, H. C.; Kanth, J. V. B.; Zaidlewicz, M, M. *J. Org.* Chem. **1998**, *63*, 5154.

[15] Long, L. H.; In A Comprehensive Treatise on Inorganic and Theoretical Chemistry; Mellor, W.J., Ed.; *Longman*: London, 1981; Supplement Vol.5, Part B1; b) Kanth, J. V. B.; Periasamy, M. *Chem.Commun.* **1990**, *1*, 1145.

[16] Salunkhe, A, M.; Burkhardt, E. R. *Tetrahedron Lett.* **1997**, *38*, 1519. [CrossRef]

[17] Periasamy, M.; Kanth, J. V. B.; Reddy. C. K. *Perkin Trans. A*. **1995**, *1*, 427. [CrossRef]

[18] Salunkhe, A, M.; Burkhardt, E. R. *Tetrahedron Lett.* **1997**, *38*, 1523. [CrossRef]

[19] Loupy, A., Ed.; Microwaves in organic synthesis, Wiley-VCH: Weinheim, 2002. [CrossRef]

[20] Hayes, L. B. *Aldrichim. Acta* **2004**, *37*, 66.

[21] Madhvi, A. S.; Smita, J.; Desai K. R. *Arch. Appl. Sci. Res*. **2012**, *4*, 645.

[22] Jacob, J. *Int. J. Chem.* **2012**, *4*, 29. [CrossRef]

[23] Varma, S. *Green Chem*. **1999**, *1*, 43. [CrossRef]

[24] Jayakumar, V. S.; Srinivas, A. K.; Hiriyana. G.; Pati. H. *Rasayan J. Chem*. **2008**, *1*, 326.

[25] Pelter, A.; Smith, K.; Brown, H. C. Borane reagents, *Academic press*, London, 1988.

[26] Brown, H. C.; Organic synthesis via boranes vol.1; Aldrich chemical company, Inc.; Milwaukee, WI, 1997. [CrossRef]

[27] McKennon, M. J.; Meyers, A. I. *J. Org. Chem.* **1993**, *58*, 3568.

Orbital: The Electronic Journal of Chemistry
journal homepage: www.orbital.ufms.br
ISSN 1984-6428

| Vol 6 | | No. 1 | | January-March 2014 |

Full Paper

Synthesis and Preliminary Characterization of Manganese 3,4-(methylenedioxi)cinnamate Compound: A Simple Approach to Improve Electroanalytical Application After Incorporation to the Carbon Paste Electrode

Luiz Henrique de Oliveira, Karoline Landgraf Ribeiro, Cláudio Teodoro de Carvalho, Magno Aparecido Gonçalves Trindade*

Faculty of Science and Technology, Federal University of Grande Dourados, Rodovia Dourados-Itahum, Km 12. Dourados, MS 79804-970, Brazil.

Article history: Received: 01 February 2014; revised: 15 March 2014; accepted: 30 March 2014. Available online: 02 April 2014.

Abstract: The manganese 3,4-(methylenedioxi)cinnamate (MnMCA) compound was synthesized and characterized using thermal analysis technique to determine purity as well as stoichiometry and infrared spectroscopic data to suggest the metal-ligand coordination. The feasibility of the MnMCA compound as modifier of carbon paste electrodes was studied via electrochemical techniques such as cyclic and linear sweep voltammetry. The modified carbon paste electrode (MCPE) presented a satisfactory electrocatalytic activity for propyl gallate (PG) oxidation. The study of the instrumental and experimental parameters as well as of the voltammetric behavior showed that the MCPE exhibits better analytical performance in the detection of the PG than the glassy carbon electrode and the unmodified carbon paste electrodes. The results obtained were satisfactory concerning the use of the target MCPE-MnMCA in electroanalytical applications and detection of PG antioxidant in biodiesel sample after a simple and fast step.

Keywords: MnMCA compound; thermal analysis; electrochemical study; modified carbon paste electrodes

1. INTRODUCTION

Metal compounds have been applied in many research areas [1-4, 6, 8], particularly with modified electrodes using metal complexes, which can play an important role in electroanalytical studies, presenting satisfactory electrocatalytic properties by improving the rate of electron transfer between electrode-surface and target analyte. The most common modification is related to the incorporation of the metal-complex in the carbon paste electrodes (CPEs) [5] and this feature can provide more advantages than other electrodes, what can also be important for practical applications in electrochemical sensors [7, 8]. Regarding the CPEs, the first proposal was made by Adams in 1958 [9], which prepared a paste comprised of graphite powder and a liquid binder to give consistency to the combination. Therefore, when a modifier is admixed mechanically to the paste composition during its homogenization, the new mixture is usually called modified carbon paste electrode (MCPE) [7, 8, 10-15].

Modified carbon paste electrodes (MCPEs) have wide application in analytical chemistry and related areas. Since the first experiments, there have been considerable advances in electrodes preparation procedures, becoming usual the carbon paste modification with a specific chemical class or material in order to solve resistivity problems caused by graphite powder, as well as to improve the selectivity in the target analyte detection [7, 8, 10-15]. The MCPEs are important devices for use as working electrodes in electrochemical analysis due to their advantageous features such as selectivity, detectability, reactivity, fast responses, electrocatalytic properties, ease of surface renewal, wide working potential window, low background current and suitable electric conductivity [7]. Accordingly, the combination of MCPE and voltammetric techniques has provided a diversification in analytical applications and has been extensively studied, in order that a properly selected

*Corresponding author. E-mail: magnotr@gmail.com

modifier can supply improvement in electrocatalytic properties or serve as a catalyst of electrochemical reactions, whose characteristics are desirable for detection of target analyte on working electrode surface [7, 8, 10-15].

Recently, Ojani and co-workers [5] reported the use of electrochemical sensor based on nickel–curcumin complex modified carbon paste electrode for amoxicillin determination. Issa and co-workers [15] proposed a chemically modified carbon paste electrode with Cu(II)-selective based on the etioporphyrin I dihydrobromide as potentiometric electrode to determinate Cu(II) in real samples. All these works have justified the use of MCPEs due to the significant improvement in the catalytic property of the modifier (metal-complex), providing satisfactory electroanalytical results [14-16]. Furthermore, selectivity has been a relevant factor and attracted interest to electrochemical studies, enabling the development of devices with rapid response and appropriate for various purposes and analytical applications [5, 7, 8, 10-13, 15].

Despite the diversity of works using MCPEs to detect a variety of analytes, the influence of the 3,4-(methylenedioxi)cinnamate compound in the performance of carbon paste electrodes has not been explored. Accordingly, the purpose of the present work was synthesize and characterize the manganese 3,4-(methylenedioxi)cinnamate compound (MnMCA) in order to use it to modify CPE, aiming its application in the detection of the antioxidant propyl gallate (PG, Figure 1) in biodiesel samples. Biodiesel is relatively unstable under storage conditions, then the use of PG has been a popular choice to overcome the oxidative stability dilemma. The literature reports the enhancement of biodiesel oxidative stability by using PG antioxidant, once it contributes to avoid the oxidation chain reaction through interruption of the beginning of oxidation by its reaction with free radicals to form stable compounds [17]. Thus, electroanalytical methods to monitor the presence of antioxidants in commercial biodiesel samples are currently in demand.

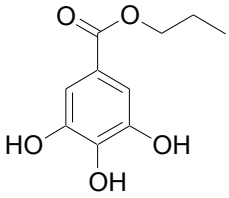

Figure 1. Chemical structure of the antioxidant propyl gallate (PG).

For the proposed method, the influence of several parameters in the detection of target antioxidant, such as paste composition and pH of the supporting electrolyte, was studied using cyclic and linear sweep voltammetry.

2. MATERIAL AND METHODS

Synthesis of manganese 3,4-(methylenedioxi)cinnamate compound

The 3,4-(methylenedioxy)cinnamic acid (CH_2OO-C_6H_3-C_2H_2-COOH) 98% pure and predominantly trans was obtained from Aldrich. Aqueous solution of sodium 3,4-(methylenedioxy)cinnamate 0.10 mol L^{-1} was prepared from 3,4-(methylenedioxy)cinnamic acid suspension by treatment with sodium hydroxide 0.10 mol L^{-1}, whose pH was adjusted around 7.5 using a pH-meter with a combined glass electrode. Aqueous solution of the bivalent metal ion was prepared by dissolving the respective chloride.

The solid-state compound was prepared by adding the ligand solution slowly, with continuous stirring to the respective metal-chloride solutions until total precipitation of the metal ions. The precipitates were then washed with distilled water until chloride ions elimination, filtered through and dried on Whatman nº 42 filter paper and kept in a desiccator over anhydrous calcium chloride.

Electrodes preparations

The CPEs were prepared by mixing graphite powder and mineral oil in a defined ratio, the mixture being macerated in a mortar until obtaining a homogeneous and consistent paste. On the other hand, MCPEs were prepared by varying the proportions of graphite powder (Aldrich), mineral oil (Aldrich) and the modifier Mn(MCA). Then the mixture containing the appropriate proportion was macerated again for approximately 20 minutes to ensure complete homogenization, obtaining a satisfactory consistency. After preparation, the carbon pastes with and without modifier were stored at approximately
-4 °C. For working electrode construction, a small amount of the prepared paste was packed into a 1.0 mL insulin plastic syringe containing a copper wire to obtain external electric contact.

Instrumentation

The characterization of the compound was performed using simultaneous TG-DTA thermal analysis system, model SDT 2960 - TA Instruments from the following experimental conditions: air flow as purge gas of 100 mL min^{-1}, heating rate of 20 °C min^{-1}, samples weighing about 5.0 mg and alumina crucibles for recording the TG-DTA curves.

The attenuate total reflectance infrared spectra for sodium 3,4-(Methylenedioxy)cinnamate, as well as for its metal-ion compounds were run on a Nicolet iS10 FT-IR spectrophotometer using an ATR accessory with Ge window and 3D structure of anhydrous compound in solid-state was optimized using Gaussian 98 program.

Voltammetric measurements were performed on a potentiostat/galvanostat (DropSens, μStat model 400) coupled to a microcomputer for data acquisition. It was used a three-electrode system comprising a platinum wire auxiliary electrode, a Ag/AgCl reference electrode and carbon paste electrodes as working electrode. An electrochemical cell with a capacity of 5.0 mL, containing a Teflon® cap with holes for the coupling of the electrodes was used for carrying out electrochemical measurements. The pH measurements of the buffer solution used as supporting electrolyte were performed in a combined glass electrode (ION, model pHB - 500) connected to a digital pH meter (Elektron, model E65-1). Deionized water used was obtained from a Milli-Q system (Millipore, model simplicity).

Solutions and instrumental measurements

Acetate buffer 0.04 mol L^{-1} used as supporting electrolyte was prepared by mixing anhydrous sodium acetate (Merck) and acetic acid (Merck), phosphate buffer 0.04 mol L^{-1} prepared with sodium phosphate dibasic monohydrate (Merck) and sodium phosphate dibasic dihydrate (Merck) and Britton-Robinson buffer prepared with acetic acid (Fluka), boric acid (Merck) and phosphoric acid (Merck). The study of the electrolyte pH was carried out in the range of 3.8 to 9.0.

Propyl Gallate (PG) standard stock solutions of (1.00×10^{-3} to 1.00×10^{-2} mol L^{-1}) were prepared by dissolving the solid in ethanol (Vetec). To register the voltammograms at glassy carbon electrode, unmodified and modified carbon paste electrode it was used an electrochemical cell containing 5.0 mL of buffer (pH desired), whose scan rate was within the potential window from -0.20 to 0.65 vs. Ag/AgCl. After each measure, the electrode surface was renewed from the removal of the surface layer and subsequent polishing on bond paper. Furthermore, before each experimental measurement the electrolytic solution was purged with gaseous nitrogen for about 10 minutes to remove the dissolved oxygen.

Preparation and analysis of biodiesel samples

Antioxidant-free soybean biodiesel sample (produced in our Laboratory) was spiked with PG in concentration of 500 mg L^{-1} employing vigorous mechanical agitation. An aliquot of spiked sample was diluted in methanol, using calibrated flasks, to achieve a final concentration of 1.00×10^{-3} mol L^{-1} (biodiesel:methanol, v/v). For the analysis, aliquots of 100 μL of the resulting solution was transferred into the electrochemical cell containing 5.0 mL of 0.04 mol L^{-1} BR buffer and agitated for 1.0 min. The resulting sample was directly analyzed, registering linear sweep voltammograms. The PG contained in the biodiesel sample was quantified using the standard addition method.

3. RESULTS AND DISCUSSION

Characterization of Mn(MCA) compound using TG-DTA technique

The characterization of the manganese compound was performed by simultaneous TG-DTA thermal analysis system using a mass sample of 5.09 mg and the recording of the TG-DTA curves is shown in Figure 2. The mass loss of the compound occurs in three steps; the first one is observed between 103-144 ºC (TG), corresponding to an endothermic peak at 142 °C (DTA) due to dehydration, which occurs in a single step with loss of two molecules of hydration water (Calculated = 7.80%, TG = 7.79%).

After the dehydration, the anhydrous compound is stable up to 255 °C and above this temperature the two following steps of thermal decomposition, which occur between 255-370 and 370-442 °C in the TG curve, respectively, correspond (DTA) to an exotherm between 280-345 °C (for second step) and to an intense peak at 428 °C (for third step) attributed to decarboxylation, oxidation and/or partial combustion of the organic matter. The total mass loss up to 450 °C is in agreement with the Mn_3O_4 as final residue. (Calculated 83.92%, TG = 84.44%), which has 99.5 % purity. As a result, it can

be attributed to the compound the following stoichiometry $Mn(CH_2OO\text{-}C_6H_3\text{-}C_2H_2\text{-}COO)_2.2H_2O$.

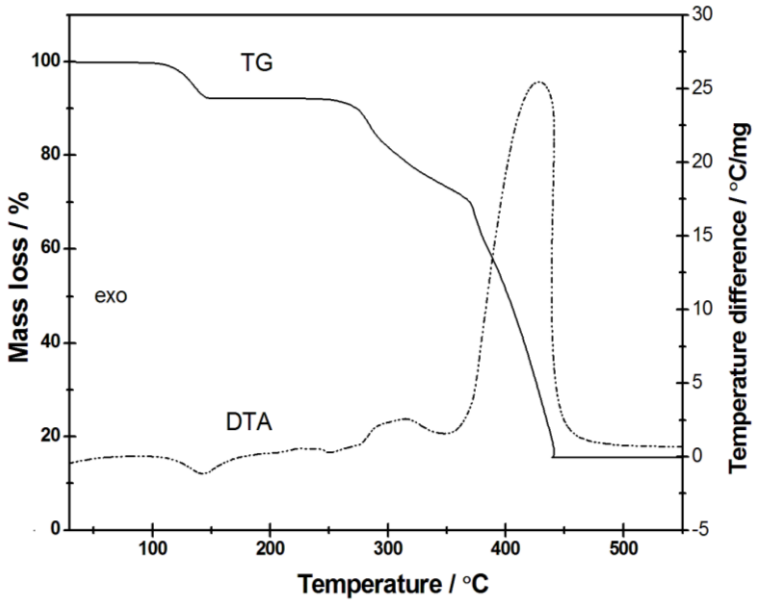

Figure 2. TG-DTA curves of manganese 3,4-(methylenedioxi)cinnamate compound obtained in air atmosphere and with 5.09 mg initial mass of the sample.

Characterization of Mn(MCA) compound using FT-IR technique

The attenuate total reflectance spectroscopic data of sodium 3,4-(methylenedioxi)cinnamate and its compound with the metal ion considered in this work were investigated by using FT-IR technique. The investigation focused mainly on the 1700-1400 cm^{-1} range because this region is potentially more informative in attempting to assign coordination sites.

In $NaCH_2OO\text{-}C_6H_3\text{-}C_2H_2\text{-}COO$, strong band at 1549 cm^{-1} and a medium intensity band located at 1413 cm^{-1} are attributed to the anti-symmetrical and symmetrical frequencies of the carboxylate groups, respectively. In the manganese compound the bands assigned to the anti-symmetrical and symmetrical frequencies are shifted to lower values relative to the corresponding frequencies in sodium salt. This behavior indicates that the coordination is carried out through the carboxylate group [18, 19]. Furthermore, the infrared spectra data suggests that the bonding of the carboxylate group to the metal is bidentate chelating, according to Figure 3.

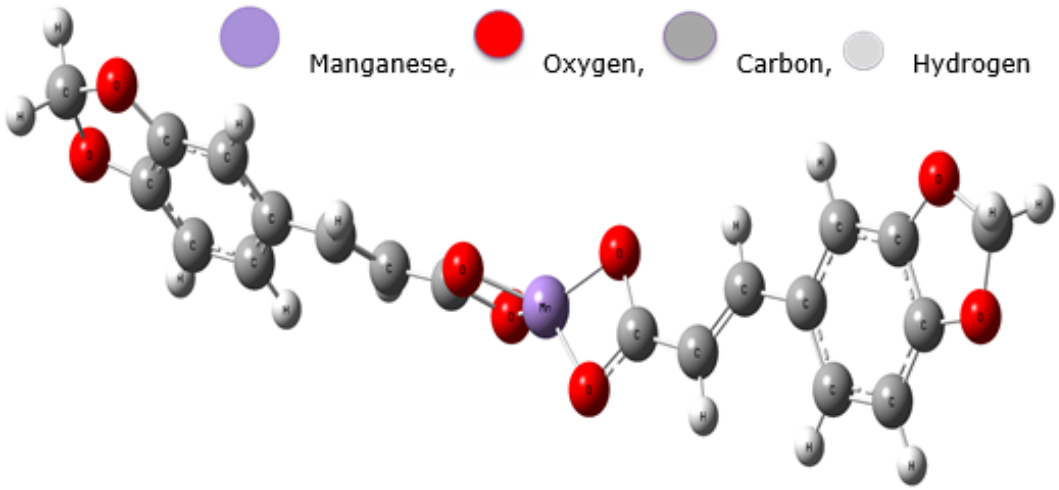

Figure 3. Metal-ligand coordination structure suggested from the FT-IR data.

Electrochemical study

Initially, it was investigated the carbon paste composition in the presence and absence of modifier by studying different ratios of graphite powder (between 65 and 80%), mineral oil (between 25 and 15%) and Mn(MCA)-modifier (between 10 and 5%). Then, the analytical performance of target electrodes was verified recording voltammograms for oxidation of PG on the CPE and MCPE surfaces, using cyclic voltammetry (CV) as electrochemical technique and comparing the voltammetric profile after each measurement. The optimized ratio for the CPE was 75% of graphite powder and 25% of mineral oil, while for MCPE it was 65% of graphite powder, 25% of mineral oil and 10% of Mn(MCA)-modifier, respectively. Moreover, the performance of paste composition in the presence and absence of modifier was evaluated in terms of its consistency during maceration and resistance to attack by the supporting electrolyte solution. For example, the voltammetric profile and the peak current intensity generated using the optimized pasta composition during the oxidation of target antioxidant was considered during this evaluation.

In order to show the role of Mn(MCA) compound as modifier with the aim of improving the CPE electroactivity range and catalytic activity, the studies were performed using cyclic voltammetry (CV) and linear sweep voltammetry (LSV) and phosphate buffer 0.04 mol L^{-1} (pH 7.0) as supporting electrolyte solution. Thus, in the Figure 4 are shown the cyclic voltammograms recorded during oxidation of propyl gallate (PG) employing the optimized paste composition in the presence (MCPE) and absence of modifier (CPE). In the mentioned experimental conditions, the voltammograms obtained are characterized for the nonappearance of oxidation (direct scan) and reduction (reverse scan) peaks in the absence of antioxidant PG during the scan within the potential window from -0.25 to +0.65 V vs. Ag/AgCl (Figure 4, a and b, respectively). However, the voltammograms obtained for electrochemical oxidation of PG (5.00×10^{-5} mol L^{-1}) are characterized by the occurrence of well-defined anodic peak ($\mathbf{I_{pa}}$) at +0.22 V vs. Ag/AgCl (on the CPE surface, Figure 4 voltammogram c) and at +0.23 V vs. Ag/AgCl (on the MCPE surface, Figure 4 voltammograms d). As previously reported by de La Fuente and co-workers [20], the anodic peak verified on the CPE and MCPE surface is attributed to the oxidation of the (R-OH) group for the oxidized form (R=O).

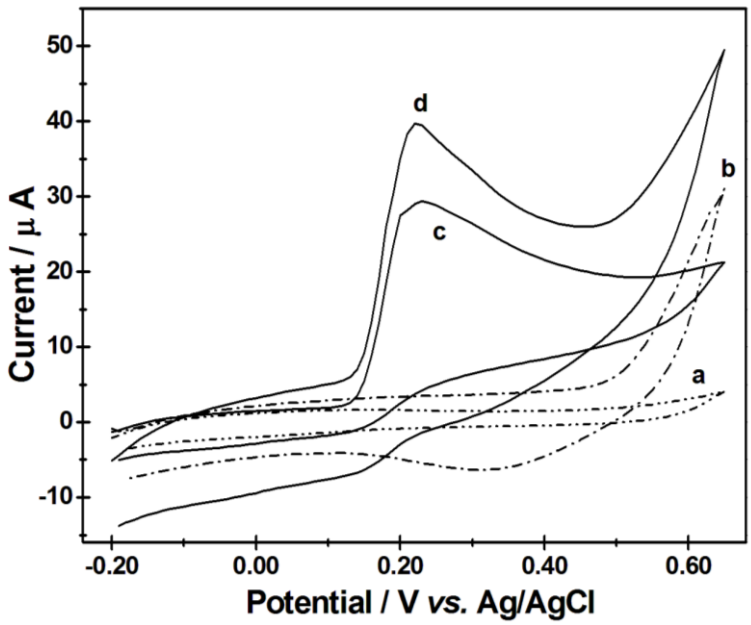

Figure 4. Cyclic voltammograms recorded under the following conditions: blank, phosphate buffer (pH 7.0) registered on the CPE (a) and MCPE (b) surfaces, respectively, and electrochemical oxidation of PG (5.00×10^{-5} mol L^{-1}) on the CPE (c) and MCPE (d) surfaces. Scan rate 100 mV s^{-1}.

Comparing both working electrode performance from the results showed in the Figure 4, it can be seen that on the CPE surface a weakest and relatively broad oxidation peak current is observed for PG detection over the potential sweep range. However, it can also see that after addition of Mn(MCA) compound to the matrix of CPE, the electrochemical response in neutral experimental

condition (pH 7.0) was significant for the PG oxidation. This improvement can be related to the voltammetric profile of the peak obtained, like current intensity and sharpness, due to the enhancement in the electron transfer rate from PG to the electrode surface. This result suggest that the incorporation of Mn(MCA) compound in the matrix of CPE provides more favorable catalytic property because the modifier acts as a redox mediator, favoring the PG oxidation process. Furthermore, this characteristic provides a suitable alternative for PG detection and it can be explored for development of alternative methodology using electroanalytical techniques. Therefore, the next step was to optimize the working conditions from the study of the experimental and instrumental parameters.

The study of the scan rate (υ) for the electrochemical oxidation of the PG (5.00×10^{-5} mol L^{-1}) on the MCPE surface using phosphate buffer 0.04 mol L^{-1} at pH 7.0 provides information about the voltammetric behavior of this process. The voltammograms were recorded in the range of -0.20 to +0.65 V vs. Ag / AgCl, varying the υ between 20 and 200 mV s^{-1}. The recorded voltammogram presented satisfactory voltammetric profile at υ smaller than 200 mV s^{-1} and after that, it was impossible to measure the exact values of the $\mathbf{I_{pa}}$ and $\mathbf{E_{pa}}$. A linear relationship between anodic peak current ($\mathbf{I_{pa}}$) and square root of the scan rate ($\upsilon^{1/2}$) was observed according to the equation: $\mathbf{I_{pa}}(\mu A) = 1.47\times\upsilon^{1/2}[(mV\ s^{-1})^{1/2}]$, (n = 7) with linear correlation coefficient of 0.9950 indicating a diffusion-controlled electrode process. In all scan rates studied, it was observed the absence of the corresponding cathodic peak in the reverse scan, suggesting irreversible nature of the PG electrochemical oxidation. The current function, $\mathbf{I_{pa}}/(\upsilon^{1/2}\mathbf{C_{PG}})$, does not change with the increase of υ, and the peak potential values ($\mathbf{E_{pa}}$) shifts slightly towards more positive potentials by increasing υ, suggesting that the electrochemical oxidation of PG presents irreversible characteristics and/or the electrode process is influenced by chemical reactions coupled to the electron transfer. For analytical purposes and considering the maximum current intensity, the υ of 100 mV s^{-1} was adopted for continuing studies.

Once the carbon paste composition was optimized, the analytical performance of the MCPE was tested comparing the voltammetric behavior obtained from different electrodes in the absence and presence of PG (5.00×10^{-5} mol L^{-1}). The Figure 5 shows the linear sweep voltammograms (LSV), recorded on the surface of the glassy carbon electrode (GCE), unmodified carbon paste electrode (CPE) and modified carbon paste electrode (MCPE) with Mn(MCA) compound to test the feasibility of using the MCPE as working electrode in electroanalysis. From Figure 5, it should be noted the absence of peak in the recorded voltammogram on the MCPE surface only in the supporting electrolyte solution (Figure 5, voltammograms a). Nonetheless, with the addition of PG (4.80×10^{-5} mol L^{-1}) in the electrochemical cell, it can be clearly seen the occurrence of a well-defined peak on the forward scan at GCE, CPE and MCPE surfaces (Figure 5, voltammograms b, c and d, respectively). From the Figure 5, the voltammogram b recorded on the MCPE surface is noticeably the one which shows a considerable response in terms of peak current intensity (named $\mathbf{I_{pa}}$), as well as improves the voltammetric profile. Again, this is indicative that the Mn(MCA) complex plays an important role in the carbon paste modification, presenting electrocatalytic property by improving the electron transfer rate from PG to MCPE-surface. For instance, the MCPE-Mn(MCA) responses ($\mathbf{I_{pa}}$ = 14.30 μA) were around two-fold higher than those obtained at the CPE ($\mathbf{I_{pa}}$ = 6.35 μA), suggesting the electrocatalytic action of Mn(MCA) compound for PG oxidation. Thus, this finding is consistent with the expected for the purposes of this work.

Voltammetric studies at different pH values

The pH of the electrolyte solution is very critical to the characteristics of PG and also to the MCPE consistence. Consequently, the effect of pH was studied in detail. Accordingly, it was evaluated the analytical performance of the MCPE under the influence of the pH between 3.8 and 9.0, recording voltammograms in the supporting electrolyte solution (phosphate buffer 0.04 mol L^{-1}). Studies at pH values higher than 9.0 were not conduced because the peak current could not be measured accurately. The voltammograms obtained for acid, neutral and basic mediums are shown in Fig. 7 (curves a-d). Besides, the PG presented higher peak current under neutral conditions than under acid and basic ones. Results show that the peak potential for oxidation of PG varies linearly with pH and is shifted to more positive values (Figure 6, inset) with linear relationship following the equation: E_{pc} (mV) = 656 – 60×pH (r = 0.998) for $3.8 \leq pH \leq 9.0$, which slope of -60 mV per pH unit indicates that the electrode process is

influenced by protonation reactions [21]. The peak current has a non-linear behavior as a function of pH, as illustrated in Figure 6 (inset). The response increases continually as pH increases from 3.8 to 7.0 and decreases significantly at pH 9.0. Thus, phosphate buffer 0.04 mol L^{-1} at pH 7.0 was chosen as supporting electrolyte solution to detect PG antioxidant on the MCPE-Mn(MCA) surface.

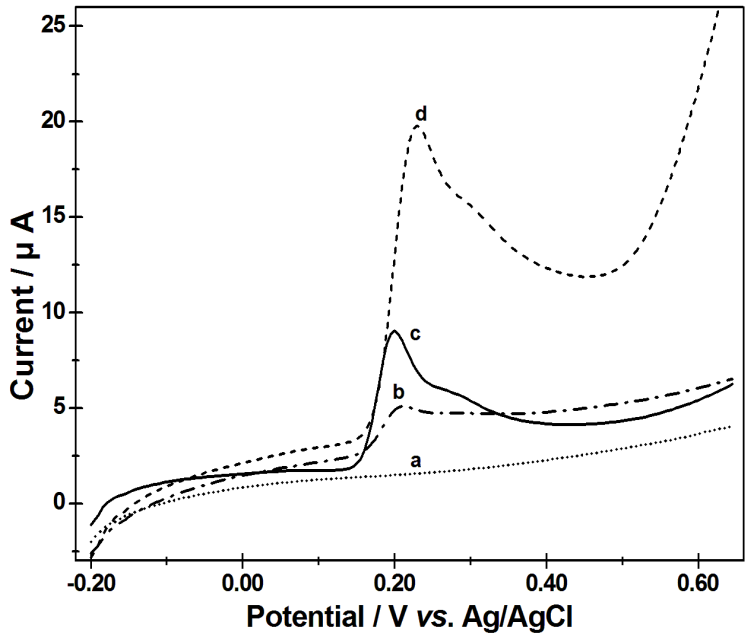

Figure 5. Linear sweep voltammograms recorded under the following conditions: (a) blank, phosphate buffer (pH 7.0) on the MCPE surface and electrochemical oxidation of PG (4.80×10^{-5} mol L^{-1}) on the GCE surface (b); CPE (c) and MCPE (d). Scan rate of 100 mV s^{-1}.

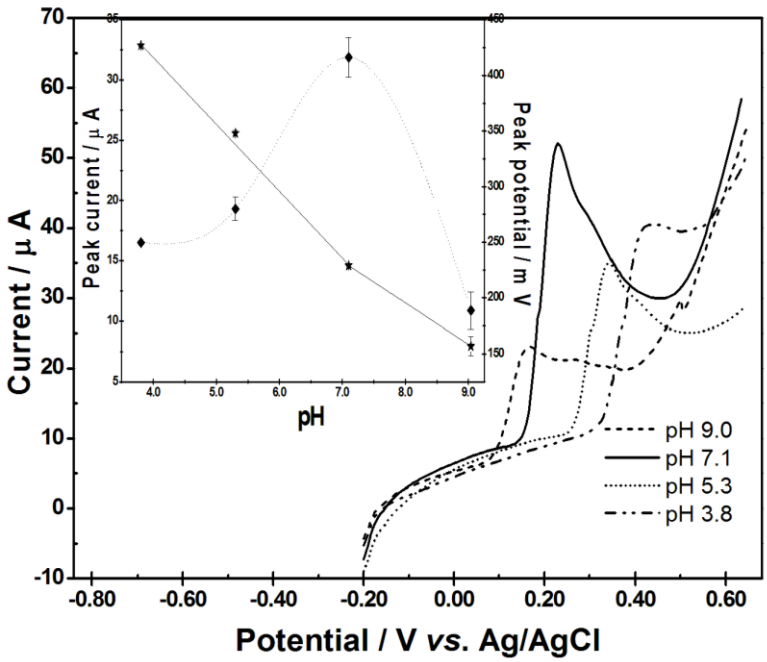

Figure 6. Linear sweep voltammograms recorded for electrochemical oxidation of 2.00×10^{-5} mol L^{-1} of PG on the MCPE surface in phosphate buffer solution between pH 3.8 and pH 9.0. Conditions: υ = 100 mV s^{-1}. Inset: Influence of pH on the peak potential and peak current response for the pH range 3.8 - 9.0.

Analytical applicability

After having optimized the working conditions regarding the work electrode composition and experimental and instrumental parameters, the PG was detected at different concentrations (4.00×10^{-6} to

2.20×10^{-5} mol L^{-1}) with the purpose of plotting the analytical curve. The Figure 7 illustrates the analytical curve obtained under these conditions, which presents a satisfactory linearity only in the concentration range of 4.00×10^{-6} to 1.40×10^{-5} mol L^{-1} for response of the peak current versus PG concentration. The linear range showed satisfactory analytical performance according to the following regression equation: $\mathbf{I_{pa}}(\mu A) = -0.21 + 1.64\times10^{5}\ C_{PG}$ (mol L^{-1}) (r = 0.998, n = 8). Then, from the obtained parameters of analytical curve it was possible to calculate the limit of detection (LOD) of the electrochemical system employing the following mathematical relationship: $3\times\mathbf{Sd_A}/m$, where $\mathbf{Sd_A}$ represents the standard deviation of the intercept and m the slope of the analytical calibration curve [22]. The preliminary studies along with estimated LOD (6.80×10^{-7} mol L^{-1}) indicate an acceptable detectability, enabling the use of the MCPE-Mn(MCA) and LSV technique in the development of a methodology for PG quantification, for example, in biofuels samples.

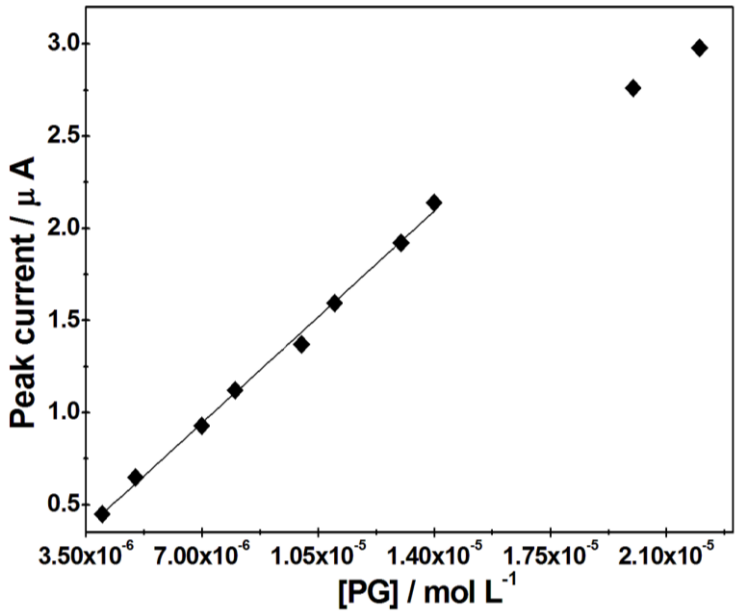

Figure 7. Dependence of the anodic peak current (I_{pa}) as a function of PG concentration. Scan rate of 100 mVs^{-1}.

The analytical application test was performed in order to detect the PG antioxidant and develop a new electroanalytical methodology. For this study, the matrix effect was evaluated by means of addition-recovery tests carried out on a biodiesel sample prepared in accordance with the experimental section (2.5). Recoveries values around 90.0% were obtained, demonstrating satisfactory precision and accuracy and indicating that the obtained results, regarding the prepared MCPE-Mn(MCA), can be considered advantageous once it was not necessary the use of expensive material such as carbon nanotubes to improve the voltammetric response. In addition, the estimated LOD is comparable to previous works reported in the literature, developed for electrochemical determination of phenolic antioxidants in a diversity of food and biodiesel samples, at different working electrodes surfaces [20, 23-29].

4. CONCLUSION

The synthesis, preliminary characterization and incorporation of Mn(MCA) compound in CPE was presented and adequately discussed. From TG-DTA analysis data, a general formula could be established for the synthesized compound providing previous information about unreported thermal stability, decomposition as well as the purity of the compound in dynamic air atmosphere. In addition, the infrared spectroscopic data suggest that the 3,4-(methylenedioxi)cinnamate acts as a chelating bidentate to the manganese metal ion.

The results obtained using electrochemical techniques such as cyclic and linear sweep

voltammetry showed that the MCPE-Mn(MCA) can be considered as a new and interesting tool in the development of working electrode to be used in electroanalysis. From electroanalytical purposes, the linear sweep voltammetric technique showed satisfactory results when compared to other ones, especially for presenting a larger analytical signal and requiring a shorter analysis time, which could be verified by the significant improvement of the voltammetric responses. Thus, the results obtained present a satisfactory analytical performance for future applications in the detection of PG in real biodiesel samples.

5. ACKNOWLEGMENTS

The authors thank Ivo Giolito Thermal Analysis Laboratory for infrastructure support, as well as FUNDECT, CAPES, UFGD and PIBIC/CNPq for financial support provided for the authors Luiz H. de Oliveira and Karoline L. Ribeiro.

6. REFERENCES AND NOTES

[1] Kanatt, S. R.; Chander, R.; Sharma, A. *Food Chem*. **2008**, *106*, 521. [CrossRef]

[2] Ronconi, L.; Aldinucci, D.; Ping, D. Q.; Fregona, D. *Anti-cancer Agents Med. Chem*. **2010**, 10, 283. [CrossRef]

[3] Silva, D. O. *Anti-cancer Agents Med. Chem*. **2010**, *10*, 312. [CrossRef]

[4] Rodríguez-Fernández, E.; Manzano, J. L.; Benito, J. J.; Hermosa, R.; Monte, E.; Criado, J. J. *J. Inorg. Biochem*. **2005**, *99*, 1558. [CrossRef]

[5] Ojani, R.; Raoof, J.-B.; Zamani, S. *Bioelectrochestry* **2012**, *85*, 44. [CrossRef]

[6] Wang, G.; Yang, J. *Surf. Coat. Tech*. **2010**, *204*, 3599. [CrossRef]

[7] Svancara, I.; Vytras, K.; Kalcher, K.; Walcarius, A.; Wang, J. *Electroanal*. **2009**, *21*, 7. [CrossRef]

[8] McCreery, R. L. *Chem. Rev*. **2008**, *108*, 2646. [CrossRef]

[9] Adams, R. N. Carbon paste electrodes, *Anal. Chem*. **1958**, *30*, 1576. [CrossRef]

[10] She, Y.; Tang, Y.; Liu, H.; He, P. *Chem. Cent. J*. **2010**, *4*, 10. [CrossRef]

[11] Radulescu, M.-C.; Chira, A.; Radulescu, M.; Bucur, B.; Bucur, M. P.; Radu, G. L. *Sensors,* **2010**, *10*, 11340. [CrossRef]

[12] Apetrei, C.; Apetrei, I. M.; Saja, J. A.; Rodriguez-Mendez, M. L. *Sensors,* **2011**, *11*, 1328. [CrossRef]

[13] Crespilho, F. N.; Rezende, M. O. O. *Quím. Nova* **2004**, *27*, 964. [CrossRef]

[14] Zhuang, R. R.; Jian, F. F. *J. Sol. State Electrochem*. **2010**, *14*, 747. [CrossRef]

[15] Issa, Y. M.; Ibrahim, H.; Shehab, O. R. *J. Electroanal. Chem.* **2012**, *666*, 11. [CrossRef]

[16] Abbaspour, A.; Norouz-sarvestani, F.; Mirahmadi, E. *Electrochim. Acta* **2012**, *76*, 404. [CrossRef]

[17] KNOTHE, G. H. *Fuel Proces. Techn*. **2007**, *88*, 677.

[18] Nakamoto, K.; Infrared and Raman Spectra of inorganic and coordination compounds, Part B. 5th ed. New York: Wiley, **1997**.

[19] Deacon, G. B.; Phillips, R. J. *Coord. Chem. Rev*. **1980**, *33*, 227. [CrossRef]

[20] Fuente, C. L.; Acuña, J. A.; Vázquez, M. D.; Tascón, M. L.; Batanero, P. S. *Talanta* **1999**, *49*, 441. [CrossRef]

[21] Bard, A. J.; Faulkner, R. L.; Electrochemical methods-fundamentals and application, New York: John Wiley, **2001**.

[22] Miller, J. C.; Miller, J. N. Statistics for Analytical Chemistry, Ellis Horwood, West Sussex, **1993**.

[23] Caramit, R. P.; Andrade, A. G. F.; Souza, J. B. G.; Araujo, T.A.; Viana, L.H.; Trindade, M. A. G.; Ferreira, V. S. *Fuel* **2013**, *105*, 306. [CrossRef]

[24] Tormin, T. F.; Gimenes, D. T.; Silva, L. G.; Ruggiero, R.; Richter, E. M.; Ferreira, V. S.; Muñoz, R. A. A. *Talanta* **2010**, *82*, 1599. [CrossRef]

[25] Tormin, T. F.; Gimenes, D. T.; Richter, E. M.; Muñoz, R. A. A. *Talanta* **2011**, *85*, 1274. [CrossRef]

[26] Tormin, T. F.; Cunha, R. R.; Richter, E. M.; Muñoz, R. A. A. *Talanta* **2012**, *99*, 527. [CrossRef]

[27] Araujo, T. A.; Barbosa, A. M. J.; Viana, L. H.; Ferreira, V. S. *Colloid. Surface B* **2010**, *79*, 409. [CrossRef]

[28] Araujo, T. A.; Barbosa, A. M. J.; Viana, L. H.; Ferreira, V. S. *Fuel* **2011**, *90*, 707. [CrossRef]

[29] Ni, Y.; Wang, L.; Kokot, S. *Anal Chim Acta*, **2000**, *412*, 185. [CrossRef].

Orbital: The Electronic Journal of Chemistry
journal homepage: www.orbital.ufms.br
ISSN 1984-6428

| Vol 6 | | No. 1 | | January-March 2014 |

Short Communication

Removal of Petroleum Spill in Water by Chitin and Chitosan

Francisco Cláudio de Freitas Barros[a], Luiz Constantino Grombone Vasconcellos[b], Técia Vieira Carvalho[c] and Ronaldo Ferreira do Nascimento[a]*

[a]*Departamento de Química Analítica e Físico-Química, Universidade Federal do Ceará. Fortaleza, CE. Brasil.*
bDepartamento de Química Orgânica e Inorgânica, Universidade Federal do Ceará. Fortaleza, CE. Brasil.
[c]*PADETEC, Parque de Desenvolvimento Tecnológico, Universidade Federal do Ceará. Fortaleza, CE. Brasil.*

Article history: Received: 06 August 2013; revised: 31 December 2013; accepted: 17 February 2014. Available online: 02 April 2014.

Abstract: The present study was undertaken to evaluate the capacity of adsorption of crude oil spilled in seawater by chitin flakes, chitin powder, chitosan flakes, chitosan powder, and chitosan solution. The results showed that, although chitosan flakes had a better adsorption capacity by oil (0.379 ± 0.030 grams oil per gram of adsorbent), the biopolymer was sinking after adsorbing oil. Chitosan solution did not present such inconvenience, despite its lower adsorption capacity (0.013 ± 0.001 grams oil per gram of adsorbent). It was able to form a polymeric film on the oil slick, which allowed to restrain and to remove the oil from the samples of sea water. The study also suggests that chitosan solution 0.5% has greater efficiency against oil spills in alkaline medium than acidic medium.

Keywords: crude oil spill, biopolymers, chitosan, adsorption

1. INTRODUCTION

Crude oil: every day, 31.5 billion gallons are transported over the sea by ship; 2.73 billion gallons are consumed each day; there is also an estimative that 100 million gallons are spilled every year in marine environments [1].The spill can affect organisms by physical and toxicological processes causing an impact on the environment with disruptions in the food chain. In addition to ecological concerns, spills in shores may have economic matter in recreational areas, tourism and fisheries industry [2]. Several great disaster occurred in the last 10 years, caused by ships, oil ducts and platforms that sunk or leaked or exploded, spreading large oil slick over hundreds of square kilometers [3].

There is no efficient way to control and combat oil spills: physical restraint, removal with skimmers, cushions, or strands of natural and synthetic absorbents, addition of chemical dispersants, in-situ burning and bioremediation are not good to the environment. Natural processes such as spreading, advection, evaporation, dissolution, dispersion, emulsification, oxidation, sedimentation and degradation also contribute to remove the spilled oil on the sea [2].

Chitin is a biopolymer that comprises a linear sequence of monomeric sugars of N-acetylglucosamine. After cellulose, chitin is the most abundant biological fiber on earth. Chitin has a similar structure of cellulose, which the structural difference is the hydroxyl groups of carbon 2 is replaced by acetyl amino groups in the chitin molecule. The commercial sources of chitin are crustaceans shells especially of crab, shrimp and lobster. Chitin is also found in insects, mollusks and in fungal cell wall [4].

Chitosan is produced from the deacetylation of chitin by using strong alkaline aqueous solutions. During the course of the reaction, the N-acetyl groups linked to chitin are lost, forming units of D-glucosamine that has an amine group. Chitosan is composed by partially deacetylated polymeric chains with deacetylation degree above 50% [4].

According to Assis & Britto [5] the efficient process for the extraction of chitin and subsequent transformation for chitosan using the wastes from the creation of shrimp farmed (carciniculture) are superior to 40% of the animal weight, where 30% of these wastes could be recovered as chitin.

Chitin and chitosan have been evaluated by

*Corresponding author. E-mail: ronaldo@ufc.br

several studies as the agent for microorganisms immobilization used for removal of organic pollutants such as oil and its derivatives [6]. Chitosan has been reported as a low cost alternative in the treatment of contaminated waters containing phenolic compounds [7]. The bioremediation of oil-polluted seawater has been studied using bacteria immobilized on chitin and on chitosan flakes that degrade hydrocarbons [8]. The bioremediation of oil contaminated sediments in the shores of Singapore was conducted using osmocote mixed with chitosan [9]. The mixture caused the biodegradation of aliphatic and polycyclic aromatic hydrocarbons by native microorganisms.

Bacillus subtilis spores were encapsulated in chitosan beads crosslinked with glutaraldehyde to the biodegradation of n-hexadecane [10]. The complete biodegradation of n-alkane was reported within forty to seven days in the presence of chitin, chitosan and keratin [11].

From batch study on assessing the efficiency of different adsorbents (Mucor rouxii biomass, Absidia coerulea biomass, chitosan, and walnut shell) where used to remove oil spilled on water, chitosan showed higher adsorption capacity when compared with these materials [12].

In this work, the chitin flakes, chitin powder, chitosan flakes, chitosan powder, and chitosan solution were studied, evaluating the capacity of adsorption of crude oil spilled in simulated system containing seawater.

2. MATERIAL AND METHODS

Chitin and chitosan flakes

Chitin (white powder, molecular weight 400,000 $g.mol^{-1}$, pH 4.28) and chitosan powder (yellowish powder, 80% grade of deacetylation, molecular weight 174,205 $g.mol^{-1}$, pH 7.93), obtained from shrimp shells were provided by the company POLYMAR SA (Fortaleza-Ceará, Brazil).

The size of these materials was determined by the USP-23 method. Chitin and chitosan flakes presented particles with size high than 0.354 mm. Chitin powder presented particles with average size of 0.354 mm, while chitosan powder had particles with average size between 0.104 and 0.075 mm.

The degree of deacetylation of chitosan samples was determined by acid-base titration [13]. In this method, a chitosan solution was prepared by adding 0.5 g chitosan (flakes or powder) in 40 mL of 0.1 mol L^{-1} HCl solution. It was added 3 drops of methyl red to the chitosan solution, which was then titrated with standardized 0.1 mol L^{-1} solution of NaOH and then, repeated the same titration with blank solution (0.1 mol L^{-1} solution of HCl). The procedure was performed in triplicate. The degree of deacetylation is given by:

$$DA = [(V_B - V_G) \cdot 0.162 \cdot N \cdot 100] \div [PA \cdot (1.00 - 0.01 \cdot H)] \quad (1)$$

Where: V_B is the volume of NaOH solution spent in the blank, V_G is the volume of NaOH solution spent in the titration, N is the molality of NaOH, PA is the sample weight and H is the moisture content on the chitosan sample. Chitosan samples showed deacetylation degrees of 82.2%.

Chitosan solution

The chitosan solution was prepared by dissolving 0.5 g chitosan in 10 mL of 1.0% (w/v) acetic acid solution. The viscosity and density of the solution were determined with an Ostwald viscometer (BS/UD-7346) and a glass pycnometer, respectively. The solution presented viscosity of 3.54 ± 0.31 cp and density of 1.00342 ± 0.00082 $g.mL^{-1}$.

Determination of the biopolymers adsorption capacity

The sample of bachaquero heavy crude oil used in the experiments was supplied by Lubrificantes e Derivados de Petróleo do Nordeste - LUBNOR.

In a beaker of 1.0 L, were added 300.0 mL of distilled water, 3.0 g of petroleum, and adsorbent (flakes and powder biopolymers) varying between 4 and 10 g. The system was stirred by 15 min and the content was transferred to a basket of 0.354 mm. After one hour, the content of the basket was placed in a Petri plate previously weighed. The plate with the biopolymer and the adsorbed oil was weighed and then placed in an oven for 3.0 h at 105 °C and dried for 1.0 h. The plate containing the biopolymer flakes and oil was weighed again and the result was noted.

The procedure for the determination of the biopolymer powder adsorption capacity was similar to the biopolymer flakes. The difference is that, after stirring by 15 min, the material in the beaker was filtered in a filter paper and transferred to a Petri plate previously weighed. The plate with the biopolymer

and the adsorbed oil was weighed, placed in an oven for 3.0 hours at 105 °C and then dried for 1 h. The plate containing the biopolymer powder and oil was weighed again and adsorption capacity was determined by mass balance.

For chitosan solution, the procedure was similar to the used with biopolymer flakes and biopolymer powder, however were added 150.0 mL of 0.5% chitosan solution (in 1% w/v acetic acid solution).

The polymers adsorption capacities in flakes or powder were determined using the following calculations:

$$S_P = S_T - S_O \quad (2)$$

$$C_P = S_P / S_O \quad (3)$$

Where:

S_P= mass of oil adsorbed,

S_O= mass of dry adsorbent,

S_T= mass of the contents on the Petri plate

C_P= adsorption capacity.

For the adsorption capacity of oil by chitosan was determined by:

$$C_P = S_P / V_O \quad (4)$$

Where:

V_O= volume of solution

Application of chitosan solution in a simulated oil spill in sea water

Samples of seawater of the beach, located in the city of Fortaleza, state of Ceará, Brazil, were collected in bottles of 5.0 L. The bottles were transported to the laboratory and kept at 4 °C prior to use in experiments. The samples of seawater presented at pH 7.9.

A volume of 5.0 L of seawater was placed in a plastic container. On the surface of water, were added 7.0 g of petroleum, leaving the oil slick to spread over the water surface. After 30 min, 50.0 mL of 0.5% (w/v) chitosan solution were sprayed over the oil spill using a pneumatic spray glass.

Application of chitosan solution in a simulated oil spill in sea water at different pH values

A volume of 400.0 mL of seawater was added in two Petri plates, (A and B samples). The pH of seawater in A sample was adjusted to 3.99 with 0.1 moL^{-1} HCl solution, while the pH of seawater in B sample was corrected to 9.02 with 0.1 mol L^{-1} NaOH solution. Then 1.12 g and 1.14 g of oil were added on water surface in A and B samples, respectively. After 30 min, 50.0 mL of 0.5% chitosan solution were sprayed over the oil spill in A and B samples using a pneumatic spray glass.

3. RESULTS AND DISCUSSION

The results presented in Table 1 show that chitosan flakes is the material with better adsorption capacity (0.379 ± 0.030 grams oil per gram of adsorbent) under the experimental chosen conditions. The adsorption capacities of the biopolymers and chitosan solution were compared as shown in Figure 1. The process in which chitosan adsorbs oils and fats is not yet fully understood, but experimental observations indicate two types of mechanisms [4]:

a) Attraction of opposite charges between oil and chitosan;

b) Interlace effect, in which chitosan acts as a network, getting involved around the drops of oil and fats and trapping them.

Table 1. Adsorption capacity of biopolymer flakes, biopolymer powders and chitosan solution. All experiments were performed in duplicate.

Adsorbent	Oil Mass	Adsorbent Amount	Adsorbed Oil	Adsorption capacity
Chitin Flakes	3.06 g	9.19 g	52.24 ± 4.23 %	0.258 ± 0.022 g/g
Chitin Powder	3.18 g	9.25 g	49.35 ± 2.01 %	0.170 ± 0.004 g/g
Chitosan Flakes	3.16 g	6.09 g	72.75 ± 3.97 %	0.379 ± 0.030 g/g
Chitosan Powder	3.08 g	8.91 g	81.27 ± 13.39 %	0.281 ± 0.050 g/g
Chitosan Solution	3.08 g	150.0 mL	60.52 ± 2.01 %	0.013 ± 0.001 g/mL

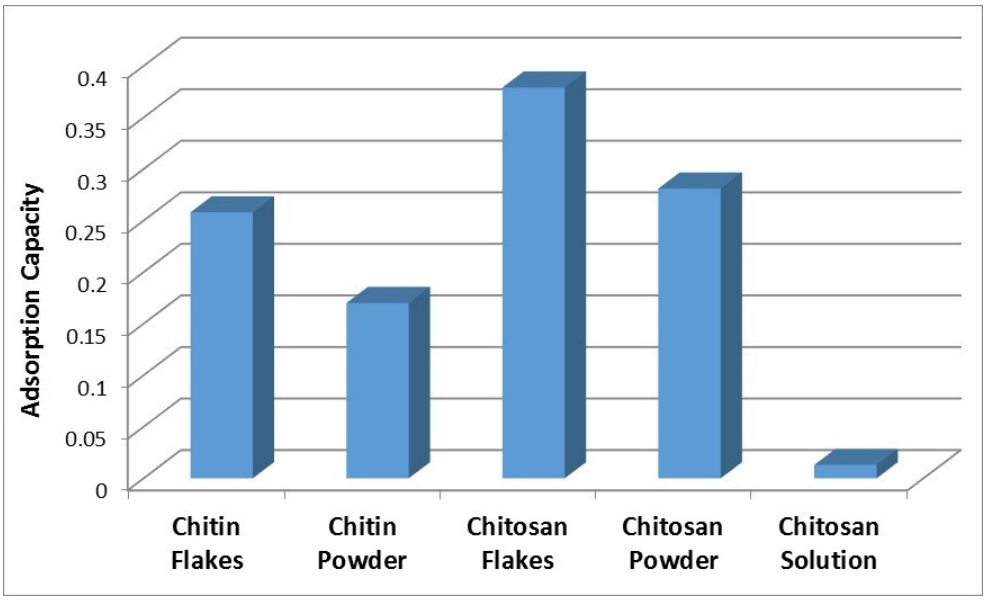

Figure 1. Histogram the adsorption capacity values of the biopolymers studied. For biopolymers flake and biopolymers powders, the adsorption capacity is expressed in mg of oil per gram of adsorbent.

Although chitosan flakes had a greater adsorption affinity by oil, initial studies showed that all the solid biopolymers have the undesired behavior of sinking after adsorbing oil, which prevent its use in the form of free particles. Chitosan solution, despite its lower adsorption capacity, does not present such inconvenience. By other hand, when oil is poured over the seawater surface, it spreads as much as possible and it tends to stick to any solid surface, like the walls of container that contains the seawater in the laboratory, and it is difficult to removal by any mechanical means.

It was observed that two hours after the application of chitosan solution, there was the formation of a biopolymer film on the oil, which prevented the oil spreading over the water surface. Furthermore, the chitosan film prevented the oil slick to stick on the walls of the container, enabling almost complete removal with the aid of a small plastic wiper.

In the samples of seawater with different pH values (A and B samples) after the addition of oil was observed that oil slicks spread freely, as expected. In sample B, the alkaline water, the oil spread with greater speed than in the acidified sample A. With the application of chitosan solution and biopolymer film formation on both samples after 2.0 h, the oil spills were contained, but with greater efficiency in the alkaline medium in sample B.

This phenomenon can be explained by the fact that chitosan is soluble in acid, such as A sample. But despite this fact, the formation of the chitosan film occurred on the oil spill in acidified seawater.

4. CONCLUSION

Chitosan flakes presented superior adsorption capacity than chitosan powder for oil. Initial test of laboratory showed that biopolymer flakes and biopolymer powders cannot be used in their free form in seawater, since, when combined with oil, become denser and sink. Chitosan was able to form a polymeric film on the oil slick, which allowed to restrain and to remove the oil from the samples of sea water. The study also suggests that chitosan solution 0.5% (m/v) has greater efficiency against oil spills in alkaline medium than acidic medium.

The chitosan solution 0.5% was able to form a polymeric film on the oil slick, which allowed to restrain and to remove the oil from the samples of sea water. Although seawater is slightly alkaline in nature, situations where its pH is acid may contribute to the decreased in efficiency on the use of chitosan solution against oil spills.

5. REFERENCES AND NOTES

[1] Oil Spill Intelligence Report, Arlington, MA, U.S.A. [Link]

[2] Spill Prevention And Response - How Its Works. American Petroleum Institute. [Link]

[3] Mitsch, W. J. *Ecol. Eng.* **2010**, *36*, 1607. [CrossRef]

[4] Muzzarelli, R. A. A. Chitin. Pergamon Press. 1st Ed. 1977.

[5] Assis, O. B. G.; De Britto, D. *Rev. Bras. Agroci.* **2008**, *14*, 91.

[6] Bashan, L. E.; Bashan, Y. *Bioresour. Technol.* **2010**, *101*, 1611. [CrossRef]

[7] Milhome, M. A. L.; Keukeleire, D.; Ribeiro, J. P.; Nascimento, R. F. *Quím. Nova* **2009**, *32*, 2122. [CrossRef]

[8] Gentili, A. R.; Cubitto, M. A.; Ferrero, M. E.; Rodriguéz, M. S. *Int. Biodeterior. Biodegrad.* **2006**, *57*, 222. [CrossRef]

[9] Xu, R.; Lau, A. N. L.; Lim, Y. G.; Obbard, J. P. *Mar. Pollut. Bull.* **2005**, *51*, 1062. [CrossRef]

[10] Barreto, R. V. G.; Hissa, D. C.; Paes, F. A.; Grangeiro, T. B.; Nascimento, R. F.; Rebelo, L. M.; Craveiro, A. A.; Melo, V. M. M. *Bioresour. Technol.* **2010**, *101*, 2121. [CrossRef]

[11] Setti, L.; Mazzieri, S.; Pifferi, P. G. *Bioresour. Technol.* **1999**, *67*, 191. [CrossRef]

[12] Srinivasan, A.; Viraraghavan, T. *Bioresour. Technol.* **2010**, *101*, 6594. [CrossRef]

[13] Broussignac, J. *Chim. Ind. Genie Chim.* **1972**, *99*, 1241.